Article

Influence of Winkler-Pasternak Foundation on the Vibrational Behavior of Plates and Shells Reinforced by Agglomerated Carbon Nanotubes

Damjan Banić [1] [iD]**, Michele Bacciocchi [2]** [iD]**, Francesco Tornabene [2],*** [iD]
and Antonio J. M. Ferreira [3]

[1]   Department of Engineering Mechanics, Faculty of Engineering, University of Rijeka, HR-51000 Rijeka,
     Croatia; dbanic@riteh.hr
[2]   Department of Civil, Chemical, Environmental and Materials Engineering (DICAM),
     School of Engineering and Architecture, University of Bologna, 40136 Bologna, Italy; michele.bacciocchi@unibo.it
[3]   Departamento de Engenharia Mecânica, Faculdade de Engenharia da Universidade do Porto,
     4200-465 Porto, Portugal; ferreira@fe.up.pt
*   Correspondence: francesco.tornabene@unibo.it

Abstract: This paper aims to investigate the effect of the Winkler-Pasternak elastic foundation on the natural frequencies of Carbon Nanotube (CNT)-reinforced laminated composite plates and shells. The micromechanics of reinforcing CNT particles are described by a two-parameter agglomeration model. CNTs are gradually distributed along the thickness direction according to various functionally graded laws. Elastic foundations are modeled according to the Winkler-Pasternak theory. The theoretical model considers several Higher-order Shear Deformation Theories (HSDTs) based on the so-called Carrera Unified Formulation (CUF). The theory behind CNTs is explained in detail. The theoretical model presented is solved numerically by means of the Generalized Differential Quadrature (GDQ) method. Several parametric studies are conducted, and their results are discussed.

Keywords: Functionally Graded Carbon Nanotubes; natural frequencies; Winkler-Pasternak elastic foundations; numerical analysis; Higher-order Shear Deformation Theories

1. Introduction

In the last few decades, due to their high potential in terms of mechanical and thermal properties such as tensile and yield strength, Carbon Nanotubes (CNTs) have attracted the interest of many scientists and researchers trying to find convenient applications for these types of nanostructure [1–11]. The application of CNTs has mainly been as a reinforcement constituent of composite materials, which are, nowadays, widely used, especially in the aerospace field and in the automotive industry [12–29]. This has led to the birth of a new class of composites called nanocomposites. In spite of the numerous works that have been written on this subject, CNTs still remain an open topic for discussion. The curiosity with regard to the effects of CNT reinforcement on various structures has led to the development of different techniques and approaches for estimating these effects as well as possible, optimized between the goals of simplicity and accuracy [27]. The theory of mixtures, due to its simplicity, is the most common approach used to describe the mechanical properties of these types of nanostructure [30,31]. Despite its simplicity, this approach neglects several aspects of the micromechanics of CNT particles, which, due to their characteristic shape, tend to agglomerate in different areas of the reinforced polymer composite. A more precise approach has been proposed in the work by Shi et al. [32], presenting a two-parameter theoretical model that closely describes the agglomeration effect of the CNT particles, whereby the homogenization,

based on the Eshelby-Mori-Tanaka scheme for granular composite materials [33], and mechanical properties are obtained. This scheme uses the so-called Hill's elastic moduli [34,35] to describe the constitutive relations of the CNT particles. For the sake of completeness, some examples concerning the agglomeration of CNTs can be found in the papers [36–38].

The present paper aims to use this approach to study the effect of agglomeration on the natural frequencies of functionally graded carbon nanotube-reinforced laminated composite plates and shells resting on the elastic foundation. Although the high structural performance of plates and shells made from conventional composites has been proved by a number of papers [39–56], by employing CNTs as a reinforcing phase, their performance can be improved even further. A gradual variation of the volume fraction of the CNT particles trough the thickness of the composite has been employed, which is characteristic to functionally graded materials (FGMs). FGMs are a recent class of composite materials designed to deal with problems of stress concentration and mechanical discontinuity [57–84]. Therefore, the term Functionally Graded Carbon Nanotubes (FG-CNTs) was introduced to refer on this type of CNT-reinforced composite. For the sake of completeness, it should be mentioned that several papers concerning structural models suitable for the mechanical analysis of these kinds of structure have been published recently [85–93]. In particular, the gradient elasticity theory was proposed by Barretta et al. [85] to this end. Alternatively, a nonlocal model can be used for this purpose, as proved in the papers by Romano and Barretta [86], Romano et al. [87], Marotti de Sciarra and Barretta [88], and Apuzzo et al. [89].

To capture the proper mechanical behavior of these structures, adequate structural models must be considered. The use of classical shell theories may result in inaccurate results; therefore, the use of Higher-order Shear Deformation Theories (HSDTs) is required. Recent developments in the area of HSDTs are found in the works by Carrera [94–98], introducing the so-called Carrera Unified Formulation (CUF). This formulation is explained in detail in the books by Tornabene et al. [99,100]. CUF represents one of the most efficient and complete approaches when studying the mechanical behavior of multilayered composite beams, plates, and shells [101–110].

In this paper, various HSDTs based on the CUF Equivalent Single Layer (ESL) approach are employed to investigate the effect of agglomeration on the natural frequencies of FG-CNT-reinforced laminated composite plates and shells resting on the elastic foundation. The elastic foundation is modeled according to the Winkler-Pasternak theory. Papers describing this type of linear elastic foundation model can be found in [111–128]. As far as nonlinear analyses are concerned, the reader can find further details in the works [129–135].

Due to its complexity, the problem is solved numerically by the means of the Generalized Differential Quadrature (GDQ) method. The GDQ is an accurate, reliable, and stable numerical technique developed by Shu in the nineties [136]. This numerical technique is described in detail in the review paper by Tornabene et al. [137]. Further details concerning this numerical approach, as well as several numerical applications, can be found in the papers [138–140]. Finally, it should be mentioned that the present approach was implemented in MATLAB code [141].

2. Theoretical Model

2.1. Geometry

The two-dimensional shell model considered in this paper is defined by the vector $\mathbf{r}(\alpha_1, \alpha_2)$ over the middle surface of the shell (Figure 1). The parameters α_1, α_2 stand for the orthogonal and principal curvilinear coordinates of the middle surface of the shell. Examples for this notation can be found in the books by Tornabene et al. [99,100]. As can be seen in Figure 1, the position vector $\mathbf{R}(\alpha_1, \alpha_2, \zeta)$ defines each point P of a generic three-dimensional shell element of constant thickness h. Position vector $\mathbf{R}(\alpha_1, \alpha_2, \zeta)$ is defined as

$$\mathbf{R}(\alpha_1, \alpha_2, \zeta) = \mathbf{r}(\alpha_1, \alpha_2) + \zeta\,\mathbf{n}(\alpha_1, \alpha_2) \tag{1}$$

where ζ is the coordinate that identifies the normal direction along the shell thickness. The outward unit normal vector $\mathbf{n}(\alpha_1, \alpha_2)$, defined along ζ, can be expressed as

$$\mathbf{n} = \frac{\mathbf{r}_{,1} \wedge \mathbf{r}_{,2}}{|\mathbf{r}_{,1} \wedge \mathbf{r}_{,2}|} \tag{2}$$

The symbol "$\wedge$" stands for the vector product, also $\mathbf{r}_{,i} = \partial \mathbf{r}/\partial \alpha_i$ for $i = 1, 2$ is introduced. The following limitations are included for $i = 1, 2$

$$\alpha_i \in \left[\alpha_i^0, \alpha_i^1\right] \tag{3}$$

where α_i^0, α_i^1 denote respectively the minimum and the maximum values of the coordinates at issue. The third coordinate ζ must be defined within the limits of the shell thickness; therefore, it is bounded as

$$\zeta \in [-h/2, h/2] \tag{4}$$

For a laminated composite structure made of l plies (Figure 1), the total thickness of the shell h can be expressed as

$$h = \sum_{k=1}^{l} h_k \tag{5}$$

where h_k denotes the thickness of the k-th ply.
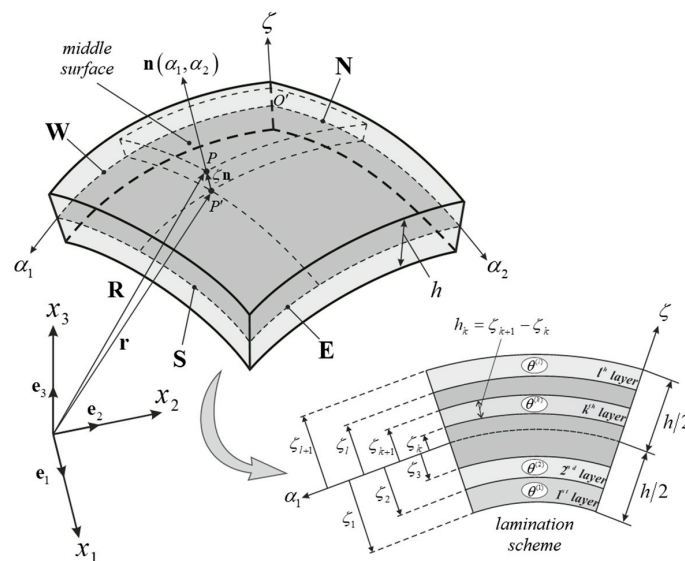
Figure 1. Doubly-curved panel representation and lamination scheme.

With the defined position vector $\mathbf{r}(\alpha_1, \alpha_2)$, the Lamé parameters $A_1(\alpha_1, \alpha_2)$ and $A_2(\alpha_1, \alpha_2)$ of the surface can be computed as

$$A_1 = \sqrt{\mathbf{r}_{,1} \cdot \mathbf{r}_{,1}}, \quad A_2 = \sqrt{\mathbf{r}_{,2} \cdot \mathbf{r}_{,2}} \tag{6}$$

where the symbol "$\cdot$" denotes the scalar product. Radii of curvature $R_1(\alpha_1, \alpha_2)$ and $R_2(\alpha_1, \alpha_2)$ of the doubly-curved reference surface, due to the hypothesis of orthogonal and principal coordinates, can be evaluated as follows

$$R_1 = -\frac{\mathbf{r}_{,1} \cdot \mathbf{r}_{,1}}{\mathbf{r}_{,11} \cdot \mathbf{n}}, \quad R_2 = -\frac{\mathbf{r}_{,2} \cdot \mathbf{r}_{,2}}{\mathbf{r}_{,22} \cdot \mathbf{n}} \tag{7}$$

with the notation $\mathbf{r}_{,ii} = \partial^2 \mathbf{r} / \partial \alpha_i^2$, for $i = 1, 2$. The parameters $H_1(\alpha_1, \alpha_2, \zeta)$ and $H_2(\alpha_1, \alpha_2, \zeta)$, which must be introduced to consider the three-dimensional size effect of the structure, are evaluated by

$$H_1 = 1 + \frac{\zeta}{R_1}, \quad H_2 = 1 + \frac{\zeta}{R_2} \tag{8}$$

2.2. Shell Formulation

The three-dimensional displacement field of the laminated composite shell can be expressed by the Carrera Unified Formulation (CUF), which was conceived to study the structural response of beams and plates. The displacement components, according to a general higher-order Equivalent Single Layer (ESL) approach, are given by

$$
\begin{aligned}
U_1(\alpha_1, \alpha_2, \zeta, t) &= \sum_{\tau=0}^{N+1} F_\tau(\zeta) u_1^{(\tau)}(\alpha_1, \alpha_2, t) \\
U_2(\alpha_1, \alpha_2, \zeta, t) &= \sum_{\tau=0}^{N+1} F_\tau(\zeta) u_2^{(\tau)}(\alpha_1, \alpha_2, t) \\
U_3(\alpha_1, \alpha_2, \zeta, t) &= \sum_{\tau=0}^{N+1} F_\tau(\zeta) u_3^{(\tau)}(\alpha_1, \alpha_2, t)
\end{aligned}
\tag{9}
$$

where U_1, U_2, U_3 are the three-dimensional displacements; F_τ represents the thickness or the shear functions and $\tau = 0, 1, 2, \ldots, N, N+1$ stands for the order of kinematic expansion; $u_1^{(\tau)}$, $u_2^{(\tau)}$, $u_3^{(\tau)}$ are the generalized displacement components or degrees of freedom of the problem. The thickness functions can be chosen freely or according to the functions listed in the book [99]. In this paper, the thickness functions are given by the power function $F_\tau = \zeta^\tau$ for $\tau = 0, 1, 2, \ldots, N$. The last order of expansion or the $(N+1)$-th order is related to the Murakami's function, by which the so-called zig-zag effect can be captured. More details about the zig-zag effect and the Murakami's function can be found in [96,97]. The Murakami's function $Z = Z(\zeta)$ is defined as

$$Z = (-1)^k \left(\frac{2}{\zeta_{k+1} - \zeta_k} \zeta - \frac{\zeta_{k+1} + \zeta_k}{\zeta_{k+1} - \zeta_k} \right) \tag{10}$$

where ζ_k and ζ_{k+1} represent, respectively, the bottom and the top coordinates of the k-th layer along the thickness direction, as shown in Figure 1. By varying the maximum order of kinematic expansion N, one can obtain different shear deformation theories. For easier denotation of these theories, the acronyms EDN and EDZN are introduced, where "E" stands for the ESL approach, "D" denotes the use of generalized displacement, and the letter "Z", if present, denotes the use of the Murakami's function.

Once the displacement field (9) is set, the generalized strains evaluated on the shell middle surface can be computed as follows

$$\boldsymbol{\varepsilon}^{(\tau)} = \mathbf{D}_\Omega \mathbf{u}^{(\tau)} \tag{11}$$

in which vector $\mathbf{u}^{(\tau)} = \mathbf{u}^{(\tau)}(\alpha_1, \alpha_2, t)$ collects generalized displacement components as

$$\mathbf{u}^{(\tau)} = \begin{bmatrix} u_1^{(\tau)} & u_2^{(\tau)} & u_3^{(\tau)} \end{bmatrix}^T \tag{12}$$

Also, the kinematic operator $\mathbf{D}_\Omega$ takes the following form

$$
\mathbf{D}_\Omega = \begin{bmatrix}
\frac{1}{A_1} \frac{\partial}{\partial \alpha_1} & \frac{1}{A_1 A_2} \frac{\partial A_2}{\partial \alpha_1} & -\frac{1}{A_1 A_2} \frac{\partial A_1}{\partial \alpha_2} & \frac{1}{A_2} \frac{\partial}{\partial \alpha_2} & -\frac{1}{R_1} & 0 & 1 & 0 & 0 \\
\frac{1}{A_1 A_2} \frac{\partial A_1}{\partial \alpha_2} & \frac{1}{A_2} \frac{\partial}{\partial \alpha_2} & \frac{1}{A_1} \frac{\partial}{\partial \alpha_1} & -\frac{1}{A_1 A_2} \frac{\partial A_2}{\partial \alpha_1} & 0 & -\frac{1}{R_2} & 0 & 1 & 0 \\
\frac{1}{R_1} & \frac{1}{R_2} & 0 & 0 & \frac{1}{A_1} \frac{\partial}{\partial \alpha_1} & \frac{1}{A_2} \frac{\partial}{\partial \alpha_2} & 0 & 0 & 1
\end{bmatrix}^T
\tag{13}
$$

All of the strains are collected in the algebraic vector $\varepsilon^{(\tau)} = \varepsilon^{(\tau)}(\alpha_1, \alpha_2, t)$, defined as

$$\varepsilon^{(\tau)} = \begin{bmatrix} \varepsilon_1^{(\tau)} & \varepsilon_2^{(\tau)} & \gamma_1^{(\tau)} & \gamma_2^{(\tau)} & \gamma_{13}^{(\tau)} & \gamma_{23}^{(\tau)} & \omega_{13}^{(\tau)} & \omega_{23}^{(\tau)} & \varepsilon_3^{(\tau)} \end{bmatrix}^T \tag{14}$$

The relation between three-dimensional strain components collected in $\varepsilon = \varepsilon(\alpha_1, \alpha_2, \zeta, t)$ and generalized strains (14) can be expressed as follows

$$\varepsilon = \sum_{\tau=0}^{N+1} \mathbf{Z}^{(\tau)} \varepsilon^{(\tau)} \tag{15}$$

where ε is described as

$$\varepsilon = \begin{bmatrix} \varepsilon_1 & \varepsilon_2 & \gamma_{12} & \gamma_{1n} & \gamma_{2n} & \varepsilon_n \end{bmatrix}^T \tag{16}$$

It should be specified that the subscript n in (16) denotes those strain components that involve the direction perpendicular to the shell middle surface. The matrix $\mathbf{Z}^{(\tau)}$ is described, for each order of kinematic expansion τ, as follows

$$\mathbf{Z}^{(\tau)} = \begin{bmatrix} \frac{F_\tau}{H_1} & 0 & 0 & 0 & 0 & 0 & 0 & 0 & 0 \\ 0 & \frac{F_\tau}{H_2} & 0 & 0 & 0 & 0 & 0 & 0 & 0 \\ 0 & 0 & \frac{F_\tau}{H_1} & \frac{F_\tau}{H_2} & 0 & 0 & 0 & 0 & 0 \\ 0 & 0 & 0 & 0 & \frac{F_\tau}{H_1} & 0 & \frac{\partial F_\tau}{\partial \zeta} & 0 & 0 \\ 0 & 0 & 0 & 0 & 0 & \frac{F_\tau}{H_2} & 0 & \frac{\partial F_\tau}{\partial \zeta} & 0 \\ 0 & 0 & 0 & 0 & 0 & 0 & 0 & 0 & \frac{\partial F_\tau}{\partial \zeta} \end{bmatrix} \tag{17}$$

The stress results for each order τ of kinematic expansion can be calculated over the generalized strains (11) as

$$\mathbf{S}^{(\tau)} = \sum_{\eta=0}^{N+1} \mathbf{A}^{(\tau\eta)} \varepsilon^{(\eta)} \tag{18}$$

where the algebraic vector $\mathbf{S}^{(\tau)} = \mathbf{S}^{(\tau)}(\alpha_1, \alpha_2, t)$ is taken as

$$\mathbf{S}^{(\tau)} = \begin{bmatrix} N_1^{(\tau)} & N_2^{(\tau)} & N_{12}^{(\tau)} & N_{21}^{(\tau)} & T_1^{(\tau)} & T_2^{(\tau)} & P_1^{(\tau)} & P_2^{(\tau)} & S_3^{(\tau)} \end{bmatrix}^T \tag{19}$$

The constitutive operator $\mathbf{A}^{(\tau\eta)}$ is defined as follows

$$\mathbf{A}^{(\tau\eta)} = \begin{bmatrix} A_{11(20)}^{(\tau\eta)} & A_{12(11)}^{(\tau\eta)} & A_{16(20)}^{(\tau\eta)} & A_{16(11)}^{(\tau\eta)} & 0 & 0 & 0 & 0 & A_{13(10)}^{(\tau\tilde{\eta})} \\ A_{12(11)}^{(\tau\eta)} & A_{22(02)}^{(\tau\eta)} & A_{26(11)}^{(\tau\eta)} & A_{26(02)}^{(\tau\eta)} & 0 & 0 & 0 & 0 & A_{23(01)}^{(\tau\tilde{\eta})} \\ A_{16(20)}^{(\tau\eta)} & A_{26(11)}^{(\tau\eta)} & A_{66(20)}^{(\tau\eta)} & A_{66(11)}^{(\tau\eta)} & 0 & 0 & 0 & 0 & A_{36(10)}^{(\tau\tilde{\eta})} \\ A_{16(11)}^{(\tau\eta)} & A_{26(02)}^{(\tau\eta)} & A_{66(11)}^{(\tau\eta)} & A_{66(02)}^{(\tau\eta)} & 0 & 0 & 0 & 0 & A_{36(01)}^{(\tau\tilde{\eta})} \\ 0 & 0 & 0 & 0 & A_{44(20)}^{(\tau\eta)} & A_{45(11)}^{(\tau\eta)} & A_{44(10)}^{(\tau\tilde{\eta})} & A_{45(10)}^{(\tau\tilde{\eta})} & 0 \\ 0 & 0 & 0 & 0 & A_{45(11)}^{(\tau\eta)} & A_{55(02)}^{(\tau\eta)} & A_{45(01)}^{(\tau\tilde{\eta})} & A_{55(01)}^{(\tau\tilde{\eta})} & 0 \\ 0 & 0 & 0 & 0 & A_{44(10)}^{(\tilde{\tau}\eta)} & A_{45(01)}^{(\tilde{\tau}\eta)} & A_{44(00)}^{(\tilde{\tau}\tilde{\eta})} & A_{45(00)}^{(\tilde{\tau}\tilde{\eta})} & 0 \\ 0 & 0 & 0 & 0 & A_{45(10)}^{(\tilde{\tau}\eta)} & A_{55(01)}^{(\tilde{\tau}\eta)} & A_{45(00)}^{(\tilde{\tau}\tilde{\eta})} & A_{55(00)}^{(\tilde{\tau}\tilde{\eta})} & 0 \\ A_{13(10)}^{(\tilde{\tau}\eta)} & A_{23(01)}^{(\tilde{\tau}\eta)} & A_{36(10)}^{(\tilde{\tau}\eta)} & A_{36(01)}^{(\tilde{\tau}\eta)} & 0 & 0 & 0 & 0 & A_{33(00)}^{(\tilde{\tau}\tilde{\eta})} \end{bmatrix} \tag{20}$$

where the elastic constant in (20) can be evaluated according to the following expressions

$$A^{(\tau\eta)}_{nm\,(pq)} = \sum_{k=1}^{l} \int_{\zeta_k}^{\zeta_{k+1}} \overline{B}^{(k)}_{nm} F_\eta F_\tau \frac{H_1 H_2}{H_1^p H_2^q} d\zeta$$

$$A^{(\tilde{\tau}\eta)}_{nm\,(pq)} = \sum_{k=1}^{l} \int_{\zeta_k}^{\zeta_{k+1}} \overline{B}^{(k)}_{nm} F_\eta \frac{\partial F_\tau}{\partial \zeta} \frac{H_1 H_2}{H_1^p H_2^q} d\zeta$$

$$A^{(\tau\tilde{\eta})}_{nm\,(pq)} = \sum_{k=1}^{l} \int_{\zeta_k}^{\zeta_{k+1}} \overline{B}^{(k)}_{nm} \frac{\partial F_\eta}{\partial \zeta} F_\tau \frac{H_1 H_2}{H_1^p H_2^q} d\zeta$$

$$A^{(\tilde{\tau}\tilde{\eta})}_{nm\,(pq)} = \sum_{k=1}^{l} \int_{\zeta_k}^{\zeta_{k+1}} \overline{B}^{(k)}_{nm} \frac{\partial F_\eta}{\partial \zeta} \frac{\partial F_\tau}{\partial \zeta} \frac{H_1 H_2}{H_1^p H_2^q} d\zeta$$

(21)

for $\tau, \eta = 0, 1, 2, \dots, N, N+1$, $n, m = 1, 2, 3, 4, 5, 6$, and $p, q = 0, 1, 2$. The superscripts η, τ on the left-hand side of (21) denote the use of the corresponding thickness functions F_η, F_τ, where the tilde denotes that the derivative of the corresponding thickness function with respect to ζ has been used. Due to the dependence of all the quantities F_η, F_τ, H_1, H_2 in (21) on the thickness coordinate ζ, the numerical method must be introduced to solve the problem. The notation $\overline{B}^{(k)}_{nm}$ is related to the elastic constants of the material $\overline{C}^{(k)}_{nm}$ as follows

$$\overline{B}^{(k)}_{nm} = \overline{C}^{(k)}_{nm} \quad \text{for} \quad n, m = 1, 2, 3, 6$$
$$\overline{B}^{(k)}_{nm} = \kappa \overline{C}^{(k)}_{nm} \quad \text{for} \quad n, m = 4, 5$$

(22)

where κ is the shear correction factor, the value of which will be specified in the notation representative of the structural model through a proper superscript. This model assumes that each layer of the laminated composite is made of linearly elastic and homogenous materials. The plies are perfectly joined together, and both orthotropic and isotropic mediums can be taken into account. It should be recalled that the elastic constants $\overline{C}^{(k)}_{nm}$ are evaluated in the geometric reference system $O'\alpha_1\alpha_2\zeta$ through proper transformations that take into account the orientation of the material [46,99]. If the k-th layer is orthotropic, the stress-strain relation is given as

$$
\begin{bmatrix}
\sigma_1^{(k)} \\
\sigma_2^{(k)} \\
\tau_{12}^{(k)} \\
\tau_{1n}^{(k)} \\
\tau_{2n}^{(k)} \\
\sigma_n^{(k)}
\end{bmatrix}
=
\begin{bmatrix}
\overline{C}_{11}^{(k)} & \overline{C}_{12}^{(k)} & \overline{C}_{16}^{(k)} & 0 & 0 & \overline{C}_{13}^{(k)} \\
\overline{C}_{12}^{(k)} & \overline{C}_{22}^{(k)} & \overline{C}_{26}^{(k)} & 0 & 0 & \overline{C}_{23}^{(k)} \\
\overline{C}_{16}^{(k)} & \overline{C}_{26}^{(k)} & \overline{C}_{66}^{(k)} & 0 & 0 & \overline{C}_{36}^{(k)} \\
0 & 0 & 0 & \overline{C}_{44}^{(k)} & \overline{C}_{45}^{(k)} & 0 \\
0 & 0 & 0 & \overline{C}_{45}^{(k)} & \overline{C}_{55}^{(k)} & 0 \\
\overline{C}_{13}^{(k)} & \overline{C}_{23}^{(k)} & \overline{C}_{36}^{(k)} & 0 & 0 & \overline{C}_{33}^{(k)}
\end{bmatrix}
\begin{bmatrix}
\varepsilon_1^{(k)} \\
\varepsilon_2^{(k)} \\
\gamma_{12}^{(k)} \\
\gamma_{1n}^{(k)} \\
\gamma_{2n}^{(k)} \\
\varepsilon_n^{(k)}
\end{bmatrix}
$$

(23)

in which the elastic constants $\overline{C}^{(k)}_{nm}$ can be related to the nine independent engineering constants of the material—$E_1^{(k)}, E_2^{(k)}, E_3^{(k)}, G_{12}^{(k)}, G_{13}^{(k)}, G_{23}^{(k)}, \nu_{12}^{(k)}, \nu_{13}^{(k)}, \nu_{23}^{(k)}$—as specified in the book by Tornabene et al. [99]. It should be recalled that the hypothesis of plane stress is needed in lower-order theories, such as the Reissner-Mindlin theory or First-order Shear Deformation Theory (FSDT). When needed, the reduced elastic coefficients $\overline{Q}^{(k)}_{nm}$ are used. The meaning of these coefficients is explained in detail in [99].

On the other hand, the elastic foundation, studied in this paper, is approximated by applying uniformly distributed springs at the top and/or bottom surfaces of the shell (Figure 2). The stiffnesses

of the springs are denoted by $k_{1f}^{(\pm)}$, $k_{2f}^{(\pm)}$, and $k_{3f}^{(\pm)}$ along the three coordinate directions α_1, α_2, and ζ, respectively. Superscripts $(+)$ or $(-)$ denote that these springs are located on the top or the bottom surface of the shell, respectively. The elastic foundation is modeled according to the Winkler-Pasternak elastic foundation theory. In this paper, only the elastic foundations with the uniform thickness $h_f^{(\pm)}$ are considered. Further information about this theory can be found in the papers [126–128,135] and in the book [99]. Forces produced by the springs along the three coordinate directions can be written in the form of generalized external load vector of the foundation $\mathbf{q}_f^{(\tau)}$ as

$$\mathbf{q}_f^{(\tau)} = -\sum_{\eta=0}^{N+1} \mathbf{L}_f^{(\tau\eta)} \mathbf{u}^{(\eta)} - \sum_{\eta=0}^{N+1} \mathbf{M}_f^{(\tau\eta)} \ddot{\mathbf{u}}^{(\eta)} \tag{24}$$

for $\tau = 0, 1, 2, \ldots, N, N+1$, where the operators $\mathbf{L}_f^{(\tau\eta)}$ and $\mathbf{M}_f^{(\tau\eta)}$ are the stiffness matrix and inertia matrix, respectively, of the linear elastic foundation. Vector $\ddot{\mathbf{u}}^{(\tau)} = \ddot{\mathbf{u}}^{(\tau)}(\alpha_1, \alpha_2, t)$ collects the generalized acceleration components that correspond to the generalized displacements

$$\ddot{\mathbf{u}}^{(\tau)} = \begin{bmatrix} \ddot{u}_1^{(\tau)} & \ddot{u}_2^{(\tau)} & \ddot{u}_3^{(\tau)} \end{bmatrix}^T \tag{25}$$

The operator $\mathbf{L}_f^{(\tau\eta)}$ takes the following form

$$\mathbf{L}_f^{(\tau\eta)} = \begin{bmatrix} L_{f1}^{(\tau\eta)\alpha_1} & 0 & 0 \\ 0 & L_{f2}^{(\tau\eta)\alpha_2} & 0 \\ 0 & 0 & L_{f3}^{(\tau\eta)\alpha_3} \end{bmatrix} \tag{26}$$

with the quantities $L_{f1}^{(\tau\eta)\alpha_1}$, $L_{f2}^{(\tau\eta)\alpha_2}$, $L_{f3}^{(\tau\eta)\alpha_3}$ defined as follows

$$L_{f1}^{(\tau\eta)\alpha_1} = k_{1f}^{(-)} F_\eta^{\alpha_1(-)} F_\tau^{\alpha_1(-)} H_1^{(-)} H_2^{(-)} + k_{1f}^{(+)} F_\eta^{\alpha_1(+)} F_\tau^{\alpha_1(+)} H_1^{(+)} H_2^{(+)}$$

$$L_{f2}^{(\tau\eta)\alpha_2} = k_{2f}^{(-)} F_\eta^{\alpha_2(-)} F_\tau^{\alpha_2(-)} H_1^{(-)} H_2^{(-)} + k_{2f}^{(+)} F_\eta^{\alpha_2(+)} F_\tau^{\alpha_2(+)} H_1^{(+)} H_2^{(+)} \tag{27}$$

$$L_{f3}^{(\tau\eta)\alpha_3} = \left(k_{3f}^{(-)} - G_f^{(-)} \nabla_{(-)}^2\right) F_\eta^{\alpha_3(-)} F_\tau^{\alpha_3(-)} H_1^{(-)} H_2^{(-)} + \left(k_{3f}^{(+)} - G_f^{(+)} \nabla_{(+)}^2\right) F_\eta^{\alpha_3(+)} F_\tau^{\alpha_3(+)} H_1^{(+)} H_2^{(+)}$$

where $\nabla_{(\pm)}^2$ represents the Laplacian operator in curvilinear orthogonal coordinates applied at the top or the bottom surfaces of the shell defined below

$$\nabla_{(\pm)}^2 = \left(\frac{1}{A_1^2\left(H_1^{(\pm)}\right)^2}\frac{\partial^2}{\partial\alpha_1^2} + \frac{1}{A_2^2\left(H_2^{(\pm)}\right)^2}\frac{\partial^2}{\partial\alpha_2^2} + \left(\frac{1}{A_1^2 A_2\left(H_1^{(\pm)}\right)^2}\frac{\partial A_2}{\partial\alpha_1} - \frac{h}{2A_1^2 R_2^2\left(H_1^{(\pm)}\right)^2 H_2^{(\pm)}}\frac{\partial R_2}{\partial\alpha_1} + \right.$$

$$\left. - \frac{1}{A_1^3\left(H_1^{(\pm)}\right)^2}\frac{\partial A_1}{\partial\alpha_1} + \frac{h}{2A_1^2 R_1^2\left(H_1^{(\pm)}\right)^3}\frac{\partial R_1}{\partial\alpha_1}\right)\frac{\partial}{\partial\alpha_1} + \left(\frac{1}{A_1 A_2^2\left(H_2^{(\pm)}\right)^2}\frac{\partial A_1}{\partial\alpha_2} - \frac{h}{2A_2^2 R_1^2\left(H_2^{(\pm)}\right)^2 H_1^{(\pm)}}\frac{\partial R_1}{\partial\alpha_2} + \right. \tag{28}$$

$$\left. - \frac{1}{A_2^3\left(H_2^{(\pm)}\right)^2}\frac{\partial A_2}{\partial\alpha_2} + \frac{h}{2A_2^2 R_2^2\left(H_2^{(\pm)}\right)^3}\frac{\partial R_2}{\partial\alpha_2}\right)\frac{\partial}{\partial\alpha_2}\right)$$

where

$$H_1^{(\pm)} = 1 \pm \frac{h}{2R_1}, \qquad H_2^{(\pm)} = 1 + \frac{h}{2R_2} \tag{29}$$

The quantity $G_f^{(\pm)}$ is the shear modulus of the elastic foundation, according to the Pasternak model. On the other hand, the operator $\mathbf{M}_f^{(\tau\eta)}$ is defined as

$$\mathbf{M}_f^{(\tau\eta)} = \begin{bmatrix} I_{f1}^{(\tau\eta)\alpha_1} & 0 & 0 \\ 0 & I_{f2}^{(\tau\eta)\alpha_2} & 0 \\ 0 & 0 & I_{f3}^{(\tau\eta)\alpha_3} \end{bmatrix} \tag{30}$$

with the foundation inertial components $I_{f1}^{(\tau\eta)\alpha_1}$, $I_{f2}^{(\tau\eta)\alpha_2}$, $I_{f3}^{(\tau\eta)\alpha_3}$ defined as follows

$$
\begin{aligned}
I_{f1}^{(\tau\eta)\alpha_1} &= \tfrac{1}{3}\rho_f^{(-)}h_f^{(-)}F_\eta^{\alpha_1(-)}F_\tau^{\alpha_1(-)}H_1^{(-)}H_2^{(-)} + \tfrac{1}{3}\rho_f^{(+)}h_f^{(+)}F_\eta^{\alpha_1(+)}F_\tau^{\alpha_1(+)}H_1^{(+)}H_2^{(+)} \\
I_{f2}^{(\tau\eta)\alpha_2} &= \tfrac{1}{3}\rho_f^{(-)}h_f^{(-)}F_\eta^{\alpha_2(-)}F_\tau^{\alpha_2(-)}H_1^{(-)}H_2^{(-)} + \tfrac{1}{3}\rho_f^{(+)}h_f^{(+)}F_\eta^{\alpha_2(+)}F_\tau^{\alpha_2(+)}H_1^{(+)}H_2^{(+)} \\
I_{f3}^{(\tau\eta)\alpha_3} &= \tfrac{1}{3}\rho_f^{(-)}h_f^{(-)}F_\eta^{\alpha_3(-)}F_\tau^{\alpha_3(-)}H_1^{(-)}H_2^{(-)} + \tfrac{1}{3}\rho_f^{(+)}h_f^{(+)}F_\eta^{\alpha_3(+)}F_\tau^{\alpha_3(+)}H_1^{(+)}H_2^{(+)}
\end{aligned}
\tag{31}
$$

where $\rho_f^{(\pm)}$ is the density of the elastic foundation.

Finally, the equations of motion and the corresponding boundary conditions are deduced [99]. For each order τ of kinematic expansion, the three equations of motion can be written in matrix form as follows

$$\mathbf{D}_\Omega^* \mathbf{S}^{(\tau)} + \mathbf{q}_f^{(\tau)} = \sum_{\eta=0}^{N+1} \mathbf{M}^{(\tau\eta)} \ddot{\mathbf{u}}^{(\eta)} \tag{32}$$

in which $\mathbf{D}_\Omega^*$ represents the equilibrium differential operator defined as

$$\mathbf{D}_\Omega^* = \begin{bmatrix}
\frac{1}{A_1}\frac{\partial}{\partial\alpha_1} + \frac{1}{A_1 A_2}\frac{\partial A_2}{\partial\alpha_1} & -\frac{1}{A_1 A_2}\frac{\partial A_1}{\partial\alpha_2} & -\frac{1}{R_1} \\[2mm]
-\frac{1}{A_1 A_2}\frac{\partial A_2}{\partial\alpha_1} & \frac{1}{A_2}\frac{\partial}{\partial\alpha_2} + \frac{1}{A_1 A_2}\frac{\partial A_1}{\partial\alpha_2} & -\frac{1}{R_2} \\[2mm]
\frac{1}{A_1 A_2}\frac{\partial A_1}{\partial\alpha_2} & \frac{1}{A_1}\frac{\partial}{\partial\alpha_1} + \frac{1}{A_1 A_2}\frac{\partial A_2}{\partial\alpha_1} & 0 \\[2mm]
\frac{1}{A_2}\frac{\partial}{\partial\alpha_2} + \frac{1}{A_1 A_2}\frac{\partial A_1}{\partial\alpha_2} & \frac{1}{A_1 A_2}\frac{\partial A_2}{\partial\alpha_1} & 0 \\[2mm]
\frac{1}{R_1} & 0 & \frac{1}{A_1}\frac{\partial}{\partial\alpha_1} + \frac{1}{A_1 A_2}\frac{\partial A_2}{\partial\alpha_1} \\[2mm]
0 & \frac{1}{R_2} & \frac{1}{A_2}\frac{\partial}{\partial\alpha_2} + \frac{1}{A_1 A_2}\frac{\partial A_1}{\partial\alpha_2} \\[2mm]
-1 & 0 & 0 \\[2mm]
0 & -1 & 0 \\[2mm]
0 & 0 & -1
\end{bmatrix}^T \tag{33}$$

The inertia matrix $\mathbf{M}^{(\tau\eta)}$ is defined as follows, for $\tau, \eta = 0, 1, 2, \ldots, N, N+1$

$$\mathbf{M}^{(\tau\eta)} = \begin{bmatrix} I^{(\tau\eta)} & 0 & 0 \\ 0 & I^{(\tau\eta)} & 0 \\ 0 & 0 & I^{(\tau\eta)} \end{bmatrix} \tag{34}$$

where the inertia terms $I^{(\tau\eta)}$ are evaluated for $\tau, \eta = 0, 1, 2, \ldots, N, N+1$ once the mass density $\rho^{(k)}$ of the k-th layer is introduced

$$I^{(\tau\eta)} = \sum_{k=1}^{l} \int_{\zeta_k}^{\zeta_{k+1}} \rho^{(k)} F_\tau F_\eta H_1 H_2 d\zeta \tag{35}$$

All the results are summarized in the fundamental system of equations with the size of $3 \times (N+2)$ equilibrium equations, in which, for each order $\tau = 0, 1, 2, \ldots, N, N+1$ of kinematic expansion, the compact form is written as follows

$$\sum_{\eta=0}^{N+1} \left(\mathbf{L}^{(\tau\eta)} - \mathbf{L}_f^{(\tau\eta)} \right) \mathbf{u}^{(\eta)} = \sum_{\eta=0}^{N+1} \left(\mathbf{M}^{(\tau\eta)} + \mathbf{M}_f^{(\tau\eta)} \right) \ddot{\mathbf{u}}^{(\eta)} \tag{36}$$

where the fundamental operator $\mathbf{L}^{(\tau\eta)} = \mathbf{D}_\Omega^* \mathbf{A}^{(\tau\eta)} \mathbf{D}_\Omega$ is a 3×3 matrix defined as shown below

$$\mathbf{L}^{(\tau\eta)} = \begin{bmatrix} L_{11}^{(\tau\eta)} & L_{12}^{(\tau\eta)} & L_{13}^{(\tau\eta)} \\ L_{21}^{(\tau\eta)} & L_{22}^{(\tau\eta)} & L_{23}^{(\tau\eta)} \\ L_{31}^{(\tau\eta)} & L_{32}^{(\tau\eta)} & L_{33}^{(\tau\eta)} \end{bmatrix} \tag{37}$$

The explicit definitions of the term $L_{fg}^{(\tau\eta)}$, for $f, g = 1, 2, 3$ can be found in the book by Tornabene et al. [99]. To solve the elastic problem at hand, the proper boundary conditions must be enforced for each order of kinematic expansion $\tau = 0, 1, 2, \ldots, N, N+1$. In this work, only the restrains of the whole edge are considered as completely clamped (C), simply-supported (S) or free (F). If the edge is identified by $\alpha_1 = \alpha_1^0$ or $\alpha_1 = \alpha_1^1$, for $\alpha_2^0 \leq \alpha_2 \leq \alpha_2^1$, one gets:

$$\begin{aligned} \text{C} \quad &\to \quad u_1^{(\tau)} = u_2^{(\tau)} = u_3^{(\tau)} = 0 \\ \text{S} \quad &\to \quad N_1^{(\tau)} = 0, \ \ u_2^{(\tau)} = u_3^{(\tau)} = 0 \\ \text{F} \quad &\to \quad N_1^{(\tau)} = N_{12}^{(\tau)} = T_1^{(\tau)} = 0 \end{aligned} \tag{38}$$

On the other hand, if the edge is characterized by $\alpha_2 = \alpha_2^0$ or $\alpha_2 = \alpha_2^1$, for $\alpha_1^0 \leq \alpha_1 \leq \alpha_1^1$, the following conditions are obtained

$$\begin{aligned} \text{C} \quad &\to \quad u_1^{(\tau)} = u_2^{(\tau)} = u_3^{(\tau)} = 0 \\ \text{S} \quad &\to \quad N_2^{(\tau)} = 0, \ \ u_1^{(\tau)} = u_3^{(\tau)} = 0 \\ \text{F} \quad &\to \quad N_{21}^{(\tau)} = N_2^{(\tau)} = T_2^{(\tau)} = 0 \end{aligned} \tag{39}$$

To generalize the boundary conditions applied, the notation XXXX is introduced, where X is replaced either with C (clamped), S (simply-supported) or F (free). The edges are referred in the sequence WSEN, where each edge is denoted by the following coordinates

$$\begin{aligned} \text{West edge (W)} \quad &\to \quad \alpha_1^0 \leq \alpha_1 \leq \alpha_1^1, \ \alpha_2 = \alpha_2^0 \\ \text{South edge (S)} \quad &\to \quad \alpha_1 = \alpha_1^1, \ \alpha_2^0 \leq \alpha_2 \leq \alpha_2^1 \\ \text{East edge (E)} \quad &\to \quad \alpha_1^0 \leq \alpha_1 \leq \alpha_1^1, \ \alpha_2 = \alpha_2^1 \\ \text{North edge (N)} \quad &\to \quad \alpha_1 = \alpha_1^0, \ \alpha_2^0 \leq \alpha_2 \leq \alpha_2^1 \end{aligned} \tag{40}$$

So, the boundary conditions noted as CCFF mean that the West and the South edges are clamped and the last two edges are free.
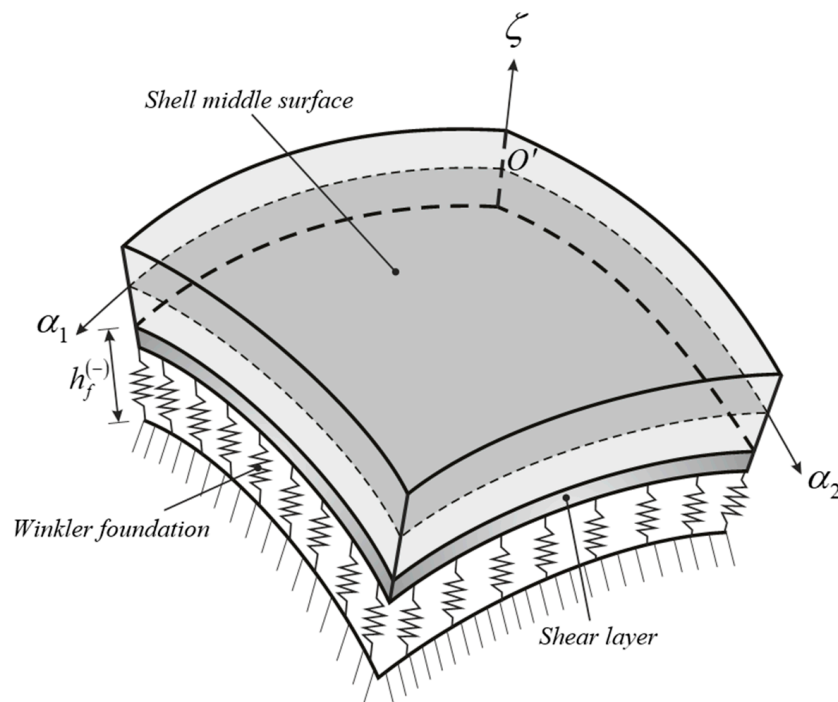
Figure 2. Doubly-curved panel representation and description.

2.3. Functionally Graded Carbon Nanotube Reinforced Composite Structures

The characteristic shape of CNTs is one of the main factors that causes the agglomeration of these particles when scattered in a polymer matrix [24–27,32]. Thus, in some regions of the Carbon Nanotube-reinforced ply, the concentration of CNTs is higher than the average volume fraction in the ply itself. According to the micromechanical model presented by Shi et al. [32], these areas can be assumed to be spherically shaped inclusions with different elastic properties from the surrounding matrix, as depicted in Figure 3a. Therefore, CNTs are contained both in the matrix and in the spherical inclusions. The overall volume of the lamina W is given by the following relation

$$W = W_r + W_m \tag{41}$$

in which W_m is the volume of the matrix. W_r denotes the volume of CNTs embedded in the lamina, which can be further separated as

$$W_r = W_r^{in} + W_r^{m} \tag{42}$$

where W_r^{in} and W_r^{m} indicate the volume of CNTs scattered in the inclusions and in the matrix, respectively. The mass fraction of CNTs, w_r, and of the matrix, w_m, can be expressed by the theory of mixture as

$$w_r = \frac{M_r}{M_r + M_m}, \quad w_m = \frac{M_m}{M_r + M_m} \tag{43}$$

Analogously, the volume fraction can be expressed as

$$V_r = \frac{W_r}{W}, \quad V_m = \frac{W_m}{W} \tag{44}$$

In which the relation $V_r + V_m = 1$ must hold. In this paper, Functionally Graded Carbon Nanotube (FG-CNT)-reinforced composite is considered. This term specifies a structure with the reinforcing

phase made of CNTs, which has a gradual distribution along the thickness direction. Further on, if the FG-CNT-reinforced composite is to be considered, the volume fraction of CNTs V_r can be characterized by a continuous gradual variation from the bottom to the top surface of the lamina assuming

$$V_r(\zeta) = V_r^* V_C(\zeta) \tag{45}$$

where V_r^* is the CNT volume fraction value and $V_C(\zeta)$ is through-the-thickness distribution. Depending on the CNT mass fraction w_r and on the density of both CNT ρ_r and the matrix ρ_m, CNT volume fraction value V_r^* is given as

$$V_r^* = \left(\frac{\rho_r}{w_r \rho_m} - \frac{\rho_r}{\rho_m} + 1\right)^{-1} \tag{46}$$

On the other hand, the function $V_C(\zeta)$ introduced in (45) can be defined by various distributions as described in [75,83]. The superscript k will be introduced in the following to specify that the through-the-thickness distribution $V_C(\zeta)$ should be defined for each layer, when laminated configurations are analyzed. In other words, the quantity at hand will be indicated as $V_C^{(k)}(\zeta)$. In this paper, the five-parameter exponential law (5P), two-parameter exponential (2P-E) and two-parameter Weibull (2P-W) functions are considered. To describe through the thickness CNTs distribution the following notation has been used

$$FG - CNT_{\text{bottom(distribution)}(a^{(k)}/b^{(k)}/...)}^{\text{top}} \tag{47}$$

where superscript "top" indicates the material on the upper surface of the lamina, while the subscript "bottom" indicates the material on the lower surface of the lamina. The subscript "(distribution)" designates instead the through-the-thickness distribution used to describe the volume fraction $V_C^{(k)}(\zeta)$ as (5P), (2P-E) or (2P-W), if the distribution is, five parameter exponential law, two parameter exponential function or two parameter Weibull function, respectively. Finally, the expression "$(a^{(k)}/b^{(k)}/\ldots)$" specifies the parameters that describe these distributions and control the volume fraction profile along the thickness h_k of the k-th lamina. Depending on the material used on the top or bottom surfaces of the lamina, different expressions have to be used for all of the stated distributions. In particular, if the top material is CNTs and the bottom material is polymer matrix (PM), the through-the-thickness distributions $V_C^{(k)}(\zeta)$ can be written as follows

Five-parameter exponential law $FG - CNT_{PM(5P)(a^{(k)}/b^{(k)}/c^{(k)}/d^{(k)}/p^{(k)})}^{\text{CNT}}$

$$V_C^{(k)}(\zeta) = \left(d^{(k)} - a^{(k)}\left(\frac{\zeta_{k+1} - \zeta}{h_k}\right) + b^{(k)}\left(\frac{\zeta_{k+1} - \zeta}{h_k}\right)^{c^{(k)}}\right)^{p^{(k)}} \tag{48}$$

Two-parameter exponential function $FG - CNT_{PM(2P-E)(a^{(k)}/b^{(k)})}^{\text{CNT}}$

$$V_C^{(k)}(\zeta) = \left(\frac{\exp\left(a^{(k)}\left(\frac{\zeta - \zeta_k - h_k/2}{h_k} + \frac{1}{2}\right)\right) - 1}{\left(\exp\left(\frac{a^{(k)}}{2}\right) - 1\right)\left(\exp\left(a^{(k)}\frac{\zeta - \zeta_k - h_k/2}{h_k}\right) + 1\right)}\right)^{b^{(k)}} \tag{49}$$

Weibull function $FG - CNT_{PM(2P-W)(a^{(k)}/b^{(k)})}^{\text{CNT}}$

$$V_C^{(k)}(\zeta) = 1 - \exp\left(-\left(\frac{1}{a^{(k)}}\frac{\zeta - \zeta_k}{h_k}\right)^{b^{(k)}}\right) \tag{50}$$

Moreover, if top and bottom materials are reversed, the following distributions apply

Five-parameter exponential law $FG - CNT_{CNT(5P)(a^{(k)}/b^{(k)}/c^{(k)}/d^{(k)}/p^{(k)})}^{PM}$

$$
V_C^{(k)}(\zeta) = \left(d^{(k)} - a^{(k)} \left(\frac{\zeta - \zeta_k}{h_k} \right) + b^{(k)} \left(\frac{\zeta - \zeta_k}{h_k} \right)^{c^{(k)}} \right)^{p^{(k)}}
\tag{51}
$$

Two-parameter exponential function $FG - CNT_{CNT(2P-E)(a^{(k)}/b^{(k)})}^{PM}$

$$
V_C^{(k)}(\zeta) = 1 - \left(\frac{\exp\left(a^{(k)} \left(\frac{\zeta - \zeta_k - h_k/2}{h_k} + \frac{1}{2} \right) \right) - 1}{\left(\exp\left(\frac{a^{(k)}}{2} \right) - 1 \right) \left(\exp\left(a^{(k)} \frac{\zeta - \zeta_k - h_k/2}{h_k} \right) + 1 \right)} \right)^{b^{(k)}}
\tag{52}
$$

Weibull function $FG - CNT_{CNT(2P-W)(a^{(k)}/b^{(k)})}^{PM}$

$$
V_C^{(k)}(\zeta) = \exp\left(-\left(\frac{1}{a^{(k)}} \frac{\zeta - \zeta_k}{h_k} \right)^{b^{(k)}} \right)
\tag{53}
$$

Further on, the total volume of the reinforcing phase V_r is separated as follows

$$
V_r = V_r^{in} + V_r^m
\tag{54}
$$

where V_r^{in} is the volume of CNTs in the inclusions and V_r^m is the volume of the nanoparticles scattered in the matrix. Two parameters that characterize the agglomeration of CNTs have to be introduced

$$
\mu_1 = \frac{W_{in}}{W}, \quad \mu_2 = \frac{W_r^{in}}{W_r}
\tag{55}
$$

The parameter μ_1 specifies the effective volume of the inclusions W_{in} with respect to the overall volume of the layer W. Therefore, if $\mu_1 = 1$, there is no agglomeration, and the CNTs are uniformly scattered in the polymer matrix. The second parameter μ_2 defines the portion of CNT volume embedded in the inclusions W_r^{in} with respect to the total volume of CNTs W_r. Therefore, if $\mu_2 = 1$, all the nanoparticles are allocated in the spherical inclusions. To obtain the intermediate cases between the two limit cases, the following limitation must be introduced

$$
\mu_2 \geq \mu_1
\tag{56}
$$

It should be specified that it is possible to increase the CNT spatial heterogeneity for a generic value of $\mu_1 < 1$ if higher values of μ_2 are taken, meeting the requirement defined in (56). By the use of the relations (44), (54) and (55), the following relations that correlate the agglomeration parameters can be obtained

$$
\begin{aligned}
\frac{W_r^{in}}{W_{in}} &= \frac{V_r \mu_2}{\mu_1} \\
\frac{W_r^m}{W - W_{in}} &= \frac{V_r (1 - \mu_2)}{1 - \mu_1}
\end{aligned}
\tag{57}
$$

for $\mu_2 > \mu_1$. After defining the micromechanics of the particle agglomeration, next step is to define properties of the CNT-reinforced composite layer. In order to do so, the mechanical properties of the polymer matrix and the hybrid inclusions have to be evaluated. For this purpose, in this paper, the Eshelby-Mori-Tanaka approach is considered. Readers can find more information about other methods in the work by Shi et al. [32]. This method assumes that CNTs are randomly oriented in the

inclusions, and are made of a transversely isotropic material. The bulk modulus K_{in} and the shear modulus G_{in} of the spherical inclusions are given by

$$K_{in}(\zeta) = K_m + \frac{V_r \mu_2 (\delta_r - 3K_m \alpha_r)}{3(\mu_1 - V_r \mu_2 + V_r \mu_2 \alpha_r)}$$

$$G_{in}(\zeta) = G_m + \frac{V_r \mu_2 (\eta_r - 2G_m \beta_r)}{2(\mu_1 - V_r \mu_2 + V_r \mu_2 \beta_r)}$$

(58)

The same moduli for the hybrid matrix are given by

$$K_{out}(\zeta) = K_m + \frac{V_r (1 - \mu_2)(\delta_r - 3K_m \alpha_r)}{3(1 - \mu_1 - V_r (1 - \mu_2) + V_r (1 - \mu_2) \alpha_r)}$$

$$G_{out}(\zeta) = G_m + \frac{V_r (1 - \mu_2)(\eta_r - 2G_m \beta_r)}{2(1 - \mu_1 - V_r (1 - \mu_2) + V_r (1 - \mu_2) \beta_r)}$$

(59)

where K_m and G_m denote the bulk modulus and the shear modulus of the isotropic matrix. It should be mentioned that the subscripts "*in*" and "*out*" are associated with the mechanical properties of the inclusions and of the matrix enriched with scattered CNTs, respectively. From the theory of elasticity, it is known that

$$K_m = \frac{E_m}{3(1 - 2\nu_m)}, \quad G_m = \frac{E_m}{2(1 + \nu_m)}$$

(60)

where E_m is the elastic modulus and ν_m the Poisson's ratio. The rest of the unknown quantities from (58) and (59) are defined as

$$\alpha_r = \frac{3(K_m + G_m) + k_r + l_r}{3(G_m + k_r)}$$

$$\beta_r = \frac{1}{5}\left(\frac{4G_m + 2k_r + l_r}{3(G_m + k_r)} + \frac{4G_m}{G_m + p_r} + \frac{2(G_m(3K_m + G_m) + G_m(3K_m + 7G_m))}{G_m(3K_m + G_m) + m_r(3K_m + 7G_m)}\right)$$

$$\delta_r = \frac{1}{3}\left(n_r + 2l_r + \frac{(2k_r + l_r)(3K_m + G_m - l_r)}{G_m + k_r}\right)$$

$$\eta_r = \frac{1}{5}\left(\frac{2}{3}(n_r - l_r) + \frac{8G_m p_r}{G_m + p_r} + \frac{2(k_r - l_r)(2G_m + l_r)}{3(G_m + k_r)} + \frac{8m_r G_m(3K_m + 4G_m)}{3K_m(m_r + G_m) + G_m(7m_r + G_m)}\right)$$

(61)

where k_r, l_r, m_r, n_r, p_r are the Hill's elastic moduli of the nanoparticles. The reader can find further descriptions of these quantities in [27]. In brief, the mechanical characterization of a single CNT is given by the so-called Hill's elastic moduli, since it is assumed to be an equivalent continuum cylindrical shell, as shown in Figure 3b [7]. Values for these quantities are given for different Single-Walled Carbon Nanotubes (SWCNTs) for various chiral indices that can be found in literature. In this paper, only armchair-type SWCNTs are considered, as shown in Table 1 with the notation SWCNT(Δ, Δ), where Δ stands for the chiral index. After obtaining values from (58) and (59), the Mori-Tanaka method gives the effective bulk and shear modulus of the CNT-reinforced layer as

$$K(\zeta) = K_{out}\left(1 + \frac{\mu\left(\frac{K_{in}}{K_{out}} - 1\right)}{1 + (1 - \mu)\left(\frac{K_{in}}{K_{out}} - 1\right)\frac{1 + \nu_{out}}{3 - 3\nu_{out}}}\right)$$

$$G(\zeta) = G_{out}\left(1 + \frac{\mu\left(\frac{G_{in}}{G_{out}} - 1\right)}{1 + (1 - \mu)\left(\frac{G_{in}}{G_{out}} - 1\right)\frac{8 - 10\nu_{out}}{15 - 15\nu_{out}}}\right)$$

(62)

where ν_{out} is the Poisson's ratio of the hybrid matrix defined as

$$\nu_{out}(\zeta) = \frac{3K_{out} - 2G_{out}}{6K_{out} + 2G_{out}}$$

(63)

The resulting reinforced layer, as specified in the works [24], is isotropic. Therefore, the Young modulus $E(\zeta)$ and the Poisson's ratio $\nu(\zeta)$ are evaluated through the following expressions

$$E(\zeta) = \frac{9KG}{3K + G}, \quad \nu(\zeta) = \frac{3K - 2G}{6K + 2G} \tag{64}$$

At the end, density $\rho(\zeta)$ of the reinforced layer is evaluated by Mixture theory as

$$\rho(\zeta) = (\rho_r - \rho_m)V_r + \rho_m \tag{65}$$

where ρ_r is the density of the CNTs and ρ_m density of the polymer matrix. Further details concerning the present approach are illustrated in depth in the works by Tornabene et al. [24–27].
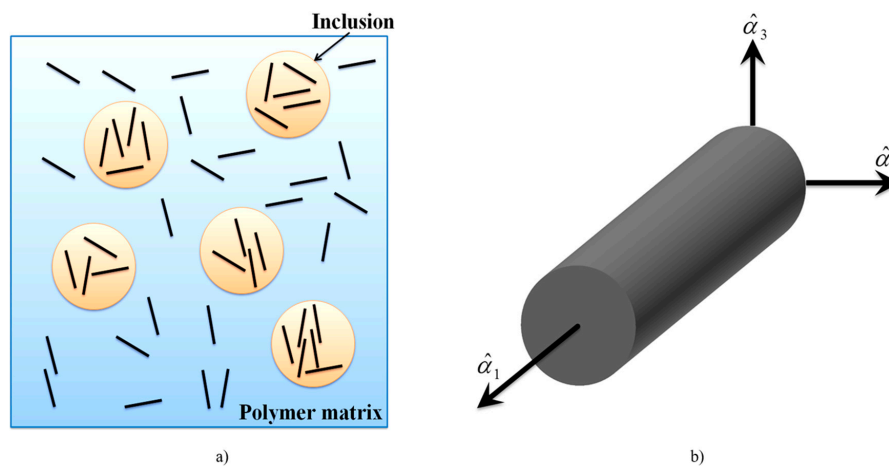
Figure 3. CNT reinforced composite layer: (**a**) shell element with inclusion model of CNT agglomeration; (**b**) effective CNT fiber and local co-ordinate system representation.

Table 1. Hill's elastic moduli for several Single-Walled Carbon Nanotubes.

Carbon Nanotubes	k_r [GPa]	l_r [GPa]	m_r [GPa]	n_r [GPa]	p_r [GPa]	Refs.
SWCNT (5,5)	536	184	132	2143	791	[9,12]
SWCNT (6,6)	9.9	8.4	4.4	457.6	27	[8]
SWCNT (10,10)	271	88	17	1089	442	[9]
SWCNT (15,15)	181	58	5	726	301	[9]
SWCNT (20,20)	136	43	2	545	227	[9,12]
SWCNT (50,50)	55	17	0.1	218	92	[9,12]

3. Numerical Scheme

After the fundamental system of Equation (36), along with the proper boundary conditions of (38)–(40), is set, a numerical scheme has to be implemented in order to obtain the solution. In this paper, the fundamental system of equations is solved by the Generalized Differential Quadrature (GDQ) method. Although, only fundamental aspects of this techniques are presented in the current paper, the reader can find further information about this method in [137]. Using this approach, the n-th derivative at a generic point x_i of a sufficiently smooth one-dimensional function $f(x)$ is obtained as a weighted linear sum of the function values at some chosen grid points

$$\left. \frac{d^n f(x)}{dx^n} \right|_{x=x_i} \cong \sum_{j=1}^{I_N} \varsigma_{ij}^{(n)} f(x_j) \tag{66}$$

for $i = 1, 2, \ldots, I_N$, where quantities $\varsigma_{ij}^{(n)}$ represent the weighting coefficients of the sum. To obtain the solution, weighting coefficients $\varsigma_{ij}^{(n)}$ have to be evaluated at each grid point, as highlighted in the review paper by Tornabene et al. [137]. Additionally, if adequate solutions are to be acquired, proper grid distribution is needed. In this paper, Chebyshev-Gauss-Lobatto grid distribution has been chosen to discretize the domain under consideration. If Expression (66) is extended on a two-dimensional problem, the points of the shell middle surface are placed according to the following Expressions along the principal co-ordinates α_1, α_2

$$\alpha_{1i} = \left(1 - \cos\left(\frac{i-1}{I_N - 1}\pi \right) \right) \frac{(\alpha_1^1 - \alpha_1^0)}{2} + \alpha_1^0 \tag{67}$$

for $i = 1, 2, \ldots, I_N$ with $\alpha_1 \in \left[\alpha_1^0, \alpha_1^1 \right]$, and

$$\alpha_{2j} = \left(1 - \cos\left(\frac{j-1}{I_M - 1}\pi \right) \right) \frac{(\alpha_2^1 - \alpha_2^0)}{2} + \alpha_2^0 \tag{68}$$

for $j = 1, 2, \ldots, I_M$ with $\alpha_2 \in \left[\alpha_2^0, \alpha_2^1 \right]$, in which I_N, I_M are the total number of nodes along α_1, α_2, respectively. To solve the fundamental system of equations the separation of variables is to be used. The generalized displacements can be expressed as

$$\mathbf{u}^{(\tau)}(\alpha_1, \alpha_2, t) = \mathbf{U}^{(\tau)}(\alpha_1, \alpha_2)e^{i\omega t} \tag{69}$$

where $\mathbf{U}^{(\tau)} = \left[\begin{array}{ccc} U_1^{(\tau)}(\alpha_1, \alpha_2) & U_2^{(\tau)}(\alpha_1, \alpha_2) & U_3^{(\tau)}(\alpha_1, \alpha_2) \end{array} \right]^T$ denotes the mode shape vector, whose components are the amplitude of the modes at issue, whereas ω is the circular frequency of the system, which allows the natural frequency to be defined as $f = \omega/2\pi$. If Expression (69) and its second-order temporal derivative are substituted in (36), the fundamental system of Equation (36) becomes

$$\sum_{\eta=0}^{N+1} \left(\mathbf{L}^{(\tau\eta)} - \mathbf{L}_f^{(\tau\eta)} \right) \mathbf{U}^{(\eta)} + \omega^2 \sum_{\eta=0}^{N+1} \left(\mathbf{M}^{(\tau\eta)} + \mathbf{M}_f^{(\tau\eta)} \right) \mathbf{U}^{(\eta)} = \mathbf{0} \tag{70}$$

for $\tau = 0, 1, 2, \ldots, N, N+1$. Once the GDQ method is applied, the following discrete form of Equation (70) is obtained

$$\mathbf{K}\boldsymbol{\delta} = \omega^2 \mathbf{M}\boldsymbol{\delta} \tag{71}$$

in which $\mathbf{K}$ is the discrete global stiffness matrix, $\mathbf{M}$ is the discrete inertia matrix, $\boldsymbol{\delta}$ the discrete mode shape vector. It should be mentioned that $\mathbf{K}$, $\mathbf{M}$ include the effect of the elastic foundation, too.

Finally, the numerical problem can be simplified by isolating the components related to the boundary nodes (*b*) from the inner ones (*d*). Through the kinematic condensation of non-domain degrees of freedom, System (71) can be rewritten as

$$\left(\mathbf{K}_{dd} - \mathbf{K}_{db}(\mathbf{K}_{bb})^{-1}\mathbf{K}_{bd} \right) \boldsymbol{\delta}_d = \omega^2 \mathbf{M}_{dd}\boldsymbol{\delta}_d \tag{72}$$

According to this approach, numerical instabilities and ill-conditioned matrices can be avoided. It is well known that Expression (72) represents a set of linear eigenvalue problem that allow the solution of the dynamic problem under consideration to be obtained in terms of natural frequencies.

4. Applications

In the current Section, a few applications are presented regarding the free vibration problem of laminated doubly-curved shells and plates reinforced by Carbon Nanotubes resting on elastic foundations. All of the results were obtained by MATLAB code [141]. This Section is subdivided into four Subsections. Due to a lack of papers regarding this subject, in the first Subsection, a comparison

with the FEM solution is provided. All the remaining Subsections deal with the parametric studies for free vibration presented as follows. The first parametric studies aim to present the effect of CNT volume fraction distribution, the second ones show the effect of the elastic foundation, and the last ones show the effect of CNT agglomeration parameters. In all the following applications, a Single-Walled Carbon Nanotube (SWCNT) with chiral index $\Delta = 10$ is assumed, for which values can be found in Table 1; the density of the CNTs is taken to be $\rho_r = 1400$ kg/m^3. Additionally, the matrix material has the same values in all applications: $E_m = 2.1$ GPa, $\rho_m = 1150$ kg/m^3 and $\nu_m = 0.34$. Figure 4 depicts the structures that have been considered (square plate (Figure 4a), cylindrical surface (Figure 4b) and helicoidal surface (Figure 4c)) along with the geometric parameters and position vectors $\mathbf{r}(\alpha_1, \alpha_2)$ needed for the description of the reference surfaces of such structures. In all the applications, FG-CNT material was used, the parameters and lamination schemes of which are depicted in Figure 5.

(a) Rectangular plate

$\mathbf{r}(x, y) = x\mathbf{e}_1 + y\mathbf{e}_2$

$x \in [0, L_x]$

$y \in [0, L_y]$

$L_x = L_y = 2.0\text{m}, \quad h = 0.1\text{m}$

(b) Cylindrical surface with cycloidal profile

$\mathbf{r}(\varphi, y) = \left(r_c \left(2\varphi + \sin 2\varphi \right) + y \sin \alpha \sin \varphi \right) \mathbf{e}_1 +$
$\qquad - y \cos \alpha \, \mathbf{e}_2 +$
$\qquad + \left(r_c (1 - \cos 2\varphi) - y \sin \alpha \cos \varphi \right) \mathbf{e}_3$

$y \in [0, L_y], \quad \varphi \in [\varphi_0, \varphi_1]$

$r_c = 0.5\text{m} \quad \varphi_0 = -60° \quad \varphi_1 = 60°$

$L_y = 4.0\text{m} \quad \alpha = 15° \quad h = 0.2\text{m}$

(c) Helicoid

$\mathbf{r}(\alpha_1, \alpha_2) = -a \cos(\alpha_1 + \alpha_2) \sinh(\alpha_1 - \alpha_2) \mathbf{e}_1 +$
$\qquad - a \sin(\alpha_1 + \alpha_2) \sinh(\alpha_1 - \alpha_2) \mathbf{e}_2 +$
$\qquad + a(\alpha_1 - \alpha_2) \mathbf{e}_3$

$\alpha_1 \in [\alpha_1^0, \alpha_1^1], \quad \alpha_2 \in [\alpha_2^0, \alpha_2^1]$

$\alpha_1^0 = 0 \quad \alpha_1^1 = \pi/2 \quad \alpha_2^0 = 0 \quad \alpha_2^1 = \pi/4$

$a = 2.5\text{m} \quad h = 0.3\text{m}$
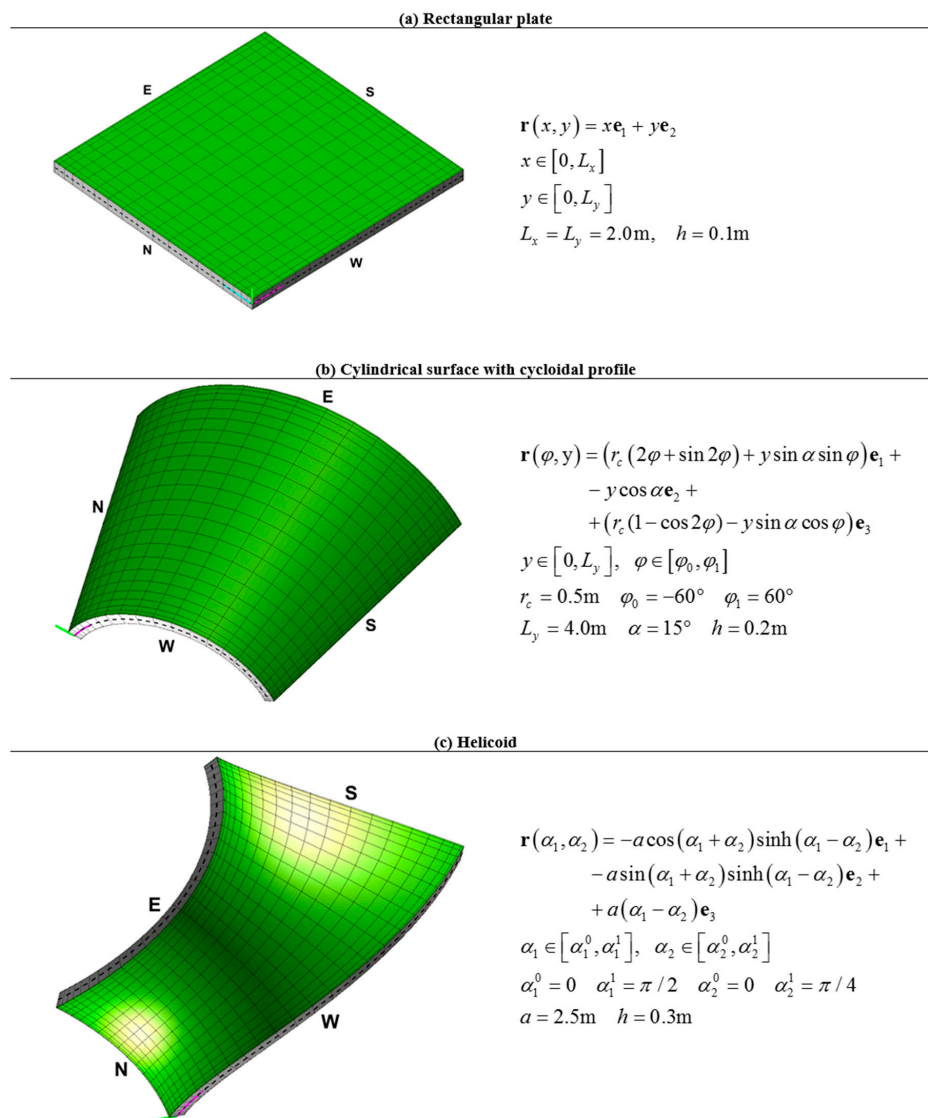
Figure 4. Three panel structures with GDQ discretization and local co-ordinate system representation. For each structure, the position vector $\mathbf{r}(\alpha_1, \alpha_2)$ is shown, along with the geometric parameters that describe the reference surface of the three structures under consideration: (**a**) rectangular plate; (**b**) cylindrical surface; (**c**) helicoid.
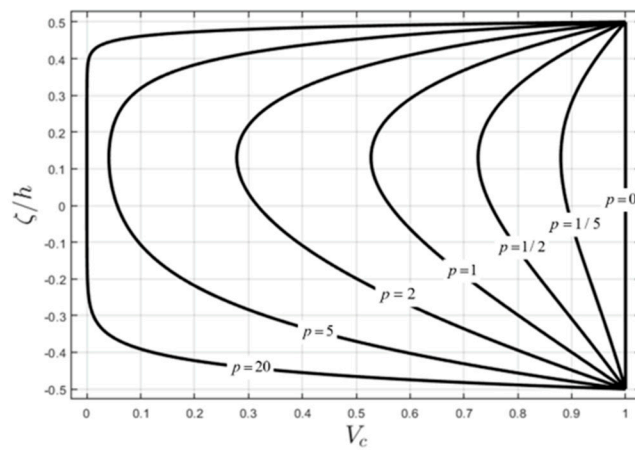
$$FG\text{-}CNT^{PM}_{CNT(5P)(a^{(1)}=1/b^{(1)}=1/c^{(1)}=4/d^{(1)}=1/p^{(1)})}$$

$$a^{(1)} = 1 \quad b^{(1)} = 1 \quad c^{(1)} = 4 \quad d^{(1)} = 1$$

$$p^{(1)} - \text{variable}$$

$$\text{top} = \text{polymer matrix}, \quad \text{bottom} = \text{CNTs}$$

$$\mu_1 = 1, \quad \mu_2 = 1, \quad w_r = 0.05, \quad h = 0.1\text{m}$$

(a)
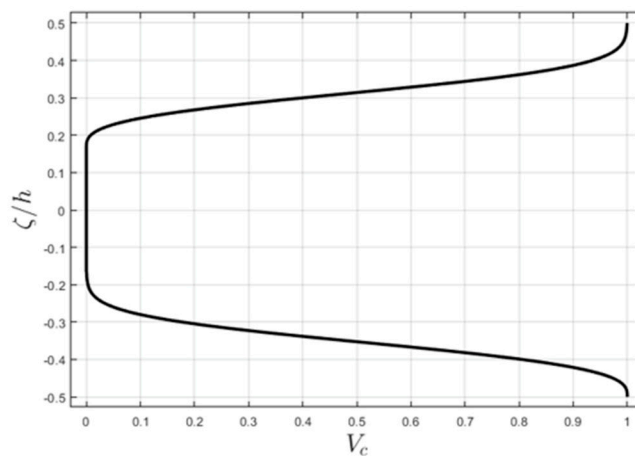
layer 1: $FG\text{-}CNT^{PM}_{CNT(2P-W)(a^{(1)}=0.5/b^{(1)}=3)}$

$$a^{(1)} = 0.5 \quad b^{(1)} = 3$$

$$\text{top} = \text{polymer matrix} \quad \text{bottom} = \text{CNTs}$$

$$\mu_1 = 0.5 \quad \mu_2 = 0.75 \quad w_r = 0.25 \quad h = 0.05\text{m}$$

layer 2: polymer matrix $\quad h = 0.1\text{m}$

layer 3: $FG\text{-}CNT^{CNT}_{PM(2P-W)(a^{(3)}=0.5/b^{(3)}=3)}$

$$a^{(3)} = 0.5 \quad b^{(3)} = 3$$

$$\text{top} = \text{CNTs} \quad \text{bottom} = \text{polymer matrix}$$

$$\mu_1 = 0.5 \quad \mu_2 = 0.75 \quad w_r = 0.25 \quad h = 0.05\text{m}$$

(b)
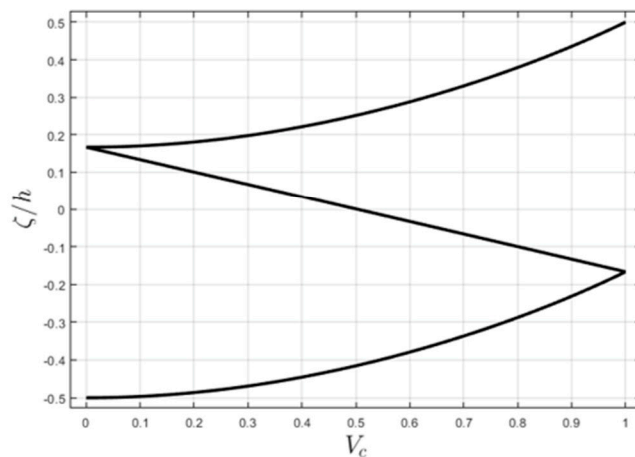
layer 1: $FG\text{-}CNT^{CNT}_{PM(2P-E)(a^{(1)}=1/b^{(1)}=0.5)}$

$$a^{(1)} = 1 \quad b^{(1)} = 0.5 \quad h = 0.1\text{m}$$

$$\text{top} = \text{CNTs} \quad \text{bottom} = \text{polymer matrix}$$

layer 2: $FG\text{-}CNT^{PM}_{CNT(5P)(a^{(2)}=1/b^{(2)}=0/c^{(2)}=0/d^{(2)}=1/p^{(2)}=1)}$

$$a^{(2)} = 1 \quad b^{(2)} = 0 \quad c^{(2)} = 0 \quad d^{(2)} = 1 \quad p^{(2)} = 1$$

$$\text{top} = \text{polymer matrix} \quad \text{bottom} = \text{CNTs}$$

$$h = 0.1\text{m}$$

layer 3: $FG\text{-}CNT^{CNT}_{PM(2P-E)(a^{(3)}=1/b^{(3)}=0.5)}$

$$a^{(3)} = 1 \quad b^{(3)} = 0.5 \quad h = 0.1\text{m}$$

$$\text{top} = \text{CNTs} \quad \text{bottom} = \text{polymer matrix}$$

(c)

Figure 5. Distributions of the CNT-reinforcing phase along the thickness. For each layer, the parameters for the distribution itself are shown: (**a**) (5P); (**b**) (2P-W); (**c**) (2P-E).

4.1. Comparison with FEM

The aim of this application is to validate the present approach by means of a comparison with results obtained through a commercial FEM code. Two examples are conducted in this Subsection: a CNT-reinforced fully clamped square plate (Figure 4a) made of single-ply of constant thickness

($h = 0.1$ m); and the same square plate with 3 layers (CNT/matrix/CNT) of various thickness (0.02 m/0.06 m/0.02 m). The agglomeration parameters and mass fraction value of the CNTs are given in Tables 2 and 3. All the phases were considered to be isotropic. The 3D FEM solution was obtained by the commercial software Strand7. Several kinematic models were considered with reference to the GDQ solution. In particular, in the first example, the following theories were used: $FSDT_{RS}^{\kappa=5/6}$, $ED2^{\kappa=5/6}$ and ED3; and in the second example, the following theories: $FSDTZ_{RS}^{\kappa=1}$, $FSDTZ_{RS}^{\kappa=5/6}$, $EDZ2^{\kappa=1}$, $EDZ2^{\kappa=5/6}$ and EDZ3. The notation *RS* means that reduced stiffness is used (hypothesis of plane stress). Analogously, κ stands for the shear correction factor. It should be noted that the zig-zag theories up to the second order of kinematic expansion are taken with and without the shear correction factor. Further details concerning this choice can be found in the following papers [101–110]. The results of the comparison can be observed in Tables 2 and 3, showing good agreement between GDQ solutions and FEM ones. It should be recalled that, in the second circumstance, only zig-zag theories were used, since the structure has a soft-core. As highlighted in [109], sandwich structures with soft inner cores require the Murakami's function to be well analyzed.

Table 2. Comparison between the first ten natural frequency variations of a CCCC square plate made of a single CNT-reinforced lamina of constant thickness $h = 0.1$ m given by GDQ method and FEM. The 3D FEM solution was obtained by commercial software Strand7.

	Uniform CNT Reinforcement Distribution			
f[Hz]	$FSDT_{RS}^{\kappa=5/6}$	$ED2^{\kappa=5/6}$	ED3	3D FEM
1	120.787	120.982	121.091	121.155
2	241.448	241.821	242.199	242.324
3	241.448	241.821	242.199	242.324
4	349.728	350.238	350.992	351.162
5	421.114	421.732	422.774	422.987
6	423.751	424.381	425.403	425.619
7	520.239	520.961	522.499	522.739
8	520.239	520.961	522.499	522.739
9	652.917	653.821	656.100	656.432
10	652.917	653.821	656.100	656.432

Table 3. Comparison between the first ten natural frequency variations of a CCCC square plate made of a 3-layered material (CNT/matrix/CNT) with various thickness $h = 0.02$ m/0.06 m/0.02 m given by GDQ method and FEM. The 3D FEM solution was obtained by commercial software Strand7.

	Lamination Scheme: $\left(FG-CNT^{PM}_{CNT(5P)(a^{(1)}=1/b^{(1)}=0/c^{(1)}=0/d^{(1)}=1/p^{(1)}=0)}/PM/FG-CNT^{PM}_{CNT(5P)(a^{(3)}=1/b^{(3)}=0/c^{(3)}=0/d^{(3)}=1/p^{(3)}=0)}\right)$					
f[Hz]	$FSDTZ_{RS}^{\kappa=1}$	$FSDTZ_{RS}^{\kappa=5/6}$	$EDZ2^{\kappa=1}$	$EDZ2^{\kappa=5/6}$	EDZ3	3D FEM
1	105.243	103.892	105.559	104.188	105.498	105.482
2	204.169	200.091	204.815	200.691	204.637	204.608
3	204.169	200.091	204.815	200.691	204.637	204.608
4	289.471	282.386	290.400	283.241	290.096	290.038
5	343.586	334.061	344.730	335.112	344.322	344.246
6	346.354	336.858	347.512	337.923	347.104	347.037
7	418.461	405.747	419.848	407.016	419.308	419.190
8	418.461	405.747	419.848	407.016	419.308	419.190
9	514.520	496.736	516.310	498.371	515.554	515.393
10	514.520	496.736	516.310	498.371	515.554	515.393

4.2. Effect of Through-the-Thickness Distribution of CNTs

The following examples show the variation of the natural frequencies as a function of the volume fraction distribution along the thickness of the lamina by varying the parameter $p^{(1)}$ of a five-parameter

exponential law. A functionally graded CNT-reinforced fully clamped square plate (Figure 4a) made of a single ply of constant thickness ($h = 0.1$ m) is assumed. The agglomeration parameters and mass fraction value of the CNTs are given in Tables 4 and 5. Material was described with the five-parameter exponential law defined in Figure 5a. At the bottom of the plate, elastic foundations were applied, the parameters of which can be found in Tables 4 and 5.

Table 4. First ten natural frequency variations of a CCCC square plate (Figure 4a) made of one lamina of constant thickness $h = 0.1$ m reinforced by CNTs distributed as in Figure 5a for the different parameters $p^{(1)} = p$. The mass fraction was $w_r = 0.05$ and agglomeration parameters $\mu_1 = \mu_2 = 1$. The Chebyshev-Gauss-Lobatto grid distribution was employed, with $I_N = I_M = 21$.

	Elastic Foundation: $\rho^{(-)} = 1800\,kg/m^3$,			$h_f^{(-)} = 0.1\,m$,		$k_{3f}^{(-)} = 75 \times 10^7\,N/m^3$			
f[Hz]	$p = 0$	$p = 1/5$	$p = 1/2$	$p = 1$	$p = 2$	$p = 5$	$p = 10$	$p = 15$	$p = 20$
				FSDT$_{RS}^{\kappa=5/6}$					
1	341.557	341.153	340.590	339.761	338.431	336.089	334.456	333.695	333.244
2	379.719	378.036	375.701	372.262	366.774	357.249	350.783	347.791	345.955
3	379.719	378.036	375.701	372.262	366.774	357.249	350.783	347.791	345.955
4	430.007	426.774	422.278	415.633	404.978	386.395	373.862	368.213	361.622
5	469.071	464.709	458.633	449.631	435.144	409.749	392.584	372.274	361.622
6	470.711	466.315	460.190	451.114	436.502	410.867	392.772	372.274	364.919
7	528.685	522.691	514.326	501.897	481.810	446.124	392.772	384.850	380.340
8	528.685	522.691	514.326	501.897	481.810	446.124	393.522	385.704	381.145
9	615.397	607.148	595.607	578.371	545.185	448.132	422.311	411.447	405.105
10	615.397	607.148	595.607	578.371	545.185	448.132	422.311	411.447	405.105
				ED2$^{\kappa=5/6}$					
1	341.102	340.694	340.125	339.286	337.937	335.534	333.785	332.923	332.394
2	379.134	377.436	375.080	371.609	366.065	356.412	349.675	346.337	344.127
3	379.134	377.436	375.080	371.609	366.065	356.412	349.675	346.337	344.127
4	429.582	426.313	421.765	415.040	404.257	385.503	372.865	367.085	363.664
5	468.880	464.461	458.301	449.169	434.470	408.804	391.565	374.142	363.701
6	470.552	466.098	459.891	450.687	435.867	409.972	392.572	374.142	363.701
7	528.912	522.822	514.318	501.673	481.227	445.156	394.458	383.731	379.103
8	528.912	522.822	514.318	501.673	481.227	445.156	394.458	384.670	380.006
9	616.397	607.989	596.217	578.621	545.954	449.492	421.306	410.411	403.988
10	616.397	607.989	596.217	578.621	545.954	449.492	421.306	410.411	403.988
				ED3					
1	341.119	340.703	340.124	339.266	337.883	335.425	333.690	332.852	332.339
2	379.252	377.510	375.088	371.506	365.765	355.852	349.266	346.071	343.938
3	379.252	377.510	375.088	371.506	365.765	355.852	349.266	346.071	343.938
4	429.893	426.514	421.800	414.804	403.531	384.143	371.918	366.529	363.321
5	469.350	464.763	458.350	448.800	433.342	406.672	390.077	373.876	363.523
6	471.009	466.390	459.933	450.315	434.743	407.854	391.096	373.876	363.523
7	529.659	523.308	514.408	501.107	479.468	441.878	394.095	382.864	378.578
8	529.659	523.308	514.408	501.107	479.468	441.878	394.095	383.811	379.486
9	617.534	608.718	596.322	577.690	545.058	449.114	418.954	409.047	403.174
10	617.534	608.718	596.322	577.690	545.058	449.114	418.954	409.047	403.174

In this example, the following theories were used: FSDT$_{RS}^{\kappa=5/6}$, ED2$^{\kappa=5/6}$ and ED3. Since the lamination scheme is characterized by only one layer, the Murakami's function was not needed. Tables 4 and 5 show the first ten natural frequencies for each theory for different values of the parameter $p^{(1)}$ with two different parameters of elastic foundations. The overall behavior of the through-the-thickness distribution variation can be observed more easily from the graphs depicted in Figures 6 and 7.

Table 5. First ten natural frequency variations of a CCCC square plate (Figure 4a) made of one lamina of constant thickness $h = 0.1$ m reinforced by CNTs distributed as in Figure 5a for the different parameters $p^{(1)} = p$. The mass fraction was $w_r = 0.05$ and the agglomeration parameters $\mu_1 = \mu_2 = 1$. The Chebyshev-Gauss-Lobatto grid distribution was employed, with $I_N = I_M = 21$.

Elastic Foundation: $\rho^{(-)} = 1800\,kg/m^3$,		$h_f^{(-)} = 0.1\,m$,		$k_{3f}^{(-)} = 75 \times 10^7\,N/m^3$,		$G_f^{(-)} = 35 \times 10^7\,N/m$		
f [Hz]	$p = 0$	$p = 1/5$	$p = 1/2$	$p = 1$	$p = 2$	$p = 5$	$p = 10$	$p = 15$	$p = 20$
$\mathrm{FSDT}_{RS}^{\kappa=5/6}$									
1	612.245	611.801	611.176	607.409	545.860	447.819	392.661	372.062	361.264
2	694.928	674.844	647.287	607.409	545.860	447.819	392.661	372.062	361.264
3	694.928	674.844	647.287	610.241	608.718	533.861	465.074	439.250	425.671
4	841.143	816.155	781.879	732.290	655.761	606.022	571.512	541.063	525.069
5	882.978	881.931	880.480	878.335	796.786	652.772	604.140	603.198	592.152
6	882.978	881.931	880.480	878.335	874.733	737.097	645.461	611.039	592.152
7	1014.165	985.285	945.251	886.992	874.733	742.231	646.908	611.039	592.949
8	1091.717	1089.519	1065.496	1000.323	899.095	742.231	646.908	611.050	602.574
9	1141.685	1110.007	1085.265	1016.790	911.249	843.117	741.232	703.178	683.275
10	1167.091	1132.591	1085.265	1016.790	911.249	868.882	782.404	740.408	718.273
$\mathrm{ED2}^{\kappa=5/6}$									
1	609.884	609.437	608.802	607.835	547.042	449.412	394.399	373.763	362.913
2	695.503	675.522	648.089	608.367	547.042	449.412	394.399	373.763	362.913
3	695.503	675.522	648.089	608.367	606.200	534.043	465.263	439.426	425.831
4	840.697	815.811	781.659	732.214	655.840	602.962	573.416	542.922	526.852
5	877.187	876.030	874.415	871.974	797.669	654.451	600.059	598.222	592.267
6	877.187	876.030	874.415	871.974	867.465	739.181	647.091	611.198	592.267
7	1011.509	983.749	944.615	887.136	867.465	742.301	647.091	611.198	595.047
8	1083.926	1080.617	1063.945	1000.169	900.119	742.301	647.765	613.263	596.846
9	1135.880	1106.652	1077.028	1016.506	911.740	844.974	744.339	706.795	687.261
10	1165.706	1131.497	1084.530	1016.506	911.740	859.755	784.023	742.118	719.888
ED3									
1	610.023	609.540	608.848	607.782	547.049	449.104	394.016	373.474	362.709
2	695.772	675.763	648.289	608.502	547.049	449.104	394.016	373.474	362.709
3	695.772	675.763	648.289	608.502	605.958	534.106	465.302	439.471	425.888
4	841.121	816.194	781.989	732.474	656.005	602.386	573.017	542.643	526.687
5	877.414	876.191	874.471	871.845	797.862	654.157	599.484	597.759	592.395
6	877.414	876.191	874.471	871.845	866.972	738.858	647.157	611.288	592.395
7	1012.318	984.477	945.231	887.590	866.972	742.434	647.157	611.288	594.908
8	1084.191	1080.794	1064.835	1000.830	900.416	742.434	647.332	612.983	596.474
9	1137.009	1107.694	1077.065	1017.204	912.174	844.270	743.433	706.190	686.930
10	1166.848	1132.530	1085.420	1017.204	912.174	858.515	783.568	741.866	719.822
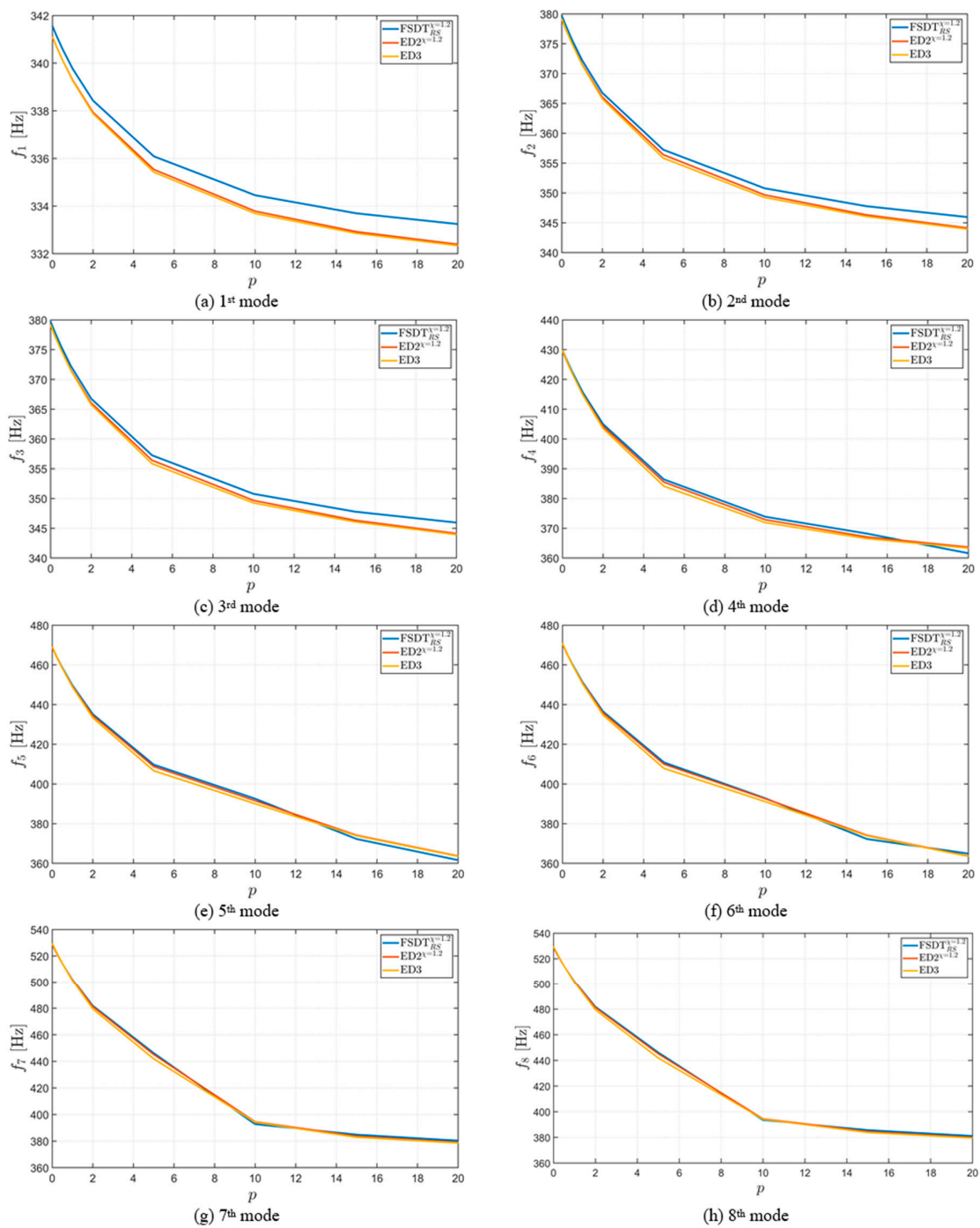
Figure 6. Frequency variations of a CCCC square plate (Figure 3a) made of one lamina of constant thickness $h = 0.1\,\text{m}$; reinforced by CNTs distributed as in Figure 5a for the different parameters $p^{(k)}$. The mass fraction was $w_r = 0.05$, and the agglomeration parameters $\mu_1 = \mu_2 = 1$. The Chebyshev-Gauss-Lobatto grid distribution was employed, with $I_N = I_M = 21$. The following mode shapes are considered: (**a**) 1st mode; (**b**) 2nd mode; (**c**) 3rd mode; (**d**) 4th mode; (**e**) 5th mode; (**f**) 6th mode; (**g**) 7th mode; (**h**) 8th mode.
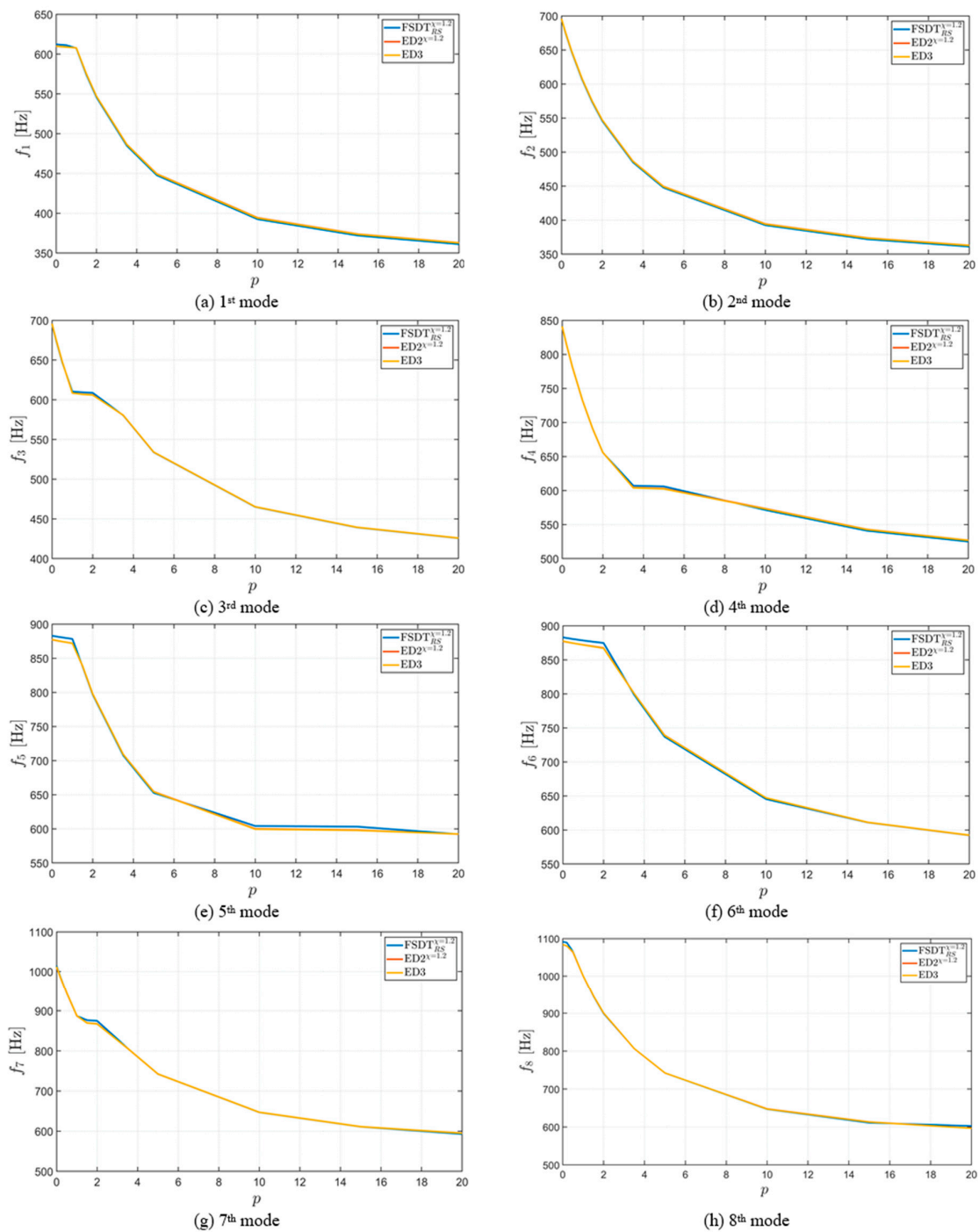
Figure 7. Frequency variations of a CCCC square plate (Figure 3a) made of one lamina of constant thickness $h = 0.1$ m reinforced by CNTs distributed as in Figure 5a for the different parameters $p^{(k)}$. The mass fraction was $w_r = 0.05$, and the agglomeration parameters $\mu_1 = \mu_2 = 1$. The Chebyshev-Gauss-Lobatto grid distribution was employed, with $I_N = I_M = 21$. The following mode shapes are considered: (**a**) 1st mode; (**b**) 2nd mode; (**c**) 3rd mode; (**d**) 4th mode; (**e**) 5th mode; (**f**) 6th mode; (**g**) 7th mode; (**h**) 8th mode.

4.3. Effect of Elastic Foundation

Following example show the variation of the natural frequencies as a function of the parameters that define elastic foundations. A cylindrical surface with cycloidal profile, as shown in Figure 4b, is assumed, with the boundary conditions CFCF. The agglomeration parameters and the mass fraction

value of the CNTs are given in Tables 6 and 7. The applied layer schemes are shown in Figure 5b. In this example, the following theories were used: $FSDT_{RS}^{\kappa=5/6}$, $FSDTZ_{RS}^{\kappa=1}$, $FSDTZ_{RS}^{\kappa=5/6}$, $ED2^{\kappa=5/6}$, $EDZ2^{\kappa=1}$, $EDZ2^{\kappa=5/6}$ and ED3. Tables 6 and 7 show the first seven natural frequencies for each theory for different values of the parameters of elastic foundation $k_{3f}^{(-)}$, $G_f^{(-)}$, respectively. The overall behavior of the variation of these elastic foundation parameters can be observed from the graphs depicted in Figures 8–11. In particular, Figures 8 and 10 show the variation of the first eight natural frequencies as a function of the foundation parameters $k_{3f}^{(-)}$ and $G_f^{(-)}$, respectively. In each graph, all the aforementioned theories have been considered. On the other hand, Figures 9 and 11 present seven different graphs (one for each structural theory), in which the variation of the first four natural frequencies are presented in terms of the foundation parameters $k_{3f}^{(-)}$ and $G_f^{(-)}$, respectively. Interesting behaviors can be observed. With reference to Figure 9, it can be noted that, initially, f_1 and f_2—as well as f_3 and f_4—are overlapped. Nevertheless, this feature changes when increasing the value of $k_{3f}^{(-)}$. Then, a bifurcation point appears, and the frequencies f_1 and f_4 are not overlapped anymore; on the other hand, the curve related to f_2 corresponds with that representing f_3. Similar observations can be made with reference to Figure 11. In particular, f_1 and f_2 exhibit an intermediate behavior in which they are overlapped. Then, the bifurcation point occurs, following which f_3 and f_4 turn out to be overlapped. In general, all these frequencies seem to follow specific paths due to the regularity of the corresponding curves.

Table 6. First seven natural frequency variations of a CFCF cylindrical surface (Figure 4b) reinforced by CNTs distributed as in Figure 5b for the different theories. The mass fraction was $w_r = 0.25$, and the agglomeration parameters $\mu_1 = 0.5$ and $\mu_2 = 0.75$. The Chebyshev-Gauss-Lobatto grid distribution was employed, with $I_N = I_M = 25$.

f [Hz]	Elastic Foundation: $\rho^{(-)} = 1800\,kg/m^3$, $h_f^{(-)} = 0.15\,m$, $G_f^{(-)} = 35 \times 10^7\,N/m^3$, $k_{3f}^{(-)}-$variable									
	$k_{3f}^{(-)}$ $[\mathbf{N/m^3}]$									
	0	5×10^7	10×10^7	15×10^7	20×10^7	25×10^7	30×10^7	45×10^7	60×10^7	75×10^7
$\mathrm{FSDT}_{RS}^{\kappa=5/6}$										
1	184.846	193.075	198.086	202.754	207.129	203.898	201.873	200.118	199.564	199.304
2	184.846	193.075	198.086	202.754	207.129	218.873	228.965	247.087	263.245	277.736
3	187.652	193.116	200.969	208.448	215.588	222.419	228.965	247.087	263.245	277.736
4	187.652	193.116	200.969	208.448	215.588	222.419	229.316	254.784	277.237	298.078
5	291.992	296.947	301.785	306.506	311.109	315.589	319.940	332.058	333.621	334.612
6	308.036	314.347	320.622	326.916	329.655	330.471	331.129	332.548	341.794	346.791
7	317.753	323.442	327.997	328.691	333.351	340.424	346.842	356.790	356.725	362.405
$\mathrm{FSDTZ}_{RS}^{\kappa=1}$										
1	184.219	192.505	197.606	202.331	206.758	205.094	202.299	200.169	199.515	199.209
2	184.219	192.505	197.606	202.331	206.758	216.930	228.242	246.493	262.630	277.094
3	187.035	192.531	200.369	207.856	215.002	221.835	228.382	246.493	262.630	277.094
4	187.035	192.531	200.369	207.856	215.002	221.835	228.382	254.379	277.254	298.542
5	292.386	297.265	302.025	306.663	311.178	315.564	319.815	331.573	332.722	333.748
6	305.049	311.703	318.371	325.151	329.973	330.106	330.426	331.618	340.856	345.563
7	311.777	317.092	322.376	327.585	332.307	337.283	341.781	354.458	356.880	362.010
$\mathrm{FSDTZ}_{RS}^{\kappa=5/6}$										
1	184.143	192.384	197.472	202.209	206.646	205.475	202.410	200.177	199.496	199.178
2	184.143	192.384	197.472	202.209	206.646	216.319	227.920	246.397	262.518	276.967
3	186.872	192.430	200.295	207.781	214.925	221.755	228.298	246.397	262.518	276.967
4	186.872	192.430	200.295	207.781	214.925	221.755	228.298	254.221	277.187	298.572
5	292.751	297.607	302.342	306.955	311.444	315.803	320.024	331.380	332.482	333.513
6	304.559	311.295	318.060	324.970	329.916	329.984	330.249	331.673	340.785	345.315
7	310.759	316.081	321.356	326.558	331.575	336.339	340.884	353.649	356.910	362.032

Table 6. *Cont.*

f[Hz]	Elastic Foundation: $\rho^{(-)} = 1800\,kg/m^3$, $h_f^{(-)} = 0.15\,m$, $G_f^{(-)} = 35 \times 10^7\,N/m^3$, $k_{3f}^{(-)}$ − variable									
	$k_{3f}^{(-)}\ [\mathbf{N/m^3}]$									
	0	5×10^7	10×10^7	15×10^7	20×10^7	25×10^7	30×10^7	45×10^7	60×10^7	75×10^7
ED2$^{\kappa=5/6}$										
1	186.687	194.391	199.212	203.714	207.942	205.231	202.692	200.560	199.876	199.550
2	186.687	194.391	199.212	203.714	207.942	218.856	229.420	247.064	262.813	276.946
3	189.190	194.656	202.246	209.490	216.418	223.054	229.420	247.064	262.813	276.946
4	189.190	194.656	202.246	209.490	216.418	223.054	229.584	254.798	276.808	297.177
5	290.128	295.022	299.799	304.461	309.005	313.429	317.727	329.757	335.300	336.145
6	316.760	323.854	328.821	333.100	333.255	333.455	333.689	334.478	339.860	346.176
7	319.144	324.040	328.821	333.474	337.991	342.370	346.620	358.671	361.209	363.034
EDZ2$^{\kappa=1}$										
1	180.565	188.140	193.540	197.799	201.800	205.576	209.157	201.174	200.003	199.511
2	180.565	188.140	193.540	197.799	201.800	205.576	209.157	238.013	252.997	266.448
3	184.068	188.981	195.359	202.253	208.846	215.163	221.221	238.013	252.997	266.448
4	184.068	188.981	195.359	202.253	208.846	215.163	221.221	238.243	258.894	277.557
5	284.270	289.130	293.880	298.523	303.058	307.484	311.800	324.042	333.242	334.058
6	297.762	303.773	309.834	316.050	322.668	327.295	331.515	332.455	334.959	343.487
7	304.543	309.302	313.956	318.507	322.956	327.295	331.515	343.413	354.283	363.689
EDZ2$^{\kappa=5/6}$										
1	179.922	187.463	192.989	197.232	201.218	204.980	208.546	201.278	200.014	199.492
2	179.922	187.463	192.989	197.232	201.218	204.980	208.546	236.706	252.078	265.484
3	182.707	188.447	194.651	201.516	208.084	214.377	220.413	237.145	252.078	265.484
4	184.399	188.447	194.651	201.516	208.084	214.377	220.413	237.145	257.315	275.870
5	283.169	288.047	292.818	297.481	302.038	306.486	310.826	323.154	333.056	333.840
6	295.135	301.128	307.161	313.323	319.812	324.824	329.049	332.330	334.212	343.052
7	302.090	306.851	311.501	316.046	320.488	324.824	329.049	341.003	351.930	361.448

Table 6. *Cont.*

f [Hz]	Elastic Foundation: $\rho^{(-)} = 1800\,kg/m^3$, $h_f^{(-)} = 0.15\,m$, $G_f^{(-)} = 35 \times 10^7\,N/m^3$, $k_{3f}^{(-)} -$ variable									
	$k_{3f}^{(-)}\ [N/m^3]$									
	0	5×10^7	10×10^7	15×10^7	20×10^7	25×10^7	30×10^7	45×10^7	60×10^7	75×10^7
	ED3									
1	179.944	187.380	193.021	197.186	201.102	204.802	208.310	201.470	200.132	199.585
2	179.944	187.380	193.021	197.186	201.102	204.802	208.310	235.652	251.237	264.508
3	183.773	188.567	194.473	201.250	207.737	213.954	219.919	236.463	251.237	264.508
4	183.773	188.567	194.473	201.250	207.737	213.954	219.919	236.463	256.022	274.312
5	282.467	287.316	292.059	296.696	301.229	305.655	309.975	322.256	333.312	334.076
6	297.790	303.700	309.683	315.855	321.671	325.916	330.051	332.599	333.315	342.323
7	303.658	308.319	312.872	317.323	321.671	325.916	330.051	341.758	352.475	361.807

Table 7. First seven natural frequency variations of a CFCF cylindrical surface (Figure 4b) reinforced by CNTs distributed as in Figure 5b for the different theories. The mass fraction was $w_r = 0.25$, and the agglomeration parameters $\mu_1 = 0.5$ and $\mu_2 = 0.75$. The Chebyshev-Gauss-Lobatto grid distribution was employed, with $I_N = I_M = 25$.

f [Hz]	Elastic Foundation: $\ae^{(-)} = 1800\,kg/m^3$, $h_f^{(-)} = 0.15\,m$, $k_{3f}^{(-)} = 35 \times 10^7\,N/m^3$, $G_f^{(-)} -$ variable									
	$G_f^{(-)}\ [N/m]$									
	0	2.5×10^7	5×10^7	10×10^7	15×10^7	20×10^7	25×10^7	30×10^7	40×10^7	50×10^7
	$FSDT_{RS}^{\kappa=5/6}$									
1	168.599	173.281	178.405	191.003	199.948	205.025	202.136	201.329	200.784	200.568
2	168.830	174.502	180.563	194.562	199.948	205.025	217.847	228.065	242.029	254.510
3	179.422	186.012	191.354	194.562	203.783	212.375	220.454	228.065	242.029	254.510
4	196.850	197.574	197.383	198.293	203.783	212.375	220.454	228.422	247.988	266.838
5	209.081	220.508	231.570	251.683	269.487	285.418	299.759	312.664	332.575	333.808
6	217.985	229.196	239.947	260.269	279.357	297.576	315.303	329.404	333.975	345.403
7	221.416	231.995	242.131	261.435	279.879	297.945	316.271	333.309	357.922	362.186

Table 7. *Cont.*

	Elastic Foundation: $\rho^{(-)} = 1800\,kg/m^3$, $h_f^{(-)} = 0.15\,m$, $k_{3f}^{(-)} = 35 \times 10^7\,N/m^3$, $G_f^{(-)}-$variable									
$f\,[\mathbf{Hz}]$	$G_f^{(-)}\;[\mathbf{N/m}]$									
	0	$\mathbf{2.5 \times 10^7}$	$\mathbf{5 \times 10^7}$	$\mathbf{10 \times 10^7}$	$\mathbf{15 \times 10^7}$	$\mathbf{20 \times 10^7}$	$\mathbf{25 \times 10^7}$	$\mathbf{30 \times 10^7}$	$\mathbf{40 \times 10^7}$	$\mathbf{50 \times 10^7}$
	FSDTZ$_{RS}^{\kappa=1}$									
1	167.461	172.625	178.139	193.361	199.328	204.487	202.887	201.673	200.941	200.662
2	167.979	173.419	179.590	193.361	199.328	204.487	216.113	227.290	241.490	253.984
3	176.909	183.501	188.640	193.859	202.715	211.470	219.686	227.404	241.490	253.984
4	194.506	196.746	196.730	193.859	202.715	211.470	219.686	227.404	247.563	267.238
5	204.223	215.187	226.865	248.291	267.196	283.977	298.937	312.247	331.707	333.025
6	208.658	220.248	231.469	252.756	272.838	292.152	311.175	329.757	333.664	344.345
7	211.364	222.921	233.901	254.767	274.935	295.786	317.795	331.099	357.960	362.235
	FSDTZ$_{RS}^{\kappa=5/6}$									
1	167.205	172.481	178.094	193.132	199.185	204.358	203.101	201.760	200.977	200.682
2	167.780	173.182	179.384	193.132	199.185	204.358	215.647	226.979	241.402	253.874
3	176.388	182.994	188.096	193.700	202.534	211.328	219.572	227.309	241.402	253.874
4	193.757	196.521	196.563	193.700	202.534	211.328	219.572	227.309	247.379	267.194
5	203.418	214.124	225.930	247.675	266.865	283.862	298.975	312.384	331.480	332.809
6	206.754	218.451	229.806	251.328	271.616	291.156	310.455	329.752	333.803	344.170
7	209.219	221.035	232.233	253.482	274.069	295.884	316.669	330.840	357.200	362.352
	ED2$^{\kappa=5/6}$									
1	168.431	173.326	178.673	193.695	200.256	205.413	203.035	202.025	201.378	201.130
2	168.758	174.459	180.707	194.765	200.256	205.413	217.793	228.346	242.305	254.731
3	179.299	185.851	191.046	194.765	203.939	212.591	220.712	228.346	242.305	254.731
4	196.981	197.679	197.401	195.695	203.939	212.591	220.712	228.616	248.166	266.624
5	208.858	220.204	231.171	251.030	268.522	284.114	298.110	310.688	331.584	335.673
6	217.770	229.240	240.295	261.333	281.292	300.631	320.215	333.253	334.565	344.308
7	221.201	232.108	242.650	263.068	283.369	307.265	324.690	338.507	361.829	364.124

Table 7. *Cont.*

| $f\,[\text{Hz}]$	$G_f^{(-)}$ [N/m]									
Elastic Foundation: $\rho^{(-)} = 1800\,kg/m^3$, $h_f^{(-)} = 0.15\,m$, $k_{3f}^{(-)} = 35 \times 10^7\,N/m^3$, $G_f^{(-)}-$**variable**										
	0	2.5×10^7	5×10^7	10×10^7	15×10^7	20×10^7	25×10^7	30×10^7	40×10^7	50×10^7
EDZ2$^{\kappa=1}$										
1	167.236	172.472	178.124	192.146	197.888	202.183	206.026	205.652	202.944	202.326
2	167.833	173.074	179.034	192.146	197.888	202.183	206.026	213.362	228.492	239.412
3	176.814	183.084	187.585	193.078	200.557	208.161	215.056	221.326	232.261	241.442
4	194.584	196.747	196.648	193.078	200.557	208.161	215.056	221.326	232.261	241.442
5	204.112	214.709	225.898	246.080	263.541	278.882	292.555	304.866	326.035	333.636
6	208.625	220.225	231.364	252.173	271.301	289.110	306.087	323.596	332.584	342.169
7	211.286	222.873	233.855	254.761	275.619	298.544	312.422	324.837	344.900	360.170
EDZ2$^{\kappa=5/6}$										
1	166.980	172.326	178.114	191.798	197.625	201.857	205.617	207.691	203.273	202.552
2	167.631	172.827	178.800	191.798	197.625	201.857	205.617	210.240	226.537	236.924
3	176.294	182.547	186.920	192.855	200.153	207.674	214.466	220.620	231.306	240.237
4	193.813	196.497	196.455	192.855	200.153	207.674	214.466	220.620	231.306	240.237
5	203.317	213.613	224.859	245.162	262.660	277.984	291.624	303.911	325.148	333.478
6	206.723	218.389	229.604	250.495	269.621	287.349	304.151	321.276	332.459	341.815
7	209.133	220.933	232.078	253.265	274.647	296.656	310.380	322.564	342.275	357.154
ED3										
1	167.259	172.489	178.170	192.009	197.704	201.876	205.559	208.802	203.701	202.970
2	167.856	173.068	178.993	192.009	197.704	201.876	205.559	208.802	225.123	234.634
3	176.871	183.085	187.476	192.984	200.265	207.662	214.302	220.272	230.507	238.906
4	194.680	196.763	196.639	192.984	200.265	207.662	214.302	220.272	230.507	238.906
5	204.223	214.827	225.954	245.940	263.121	278.119	291.422	303.369	323.983	333.744
6	208.851	220.422	231.538	252.312	271.396	289.125	305.978	323.453	332.735	340.344
7	211.554	223.103	234.067	255.009	276.214	298.269	311.825	323.781	342.863	357.017
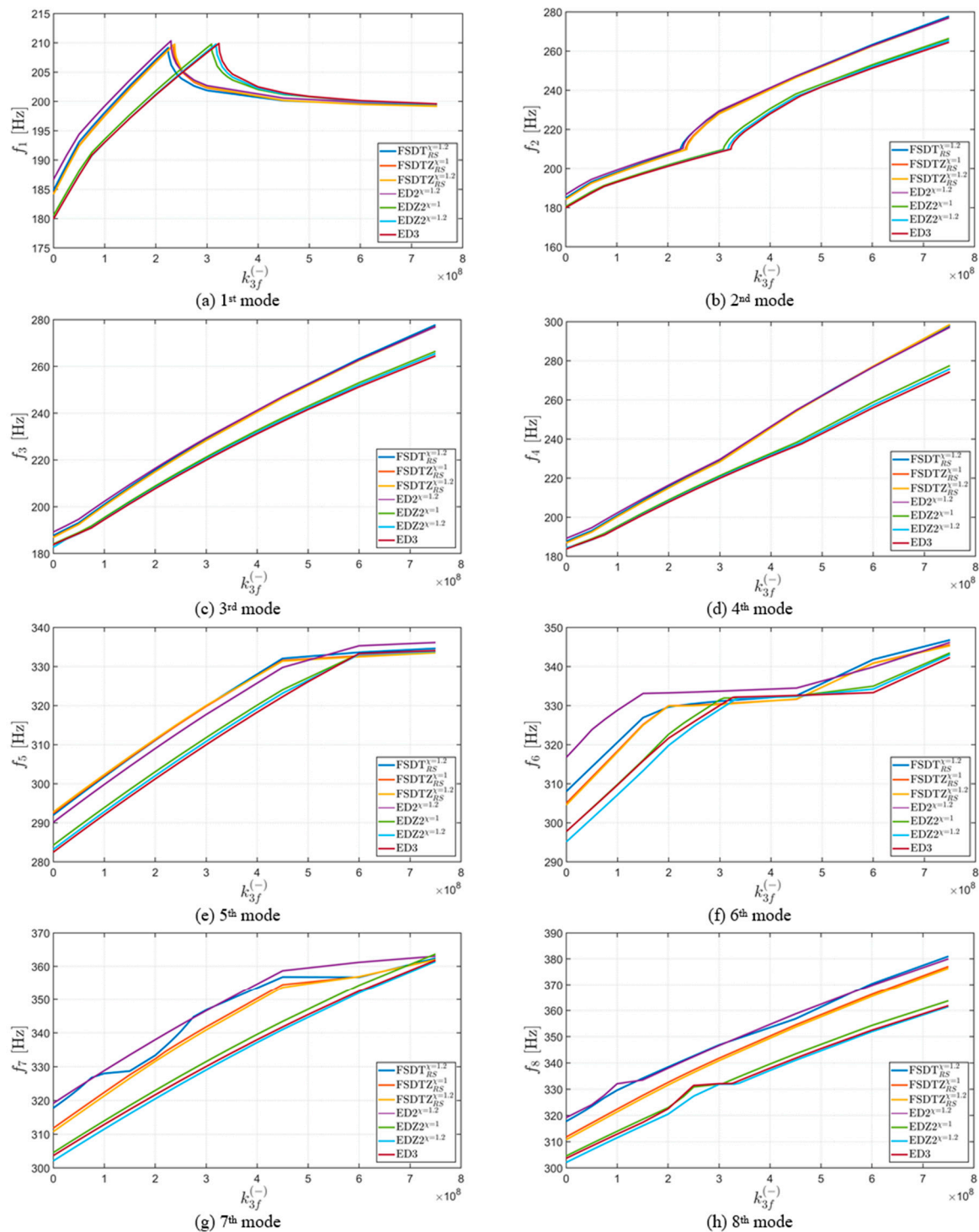
Figure 8. Frequency variations of a CFCF cylindrical surface (Figure 4b) reinforced by CNTs distributed as in Figure 5b. The mass fraction is $w_r = 0.25$, and the agglomeration parameters $\mu_1 = 0.5$ and $\mu_2 = 0.75$. The Chebyshev-Gauss-Lobatto grid distribution was employed, with $I_N = I_M = 25$. The following mode shapes are considered: (**a**) 1st mode; (**b**) 2nd mode; (**c**) 3rd mode; (**d**) 4th mode; (**e**) 5th mode; (**f**) 6th mode; (**g**) 7th mode; (**h**) 8th mode.
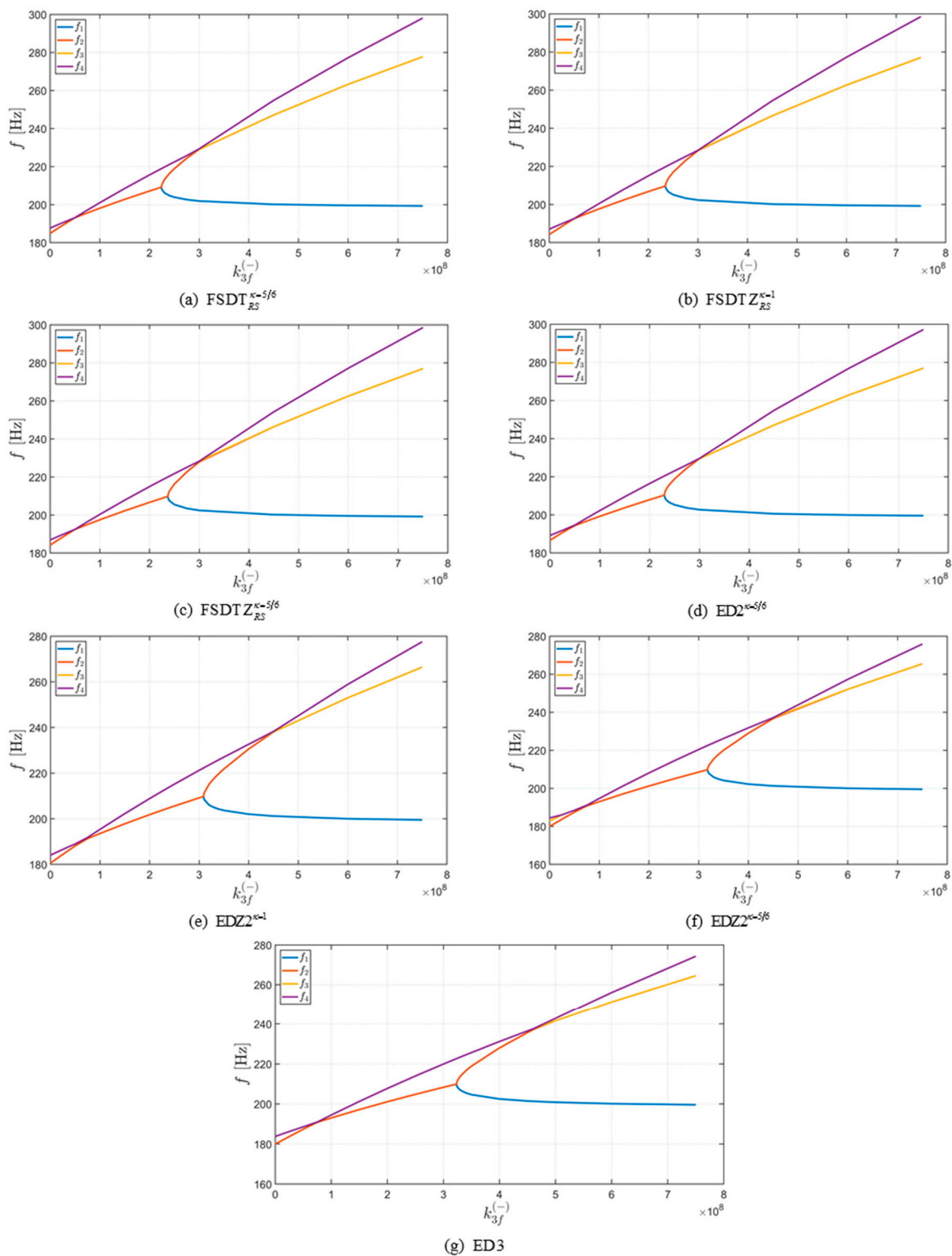
Figure 9. First four frequency modes of a CFCF cylindrical surface (Figure 4b) reinforced by CNTs distributed as in Figure 5b for the different theories: (**a**) $FSDT_{RS}^{\kappa=5/6}$; (**b**) $FSDTZ_{RS}^{\kappa=1}$; (**c**) $FSDTZ_{RS}^{\kappa=5/6}$; (**d**) $ED2^{\kappa=5/6}$; (**e**) $EDZ2^{\kappa=1}$; (**f**) $EDZ2^{\kappa=5/6}$; (**g**) ED3. The mass fraction was $w_r = 0.25$, and the agglomeration parameters $\mu_1 = 0.5$ and $\mu_2 = 0.75$. The Chebyshev-Gauss-Lobatto grid distribution was employed, with $I_N = I_M = 25$.
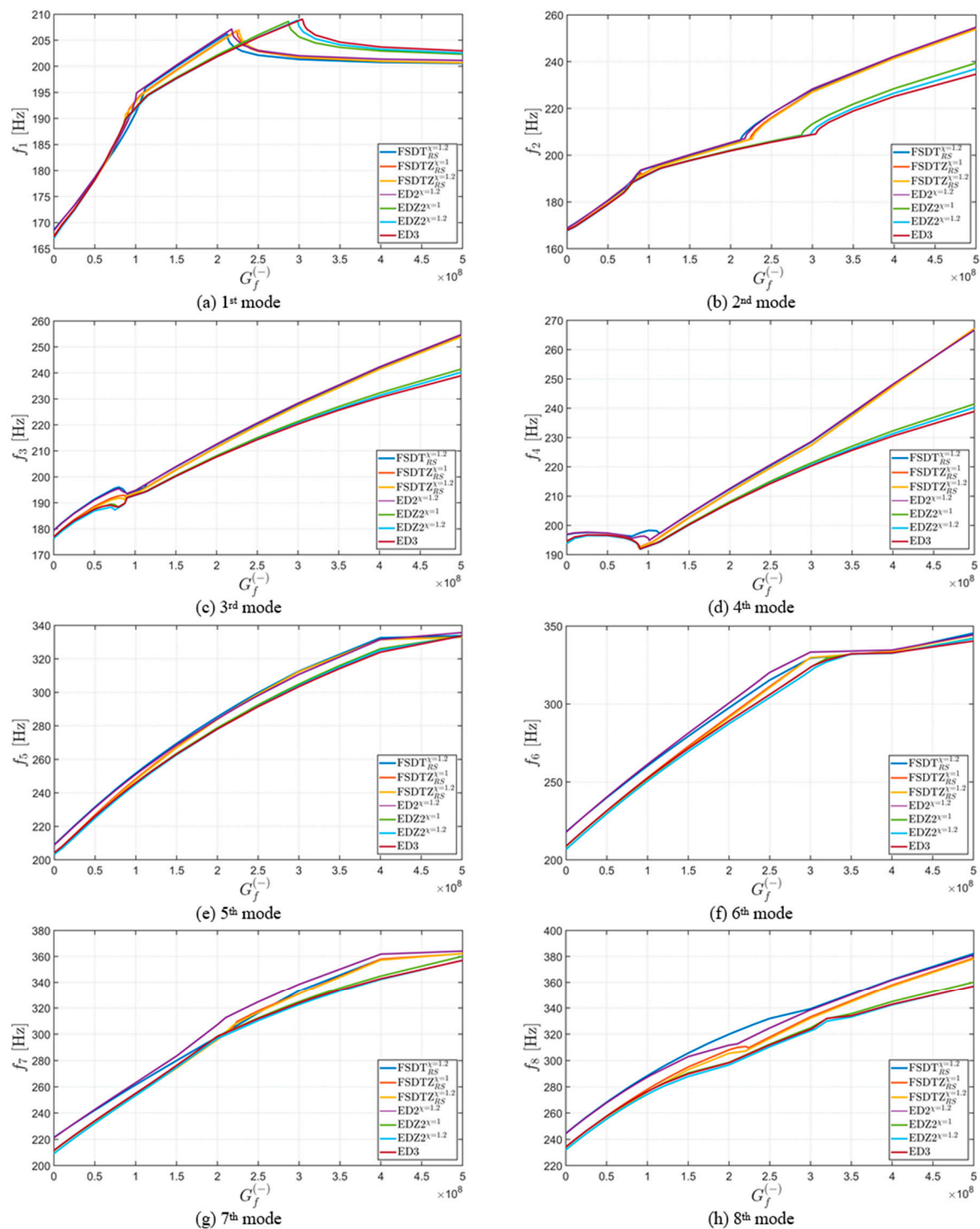
Figure 10. Frequency variations of a CFCF cylindrical surface (Figure 4b) reinforced by CNTs distributed as in Figure 5b. The mass fraction was $w_r = 0.25$, and the agglomeration parameters $\mu_1 = 0.5$ and $\mu_2 = 0.75$. The Chebyshev-Gauss-Lobatto grid distribution was employed, with $I_N = I_M = 25$. The following mode shapes are considered: (**a**) 1st mode; (**b**) 2nd mode; (**c**) 3rd mode; (**d**) 4th mode; (**e**) 5th mode; (**f**) 6th mode; (**g**) 7th mode; (**h**) 8th mode.
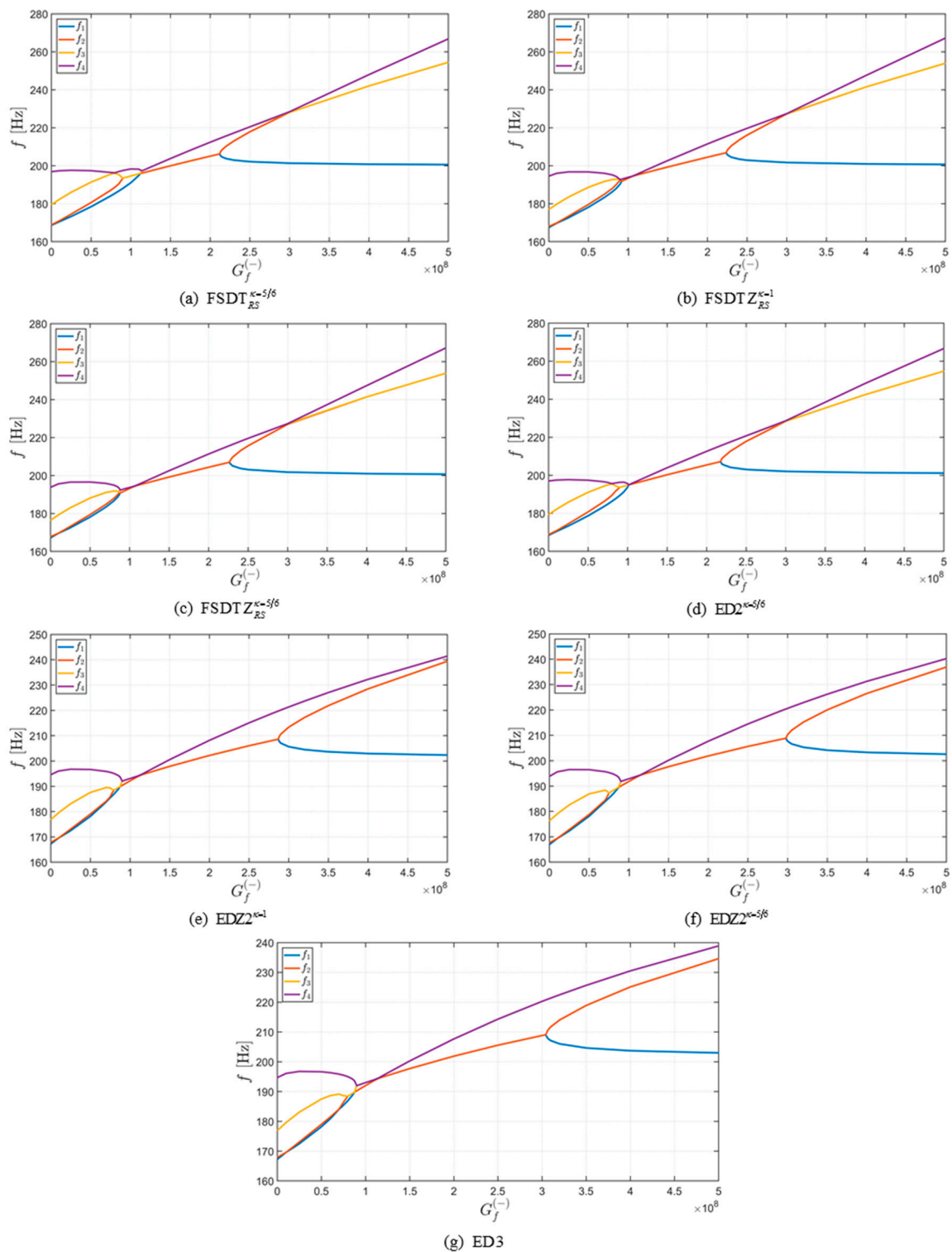
Figure 11. First four frequency modes of a CFCF cylindrical surface (Figure 4b) reinforced by CNTs distributed as in Figure 5b for the different theories: (**a**) $\text{FSDT}_{RS}^{\kappa=5/6}$; (**b**) $\text{FSDTZ}_{RS}^{\kappa=1}$; (**c**) $\text{FSDTZ}_{RS}^{\kappa=5/6}$; (**d**) $\text{ED2}^{\kappa=5/6}$; (**e**) $\text{EDZ2}^{\kappa=1}$; (**f**) $\text{EDZ2}^{\kappa=5/6}$; (**g**) ED3. The mass fraction was $w_r = 0.25$, and the agglomeration parameters $\mu_1 = 0.5$ and $\mu_2 = 0.75$. The Chebyshev-Gauss-Lobatto grid distribution was employed, with $I_N = I_M = 25$.

4.4. Effect of CNT Agglomeration

The last example shows the variation of the natural frequencies as a function of the CNT agglomeration parameters. The helicoidal surface, shown in Figure 4c, is considered, with the boundary conditions CCFF. The agglomeration parameters and the mass fraction value of the CNTs are given in Tables 8–21. The applied layer schemes are shown in Figure 5c. In this example, the following theories have been used: $FSDT_{RS}^{\kappa=5/6}$, $FSDTZ_{RS}^{\kappa=1}$, $FSDTZ_{RS}^{\kappa=5/6}$, $ED2^{\kappa=5/6}$, $EDZ2^{\kappa=1}$, $EDZ2^{\kappa=5/6}$ and ED3. Tables 8–14 show the first ten natural frequencies for the corresponding theories for different values of the mass fraction and agglomeration parameter μ_1. Tables 15–21 show the first ten natural frequencies for the corresponding theories for different values of the mass fraction and agglomeration parameter μ_2. The overall behavior of the agglomeration parameter variation can be observed from the graphs depicted in Figures 12 and 13. These graphs prove again what has been shown in the previous paper by Tornabene et al. [24] and by Shi et al. [32].

Table 8. First ten natural frequency variations for $FSDT_{RS}^{\kappa=5/6}$ theory of a CCFF helicoidal surface (Figure 4c) reinforced by CNTs distributed as in Figure 5c for different mass fractions w_r when varying the parameter of agglomeration μ_1 with $\mu_2 = 1$. The Chebyshev-Gauss-Lobatto grid distribution was employed, with $I_N = 31$, $I_M = 21$.

Theory: $bmFSDT_{RS}^{\kappa=5/6}$					
Elastic Foundation: $\rho^{(-)} = 1800\,kg/m^3$,	$h_f^{(-)} = 0.15\,m$,	$k_{2f}^{(-)} = 20 \times 10^7\,N/m^3$,	$k_{3f}^{(-)} = 35 \times 10^7\,N/m^3$		
		$w_r = 0.1$			
f [Hz]	$\mu_1 = 0.5$	$\mu_1 = 0.6$	$\mu_1 = 0.7$	$\mu_1 = 0.8$	$\mu_1 = 0.9$	$\mu_1 = 1.0$
1	98.276	102.788	107.164	111.446	115.692	119.981
2	137.440	139.576	141.583	143.676	146.134	149.371
3	145.024	147.884	151.132	154.894	159.398	165.077
4	150.836	154.383	158.466	163.330	169.320	177.030
5	152.286	156.391	161.358	167.437	175.030	184.772
6	158.895	162.661	167.003	172.170	178.547	186.817
7	162.882	167.998	173.914	180.885	189.354	200.110
8	173.308	179.363	186.463	194.930	205.273	218.402
9	175.691	182.127	189.726	198.971	210.593	225.757
10	190.617	198.324	207.173	217.583	230.219	246.202
		$w_r = 0.2$			
f [Hz]	$\mu_1 = 0.5$	$\mu_1 = 0.6$	$\mu_1 = 0.7$	$\mu_1 = 0.8$	$\mu_1 = 0.9$	$\mu_1 = 1.0$
1	101.079	106.692	112.286	117.942	123.838	130.502
2	138.378	140.959	143.764	147.486	153.515	165.695
3	146.383	150.470	155.564	162.312	172.248	189.784
4	152.605	157.722	164.325	173.361	186.905	210.836
5	154.475	160.695	169.034	180.609	196.974	222.728
6	160.765	166.205	173.231	182.920	198.397	228.139
7	165.729	173.137	182.574	195.273	213.980	246.382
8	176.702	185.566	197.020	212.505	235.255	274.353
9	179.415	188.972	201.693	219.568	246.572	293.321
10	195.088	206.179	220.291	239.254	266.975	314.206
		$w_r = 0.4$			
f [Hz]	$\mu_1 = 0.5$	$\mu_1 = 0.6$	$\mu_1 = 0.7$	$\mu_1 = 0.8$	$\mu_1 = 0.9$	$\mu_1 = 1.0$
1	102.198	108.513	114.902	121.504	128.802	140.943
2	138.047	141.006	144.696	150.665	163.203	203.896
3	146.417	151.480	158.278	168.454	186.906	239.407
4	152.875	159.297	168.266	182.033	207.073	276.940
5	155.109	163.093	174.608	191.760	218.961	293.607
6	161.061	167.884	177.473	192.898	224.360	309.017
7	166.697	175.943	188.638	207.764	241.829	334.047
8	177.994	189.121	204.556	227.804	268.910	378.557
9	180.969	193.200	210.918	238.628	288.227	418.137
10	196.973	210.800	229.781	258.221	308.089	439.135

Table 9. First ten natural frequency variations for $FSDTZ_{RS}^{\kappa=1}$ theory of a CCFF helicoidal surface (Figure 4c) reinforced by CNTs distributed as in Figure 5c for different mass fractions w_r when varying the parameter of agglomeration μ_1 with $\mu_2 = 1$. The Chebyshev-Gauss-Lobatto grid distribution was employed, with $I_N = 31$, $I_M = 21$.

Theory: $FSDTZ_{RS}^{\kappa=1}$					
$\rho^{(-)} = 1800\,kg/m^3$, $h_f^{(-)} = 0.15\,m$, $k_{2f}^{(-)} = 20 \times 10^7\,N/m^3$, $k_{3f}^{(-)} = 35 \times 10^7\,N/m^3$					
$w_r = 0.1$					
f [Hz]	$\mu_1 = 0.5$	$\mu_1 = 0.6$	$\mu_1 = 0.7$	$\mu_1 = 0.8$	$\mu_1 = 0.9$	$\mu_1 = 1.0$
1	98.298	102.811	107.187	111.469	115.713	119.996
2	137.451	139.584	141.591	143.685	146.142	149.379
3	145.054	147.911	151.155	154.912	159.410	165.078
4	150.895	154.437	158.517	163.375	169.355	177.044
5	152.340	156.449	161.416	167.491	175.072	184.794
6	158.975	162.741	167.079	172.237	178.595	186.833
7	162.962	168.086	174.004	180.966	189.414	200.125
8	173.457	179.516	186.619	195.077	205.387	218.445
9	175.786	182.215	189.798	199.022	210.623	225.766
10	190.891	198.599	207.435	217.814	230.391	246.273
$w_r = 0.2$					
f [Hz]	$\mu_1 = 0.5$	$\mu_1 = 0.6$	$\mu_1 = 0.7$	$\mu_1 = 0.8$	$\mu_1 = 0.9$	$\mu_1 = 1.0$
1	101.103	106.718	112.314	117.970	123.860	130.511
2	138.388	140.969	143.776	147.502	153.533	165.698
3	146.418	150.503	155.595	162.338	172.263	189.771
4	152.671	157.789	164.394	173.427	186.953	210.818
5	154.542	160.769	169.109	180.679	197.030	222.701
6	160.863	166.308	173.337	183.020	198.462	228.129
7	165.836	173.262	182.709	195.403	214.068	246.329
8	176.891	185.781	197.257	212.735	235.416	274.285
9	179.521	189.065	201.763	219.618	246.601	293.314
10	195.423	206.534	220.649	239.582	267.204	314.140
$w_r = 0.4$					
f [Hz]	$\mu_1 = 0.5$	$\mu_1 = 0.6$	$\mu_1 = 0.7$	$\mu_1 = 0.8$	$\mu_1 = 0.9$	$\mu_1 = 1.0$
1	102.225	108.544	114.936	121.538	128.828	140.942
2	138.058	141.018	144.714	150.693	163.240	203.866
3	146.456	151.521	158.320	168.495	186.938	239.360
4	152.949	159.379	168.359	182.133	207.159	276.830
5	155.186	163.180	174.703	191.870	219.073	293.470
6	161.176	168.014	177.619	193.040	224.456	308.923
7	166.828	176.106	188.829	207.969	241.997	333.815
8	178.222	189.403	204.888	228.156	269.192	378.214
9	181.083	193.297	210.996	238.692	288.273	418.095
10	197.364	211.239	230.258	258.706	308.475	438.735

Table 10. First ten natural frequency variations for FSDTZ$_{RS}^{\kappa=5/6}$ theory of a CCFF helicoidal surface (Figure 4c) reinforced by CNTs distributed as in Figure 5c for different mass fractions w_r when varying the parameter of agglomeration μ_1 with $\mu_2 = 1$. The Chebyshev-Gauss-Lobatto grid distribution was employed, with $I_N = 31$, $I_M = 21$.

Theory: $FSDTZ_{RS}^{\kappa=5/6}$					
Elastic Foundation: $\rho^{(-)} = 1800\,kg/m^3$, $h_f^{(-)} = 0.15\,m$, $k_{2f}^{(-)} = 20 \times 10^7\,N/m^3$, $k_{3f}^{(-)} = 35 \times 10^7\,N/m^3$					
$w_r = 0.1$					
f [Hz]	$\mu_1 = 0.5$	$\mu_1 = 0.6$	$\mu_1 = 0.7$	$\mu_1 = 0.8$	$\mu_1 = 0.9$	$\mu_1 = 1.0$
1	98.258	102.763	107.129	111.399	115.630	119.900
2	137.423	139.559	141.565	143.651	146.095	149.306
3	144.961	147.806	151.038	154.781	159.261	164.908
4	150.722	154.248	158.302	163.122	169.052	176.676
5	152.192	156.267	161.202	167.242	174.783	184.461
6	158.713	162.436	166.724	171.823	178.108	186.246
7	162.674	167.720	173.550	180.412	188.742	199.310
8	172.955	178.916	185.883	194.170	204.279	217.108
9	175.487	181.897	189.485	198.730	210.350	225.500
10	189.997	197.568	206.251	216.455	228.826	244.456
$w_r = 0.2$					
f [Hz]	$\mu_1 = 0.5$	$\mu_1 = 0.6$	$\mu_1 = 0.7$	$\mu_1 = 0.8$	$\mu_1 = 0.9$	$\mu_1 = 1.0$
1	101.058	106.661	112.241	117.881	123.755	130.393
2	138.363	140.943	143.740	147.441	153.421	165.480
3	146.318	150.387	155.461	162.179	172.065	189.504
4	152.491	157.578	164.133	173.093	186.507	210.178
5	154.374	160.560	168.856	180.372	196.491	221.839
6	160.575	165.960	172.908	182.477	197.904	227.479
7	165.499	172.819	182.135	194.662	213.093	244.971
8	176.324	185.050	196.302	211.504	233.824	272.136
9	179.221	188.769	201.492	219.361	246.331	292.986
10	194.446	205.368	219.252	237.885	265.088	311.348
$w_r = 0.4$					
f [Hz]	$\mu_1 = 0.5$	$\mu_1 = 0.6$	$\mu_1 = 0.7$	$\mu_1 = 0.8$	$\mu_1 = 0.9$	$\mu_1 = 1.0$
1	102.177	108.481	114.854	121.439	128.715	140.784
2	138.034	140.989	144.665	150.596	163.036	203.369
3	146.352	151.398	158.173	168.310	186.680	238.914
4	152.764	159.151	168.062	181.727	206.558	275.716
5	155.007	162.957	174.425	191.415	218.244	292.008
6	160.873	167.636	177.132	192.481	223.841	307.863
7	166.463	175.613	188.170	207.075	240.709	331.549
8	177.609	188.579	203.785	226.685	267.137	374.759
9	180.793	193.025	210.746	238.435	287.960	417.583
10	196.341	209.988	228.709	256.731	305.792	434.336

Table 11. First ten natural frequency variations for ED2$^{\kappa=5/6}$ theory of a CCFF helicoidal surface (Figure 4c) reinforced by CNTs distributed as in Figure 5c for different mass fractions w_r when varying the parameter of agglomeration μ_1 with $\mu_2 = 1$. The Chebyshev-Gauss-Lobatto grid distribution was employed, with $I_N = 31$, $I_M = 21$.

Theory: ED2$^{\kappa=5/6}$					
Elastic Foundation: $\rho^{(-)} = 1800\,kg/m^3$, $h_f^{(-)} = 0.15\,m$, $k_{2f}^{(-)} = 20 \times 10^7\,N/m^3$, $k_{3f}^{(-)} = 35 \times 10^7\,N/m^3$					
$w_r = 0.1$					
f [Hz]	$\mu_1 = 0.5$	$\mu_1 = 0.6$	$\mu_1 = 0.7$	$\mu_1 = 0.8$	$\mu_1 = 0.9$	$\mu_1 = 1.0$
1	97.894	102.446	106.868	111.200	115.498	119.837
2	136.937	139.191	141.300	143.475	145.999	149.295
3	144.467	147.289	150.551	154.371	158.961	164.738
4	150.691	154.330	158.473	163.375	169.394	177.129
5	152.660	156.839	161.849	167.948	175.543	185.272
6	158.439	162.211	166.579	171.782	178.201	186.528
7	162.193	167.428	173.440	180.496	189.047	199.881
8	172.779	178.909	186.051	194.552	204.945	218.150
9	176.008	182.493	190.143	199.416	211.023	226.131
10	189.979	197.824	206.789	217.298	230.016	246.067
$w_r = 0.2$					
f [Hz]	$\mu_1 = 0.5$	$\mu_1 = 0.6$	$\mu_1 = 0.7$	$\mu_1 = 0.8$	$\mu_1 = 0.9$	$\mu_1 = 1.0$
1	100.723	106.395	112.057	117.784	123.743	130.460
2	137.960	140.675	143.586	147.394	153.498	165.745
3	145.793	149.886	155.061	161.931	172.000	189.671
4	152.528	157.729	164.384	173.465	187.053	211.021
5	154.917	161.207	169.577	181.163	197.005	222.707
6	160.320	165.790	172.867	182.615	198.682	228.543
7	165.122	172.660	182.216	195.032	213.851	246.355
8	176.218	185.146	196.662	212.247	235.133	274.376
9	179.796	189.426	202.176	220.004	246.891	293.478
10	194.567	205.823	220.077	239.158	266.969	314.238
$w_r = 0.4$					
f [Hz]	$\mu_1 = 0.5$	$\mu_1 = 0.6$	$\mu_1 = 0.7$	$\mu_1 = 0.8$	$\mu_1 = 0.9$	$\mu_1 = 1.0$
1	101.864	108.252	114.722	121.404	128.766	140.951
2	137.683	140.779	144.578	150.639	163.267	204.024
3	145.819	150.929	157.852	168.182	186.792	239.451
4	152.830	159.330	168.359	182.191	207.303	277.206
5	155.588	163.638	175.184	191.874	218.971	293.756
6	160.629	167.501	177.156	193.146	224.836	309.455
7	166.135	175.527	188.366	207.644	241.865	334.180
8	177.526	188.725	204.271	227.692	269.018	378.841
9	181.399	193.701	211.408	239.014	288.443	418.095
10	196.528	210.541	229.689	258.280	308.268	439.244

Table 12. First ten natural frequency variations for EDZ2$^{\kappa=1}$ theory of a CCFF helicoidal surface (Figure 4c) reinforced by CNTs distributed as in Figure 5c for different mass fractions w_r when varying the parameter of agglomeration μ_1 with $\mu_2 = 1$. The Chebyshev-Gauss-Lobatto grid distribution was employed, with $I_N = 31$, $I_M = 21$.

Theory: $EDZ2^{\kappa=1}$					
Elastic Foundation: $\rho^{(-)} = 1800\,kg/m^3$, $\quad h_f^{(-)} = 0.15\,m$, $\quad k_{2f}^{(-)} = 20 \times 10^7\,N/m^3$, $\quad k_{3f}^{(-)} = 35 \times 10^7\,N/m^3$					
$w_r = 0.1$					
f [Hz]	$\mu_1 = 0.5$	$\mu_1 = 0.6$	$\mu_1 = 0.7$	$\mu_1 = 0.8$	$\mu_1 = 0.9$	$\mu_1 = 1.0$
1	97.929	102.482	106.906	111.238	115.534	119.867
2	136.950	139.200	141.307	143.481	146.006	149.300
3	144.509	147.330	150.589	154.405	158.988	164.754
4	150.770	154.404	158.543	163.437	169.442	177.151
5	152.733	156.916	161.926	168.019	175.601	185.303
6	158.543	162.319	166.686	171.882	178.284	186.574
7	162.309	167.555	173.571	180.620	189.145	199.925
8	173.013	179.150	186.294	194.784	205.141	218.262
9	176.110	182.593	190.232	199.487	211.072	226.155
10	190.373	198.233	207.198	217.684	230.345	246.283
$w_r = 0.2$					
f [Hz]	$\mu_1 = 0.5$	$\mu_1 = 0.6$	$\mu_1 = 0.7$	$\mu_1 = 0.8$	$\mu_1 = 0.9$	$\mu_1 = 1.0$
1	100.761	106.436	112.101	117.828	123.783	130.485
2	137.972	140.685	143.597	147.408	153.514	165.743
3	145.840	149.935	155.110	161.977	172.037	189.677
4	152.615	157.817	164.474	173.550	187.116	210.997
5	155.004	161.301	169.673	181.251	197.102	222.702
6	160.445	165.927	173.012	182.761	198.767	228.535
7	165.268	172.831	182.402	195.216	213.991	246.317
8	176.498	185.457	197.000	212.586	235.403	274.373
9	179.911	189.536	202.270	220.078	246.941	293.483
10	195.033	206.330	220.609	239.682	267.404	314.329
$w_r = 0.4$					
f [Hz]	$\mu_1 = 0.5$	$\mu_1 = 0.6$	$\mu_1 = 0.7$	$\mu_1 = 0.8$	$\mu_1 = 0.9$	$\mu_1 = 1.0$
1	101.905	108.297	114.773	121.456	128.812	140.966
2	137.694	140.791	144.595	150.667	163.304	203.979
3	145.872	150.986	157.914	168.247	186.854	239.424
4	152.926	159.435	168.475	182.314	207.407	277.054
5	155.685	163.747	175.301	192.048	219.143	293.615
6	160.772	167.667	177.348	193.306	224.958	309.332
7	166.309	175.740	188.617	207.919	242.106	333.912
8	177.849	189.109	204.718	228.181	269.452	378.513
9	181.523	193.819	211.512	239.105	288.515	418.060
10	197.055	211.143	230.364	259.003	308.927	438.971

Table 13. First ten natural frequency variations for EDZ2$^{\kappa=5/6}$ theory of a CCFF helicoidal surface (Figure 4c) reinforced by CNTs distributed as in Figure 5c for different mass fractions w_r when varying the parameter of agglomeration μ_1 with $\mu_2 = 1$. The Chebyshev-Gauss-Lobatto grid distribution was employed, with $I_N = 31$, $I_M = 21$.

Theory: *EDZ2$^{\kappa=5/6}$*					
Elastic Foundation: $\rho^{(-)} = 1800\,kg/m^3$, $\quad h_f^{(-)} = 0.15\,m$, $\quad k_{2f}^{(-)} = 20 \times 10^7\,N/m^3$, $\quad k_{3f}^{(-)} = 35 \times 10^7\,N/m^3$					
$w_r = 0.1$					
f [Hz]	$\mu_1 = 0.5$	$\mu_1 = 0.6$	$\mu_1 = 0.7$	$\mu_1 = 0.8$	$\mu_1 = 0.9$	$\mu_1 = 1.0$
1	97.885	102.430	106.843	111.165	115.447	119.768
2	136.918	139.173	141.279	143.447	145.957	149.225
3	144.416	147.224	150.469	154.270	158.835	164.578
4	150.582	154.198	158.310	163.168	169.123	176.767
5	152.576	156.728	161.705	167.761	175.301	184.961
6	158.287	162.018	166.332	171.466	177.789	185.970
7	162.001	167.168	173.097	180.044	188.451	199.084
8	172.434	178.474	185.493	193.826	203.991	216.881
9	175.865	182.324	189.953	199.208	210.798	225.880
10	189.471	197.189	205.994	216.298	228.744	244.417
$w_r = 0.2$					
f [Hz]	$\mu_1 = 0.5$	$\mu_1 = 0.6$	$\mu_1 = 0.7$	$\mu_1 = 0.8$	$\mu_1 = 0.9$	$\mu_1 = 1.0$
1	100.712	106.375	112.025	117.736	123.675	130.364
2	137.944	140.657	143.559	147.345	153.399	165.519
3	145.740	149.816	154.972	161.812	171.831	189.398
4	152.419	157.589	164.197	173.201	186.653	210.336
5	154.827	161.085	169.410	180.934	196.482	221.801
6	160.162	165.580	172.581	182.207	198.259	227.876
7	164.913	172.368	181.809	194.452	212.987	244.915
8	175.859	184.667	196.003	211.317	233.767	272.154
9	179.657	189.267	202.004	219.814	246.660	293.144
10	194.046	205.148	219.187	237.949	265.234	311.452
$w_r = 0.4$					
f [Hz]	$\mu_1 = 0.5$	$\mu_1 = 0.6$	$\mu_1 = 0.7$	$\mu_1 = 0.8$	$\mu_1 = 0.9$	$\mu_1 = 1.0$
1	101.852	108.230	114.687	121.353	128.696	140.804
2	137.668	140.760	144.544	150.567	163.094	203.466
3	145.767	150.861	157.762	168.056	186.586	238.956
4	152.724	159.191	168.163	181.893	206.788	275.907
5	155.498	163.514	175.011	191.488	218.278	292.100
6	160.473	167.289	176.856	192.825	224.335	308.240
7	165.925	175.229	187.938	207.001	240.783	331.572
8	177.170	188.238	203.580	226.671	267.343	374.944
9	181.270	193.560	211.257	238.838	288.194	417.537
10	196.020	209.874	228.786	256.984	306.175	434.423

Table 14. First ten natural frequency variations for ED3 theory of a CCFF helicoidal surface (Figure 4c) reinforced by CNTs distributed as in Figure 5c for different mass fractions w_r when varying the parameter of agglomeration μ_1 with $\mu_2 = 1$. The Chebyshev-Gauss-Lobatto grid distribution was employed, with $I_N = 31$, $I_M = 21$.

			Theory: ED3			
	Elastic Foundation: $\rho^{(-)} = 1800\,kg/m^3$,		$h_f^{(-)} = 0.15\,m$,	$k_{2f}^{(-)} = 20 \times 10^7\,N/m^3$,	$k_{3f}^{(-)} = 35 \times 10^7\,N/m^3$	
			$w_r = 0.1$			
f [Hz]	$\mu_1 = 0.5$	$\mu_1 = 0.6$	$\mu_1 = 0.7$	$\mu_1 = 0.8$	$\mu_1 = 0.9$	$\mu_1 = 1.0$
1	97.923	102.473	106.891	111.217	115.504	119.827
2	136.934	139.186	141.291	143.462	145.979	149.257
3	144.473	147.288	150.539	154.345	158.914	164.658
4	150.692	154.316	158.439	163.309	169.280	176.935
5	152.674	156.842	161.834	167.905	175.458	185.121
6	158.437	162.191	166.531	171.690	178.038	186.241
7	162.172	167.380	173.350	180.339	188.783	199.441
8	172.777	178.869	185.949	194.350	204.580	217.512
9	176.005	182.475	190.106	199.356	210.936	226.005
10	190.036	197.833	206.719	217.102	229.616	245.330
			$w_r = 0.2$			
f [Hz]	$\mu_1 = 0.5$	$\mu_1 = 0.6$	$\mu_1 = 0.7$	$\mu_1 = 0.8$	$\mu_1 = 0.9$	$\mu_1 = 1.0$
1	100.754	106.423	112.081	117.800	123.744	130.430
2	137.958	140.670	143.577	147.376	153.454	165.609
3	145.803	149.890	155.056	161.909	171.944	189.519
4	152.534	157.720	164.351	173.387	186.879	210.591
5	154.937	161.215	169.564	181.109	196.806	222.172
6	160.330	165.785	172.831	182.518	198.515	228.142
7	165.116	172.631	182.140	194.863	213.485	245.460
8	176.245	185.139	196.587	212.033	234.619	273.071
9	179.805	189.423	202.157	219.962	246.808	293.288
10	194.677	205.897	220.072	238.989	266.438	312.725
			$w_r = 0.4$			
f [Hz]	$\mu_1 = 0.5$	$\mu_1 = 0.6$	$\mu_1 = 0.7$	$\mu_1 = 0.8$	$\mu_1 = 0.9$	$\mu_1 = 1.0$
1	101.896	108.283	114.751	121.426	128.773	140.880
2	137.680	140.775	144.569	150.619	163.202	203.647
3	145.834	150.940	157.858	168.175	186.743	239.132
4	152.843	159.332	168.340	182.124	207.101	276.269
5	155.614	163.655	175.181	191.816	218.751	292.619
6	160.653	167.516	177.150	193.096	224.659	308.601
7	166.148	175.525	188.329	207.518	241.480	332.332
8	177.584	188.767	204.265	227.558	268.497	376.181
9	181.419	193.713	211.408	238.996	288.374	417.729
10	196.689	210.692	229.793	258.242	307.773	436.109

Table 15. First ten natural frequency variations for FSDT$_{RS}^{\kappa=5/6}$ theory of a CCFF helicoidal surface (Figure 4c) reinforced by CNTs distributed as ing Figure 5c for different mass fractions w_r when varying the parameter of agglomeration μ_2 with $\mu_1 = 0.5$. The Chebyshev-Gauss-Lobatto grid distribution was employed, with $I_N = 31$, $I_M = 21$.

Theory: $FSDT_{RS}^{\kappa=5/6}$					
Elastic Foundations: $\rho^{(-)} = 1800\,kg/m^3$, $\quad h_f^{(-)} = 0.15\,m$, $\quad k_{2f}^{(-)} = 20 \times 10^7\,N/m^3$, $\quad k_{3f}^{(-)} = 35 \times 10^7\,N/m^3$					
$w_r = 0.1$					
f [Hz]	$\mu_2 = 0.5$	$\mu_2 = 0.6$	$\mu_2 = 0.7$	$\mu_2 = 0.8$	$\mu_2 = 0.9$	$\mu_2 = 1.0$
1	119.985	119.692	118.625	116.255	111.188	98.276
2	149.375	149.118	148.233	146.499	143.536	137.440
3	165.084	164.643	163.108	160.026	154.598	145.024
4	177.039	176.439	174.353	170.184	162.969	150.836
5	184.783	184.021	181.364	176.043	166.882	152.286
6	186.827	186.176	183.924	179.456	171.782	158.895
7	200.122	199.290	196.388	190.559	180.355	162.882
8	218.417	217.403	213.865	206.755	194.304	173.308
9	225.774	224.581	220.435	212.198	198.179	175.691
10	246.221	244.983	240.665	231.986	216.776	190.617
$w_r = 0.2$					
f [Hz]	$\mu_2 = 0.5$	$\mu_2 = 0.6$	$\mu_2 = 0.7$	$\mu_2 = 0.8$	$\mu_2 = 0.9$	$\mu_2 = 1.0$
1	130.510	130.247	129.258	126.958	121.490	101.079
2	165.713	165.077	162.808	158.254	150.703	138.378
3	189.809	188.933	185.780	179.279	167.674	146.383
4	210.870	209.686	205.416	196.578	180.727	152.605
5	222.764	221.489	216.896	207.380	189.602	154.475
6	228.181	226.700	221.359	210.274	190.940	160.765
7	246.428	244.836	239.086	227.131	205.455	165.729
8	274.407	272.498	265.589	251.188	224.945	176.702
9	293.386	291.085	282.764	265.413	233.928	179.415
10	314.272	311.964	303.617	286.188	254.304	195.088
$w_r = 0.4$					
f [Hz]	$\mu_2 = 0.5$	$\mu_2 = 0.6$	$\mu_2 = 0.7$	$\mu_2 = 0.8$	$\mu_2 = 0.9$	$\mu_2 = 1.0$
1	140.965	140.630	139.317	136.408	130.398	102.198
2	203.983	202.646	197.476	186.422	167.062	138.047
3	239.516	237.829	231.302	217.250	191.947	146.417
4	277.085	274.885	266.346	247.848	214.086	152.875
5	293.765	291.403	282.244	262.426	226.241	155.109
6	309.188	306.533	296.237	273.856	232.491	161.061
7	334.235	331.362	320.201	295.925	251.132	166.697
8	378.771	375.384	362.210	333.476	280.140	177.994
9	418.393	414.388	398.813	364.739	300.942	180.969
10	439.392	435.351	419.642	385.338	321.356	196.973

Table 16. First ten natural frequency variations for $FSDTZ_{RS}^{\kappa=1}$ theory of a CCFF helicoidal surface (Figure 4c) reinforced by CNTs distributed as in Figure 5c for different mass fractions w_r when varying the parameter of agglomeration μ_2 with $\mu_1 = 0.5$. The Chebyshev-Gauss-Lobatto grid distribution was employed, with $I_N = 31$, $I_M = 21$.

Theory: $FSDTZ_{RS}^{\kappa=1}$					
Elastic Foundations: $\rho^{(-)} = 1800 \, kg/m^3$, $h_f^{(-)} = 0.15 \, m$, $k_{2f}^{(-)} = 20 \times 10^7 \, N/m^3$, $k_{3f}^{(-)} = 35 \times 10^7 \, N/m^3$					
$w_r = 0.1$					
f [Hz]	$\mu_2 = 0.5$	$\mu_2 = 0.6$	$\mu_2 = 0.7$	$\mu_2 = 0.8$	$\mu_2 = 0.9$	$\mu_2 = 1.0$
1	120.001	119.708	118.642	116.273	111.209	98.298
2	149.382	149.126	148.240	146.506	143.543	137.451
3	165.084	164.644	163.111	160.032	154.612	145.054
4	177.053	176.455	174.371	170.209	163.005	150.895
5	184.806	184.045	181.391	176.076	166.926	152.340
6	186.843	186.194	183.946	179.489	171.833	158.975
7	200.137	199.307	196.411	190.598	180.418	162.962
8	218.460	217.449	213.922	206.835	194.419	173.457
9	225.784	224.591	220.448	212.218	198.219	175.786
10	246.291	245.058	240.755	232.109	216.959	190.891
$w_r = 0.2$					
f [Hz]	$\mu_2 = 0.5$	$\mu_2 = 0.6$	$\mu_2 = 0.7$	$\mu_2 = 0.8$	$\mu_2 = 0.9$	$\mu_2 = 1.0$
1	130.519	130.257	129.269	126.971	121.509	101.103
2	165.717	165.081	162.814	158.263	150.715	138.388
3	189.796	188.920	185.770	179.275	167.681	146.418
4	210.852	209.669	205.406	196.581	180.756	152.671
5	222.737	221.464	216.880	207.382	189.636	154.542
6	228.171	226.692	221.356	210.285	190.981	160.863
7	246.374	244.786	239.049	227.123	205.503	165.836
8	274.340	272.436	265.546	251.194	225.039	176.891
9	293.380	291.079	282.760	265.416	233.946	179.521
10	314.205	311.904	303.582	286.213	254.445	195.423
$w_r = 0.4$					
f [Hz]	$\mu_2 = 0.5$	$\mu_2 = 0.6$	$\mu_2 = 0.7$	$\mu_2 = 0.8$	$\mu_2 = 0.9$	$\mu_2 = 1.0$
1	140.964	140.629	139.318	136.412	130.410	102.225
2	203.953	202.618	197.452	186.412	167.071	138.058
3	239.469	237.784	231.262	217.222	191.941	146.456
4	276.974	274.777	266.252	247.787	214.084	152.949
5	293.622	291.261	282.123	262.344	226.235	155.186
6	309.093	306.440	296.156	273.806	232.496	161.176
7	334.001	331.135	320.002	295.789	251.115	166.828
8	378.432	375.056	361.918	333.284	280.128	178.222
9	418.353	414.349	398.778	364.717	300.943	181.083
10	438.995	434.963	419.299	385.118	321.362	197.364

Table 17. First ten natural frequency variations for FSDTZ$_{RS}^{\kappa=5/6}$ theory of a CCFF helicoidal surface (Figure 4c) reinforced by CNTs distributed as in Figure 5c for different mass fractions w_r when varying the parameter of agglomeration μ_2 with $\mu_1 = 0.5$. The Chebyshev-Gauss-Lobatto grid distribution was employed, with $I_N = 31$, $I_M = 21$.

	Theory: $FSDTZ_{RS}^{\kappa=5/6}$					
Elastic Foundations: $\rho^{(-)} = 1800\,kg/m^3$, $h_f^{(-)} = 0.15\,m$, $k_{2f}^{(-)} = 20 \times 10^7\,N/m^3$, $k_{3f}^{(-)} = 35 \times 10^7\,N/m^3$						
			$w_r = 0.1$			
f [Hz]	$\mu_2 = 0.5$	$\mu_2 = 0.6$	$\mu_2 = 0.7$	$\mu_2 = 0.8$	$\mu_2 = 0.9$	$\mu_2 = 1.0$
1	119.905	119.613	118.550	116.189	111.139	98.258
2	149.310	149.055	148.177	146.456	143.510	137.423
3	164.914	164.476	162.949	159.882	154.482	144.961
4	176.685	176.091	174.025	169.898	162.755	150.722
5	184.472	183.714	181.072	175.781	166.678	152.192
6	186.255	185.614	183.394	178.991	171.424	158.713
7	199.322	198.503	195.645	189.908	179.867	162.674
8	217.122	216.128	212.662	205.700	193.525	172.955
9	225.517	224.325	220.181	211.946	197.921	175.487
10	244.474	243.260	239.025	230.516	215.612	189.997
			$w_r = 0.2$			
f [Hz]	$\mu_2 = 0.5$	$\mu_2 = 0.6$	$\mu_2 = 0.7$	$\mu_2 = 0.8$	$\mu_2 = 0.9$	$\mu_2 = 1.0$
1	130.401	130.139	129.153	126.859	121.409	101.058
2	165.499	164.868	162.620	158.108	150.627	138.363
3	189.528	188.657	185.518	179.050	167.501	146.318
4	210.211	209.038	204.808	196.053	180.357	152.491
5	221.875	220.615	216.077	206.685	189.274	154.374
6	227.520	226.049	220.739	209.714	190.355	160.575
7	245.015	243.445	237.773	225.985	204.625	165.499
8	272.189	270.311	263.517	249.367	223.601	176.324
9	293.051	290.754	282.446	265.123	233.682	179.221
10	311.413	309.144	300.939	283.817	252.514	194.446
			$w_r = 0.4$			
f [Hz]	$\mu_2 = 0.5$	$\mu_2 = 0.6$	$\mu_2 = 0.7$	$\mu_2 = 0.8$	$\mu_2 = 0.9$	$\mu_2 = 1.0$
1	140.806	140.472	139.168	136.276	130.292	102.177
2	203.457	202.129	196.998	186.030	166.833	138.034
3	239.023	237.343	230.844	216.854	191.665	146.352
4	275.858	273.676	265.210	246.874	213.418	152.764
5	292.157	289.820	280.752	261.136	225.341	155.007
6	308.032	305.392	295.161	272.924	231.826	160.873
7	331.732	328.895	317.872	293.907	249.706	166.463
8	374.976	371.633	358.662	330.383	277.909	177.609
9	417.841	413.842	398.295	364.285	300.606	180.793
10	434.595	430.611	415.149	381.400	318.486	196.341

Table 18. First ten natural frequency variations for ED2$^{\kappa=5/6}$ theory of a CCFF helicoidal surface (Figure 4c) reinforced by CNTs distributed as in Figure 5c for different mass fractions w_r when varying the parameter of agglomeration μ_2 with $\mu_1 = 0.5$. The Chebyshev-Gauss-Lobatto grid distribution was employed, with $I_N = 31$, $I_M = 21$.

Theory: $ED2^{\kappa=5/6}$						
Elastic Foundations: $\rho^{(-)} = 1800\,kg/m^3$, $h_f^{(-)} = 0.15\,m$, $k_{2f}^{(-)} = 20 \times 10^7\,N/m^3$, $k_{3f}^{(-)} = 35 \times 10^7\,N/m^3$						
$w_r = 0.1$						
f [Hz]	$\mu_2 = 0.5$	$\mu_2 = 0.6$	$\mu_2 = 0.7$	$\mu_2 = 0.8$	$\mu_2 = 0.9$	$\mu_2 = 1.0$
1	119.841	119.545	118.466	116.069	110.942	97.894
2	149.299	149.038	148.139	146.372	143.330	136.937
3	164.745	164.298	162.741	159.608	154.079	144.467
4	177.138	176.537	174.443	170.259	163.011	150.691
5	185.283	184.524	181.870	176.547	167.376	152.660
6	186.538	185.881	183.612	179.118	171.391	158.439
7	199.894	199.057	196.136	190.266	179.969	162.193
8	218.165	217.145	213.588	206.439	193.931	172.779
9	226.149	224.960	220.829	212.616	198.606	176.008
10	246.086	244.843	240.509	231.791	216.481	189.979
$w_r = 0.2$						
f [Hz]	$\mu_2 = 0.5$	$\mu_2 = 0.6$	$\mu_2 = 0.7$	$\mu_2 = 0.8$	$\mu_2 = 0.9$	$\mu_2 = 1.0$
1	130.468	130.204	129.208	126.889	121.370	100.723
2	165.764	165.125	162.846	158.268	150.654	137.960
3	189.696	188.816	185.646	179.102	167.383	145.793
4	211.055	209.869	205.590	196.734	180.844	152.528
5	222.742	221.466	216.862	207.340	189.995	154.917
6	228.585	227.103	221.754	210.641	190.801	160.320
7	246.401	244.805	239.039	227.046	205.276	165.122
8	274.433	272.514	265.582	251.123	224.751	176.218
9	293.544	291.248	282.949	265.649	234.278	179.796
10	314.304	311.994	303.637	286.186	254.233	194.567
$w_r = 0.4$						
f [Hz]	$\mu_2 = 0.5$	$\mu_2 = 0.6$	$\mu_2 = 0.7$	$\mu_2 = 0.8$	$\mu_2 = 0.9$	$\mu_2 = 1.0$
1	140.974	140.637	139.321	136.403	130.365	101.864
2	204.112	202.773	197.597	186.528	167.124	137.683
3	239.561	237.871	231.332	217.249	191.860	145.819
4	277.350	275.148	266.600	248.083	214.282	152.830
5	293.907	291.539	282.365	262.506	226.243	155.588
6	309.626	306.969	296.668	274.281	232.903	160.629
7	334.366	331.491	320.317	296.010	251.139	166.135
8	379.065	375.671	362.470	333.682	280.207	177.526
9	418.354	414.354	398.797	364.771	301.090	181.399
10	439.507	435.463	419.749	385.442	321.432	196.528

Table 19. First ten natural frequency variations for EDZ2$^{\kappa=1}$ theory of a CCFF helicoidal surface (Figure 4c) reinforced by CNTs distributed as in Figure 5c for different mass fractions w_r when varying the parameter of agglomeration μ_2 with $\mu_1 = 0.5$. The Chebyshev-Gauss-Lobatto grid distribution was employed, with $I_N = 31$, $I_M = 21$.

Theory: $EDZ2^{\kappa=1}$					
Elastic Foundations: $\rho^{(-)} = 1800\,kg/m^3$, $h_f^{(-)} = 0.15\,m$, $k_{2f}^{(-)} = 20 \times 10^7\,N/m^3$, $k_{3f}^{(-)} = 35 \times 10^7\,N/m^3$					
$w_r = 0.1$					
f [Hz]	$\mu_2 = 0.5$	$\mu_2 = 0.6$	$\mu_2 = 0.7$	$\mu_2 = 0.8$	$\mu_2 = 0.9$	$\mu_2 = 1.0$
1	119.872	119.575	118.498	116.102	110.976	97.929
2	149.303	149.043	148.144	146.378	143.336	136.950
3	164.761	164.315	162.759	159.629	154.108	144.509
4	177.160	176.560	174.470	170.295	163.061	150.770
5	185.314	184.556	181.907	176.593	167.437	152.733
6	186.584	185.929	183.665	179.181	171.473	158.543
7	199.938	199.102	196.190	190.337	180.067	162.309
8	218.277	217.260	213.715	206.591	194.121	173.013
9	226.173	224.984	220.857	212.653	198.665	176.110
10	246.301	245.063	240.744	232.058	216.806	190.373
$w_r = 0.2$					
f [Hz]	$\mu_2 = 0.5$	$\mu_2 = 0.6$	$\mu_2 = 0.7$	$\mu_2 = 0.8$	$\mu_2 = 0.9$	$\mu_2 = 1.0$
1	130.493	130.229	129.234	126.918	121.404	100.761
2	165.761	165.123	162.847	158.273	150.663	137.972
3	189.702	188.822	185.654	179.116	167.408	145.840
4	211.031	209.847	205.577	196.739	180.883	152.615
5	222.738	221.463	216.870	207.367	190.044	155.004
6	228.577	227.097	221.756	210.662	190.872	160.445
7	246.363	244.770	239.020	227.063	205.359	165.268
8	274.428	272.515	265.605	251.201	224.929	176.498
9	293.548	291.253	282.956	265.665	234.313	179.911
10	314.394	312.090	303.760	286.371	254.538	195.033
$w_r = 0.4$					
f [Hz]	$\mu_2 = 0.5$	$\mu_2 = 0.6$	$\mu_2 = 0.7$	$\mu_2 = 0.8$	$\mu_2 = 0.9$	$\mu_2 = 1.0$
1	140.988	140.652	139.337	136.422	130.392	101.905
2	204.066	202.729	197.559	186.506	167.129	137.694
3	239.533	237.845	231.310	217.240	191.875	145.872
4	277.198	274.999	266.470	247.999	214.277	152.926
5	293.766	291.400	282.247	262.442	226.265	155.685
6	309.501	306.847	296.564	274.217	232.913	160.772
7	334.099	331.229	320.089	295.865	251.143	166.309
8	378.733	375.349	362.195	333.522	280.270	177.849
9	418.316	414.319	398.768	364.755	301.104	181.523
10	439.228	435.198	419.534	385.362	321.609	197.055

Table 20. First ten natural frequency variations for EDZ2$^{\kappa=5/6}$ theory of a CCFF helicoidal surface (Figure 4c) reinforced by CNTs distributed as in Figure 5c for different mass fractions w_r when varying the parameter of agglomeration μ_2 with $\mu_1 = 0.5$. The Chebyshev-Gauss-Lobatto grid distribution was employed, with $I_N = 31$, $I_M = 21$.

|			Theory: $EDZ2^{\kappa=5/6}$			
	Elastic Foundations: $\rho^{(-)} = 1800\,kg/m^3$,		$h_f^{(-)} = 0.15\,m$,	$k_{2f}^{(-)} = 20 \times 10^7\,N/m^3$,	$k_{3f}^{(-)} = 35 \times 10^7\,N/m^3$	
			$w_r = 0.1$			
f [Hz]	$\mu_2 = 0.5$	$\mu_2 = 0.6$	$\mu_2 = 0.7$	$\mu_2 = 0.8$	$\mu_2 = 0.9$	$\mu_2 = 1.0$
1	119.772	119.477	118.403	116.013	110.903	97.885
2	149.229	148.971	148.079	146.326	143.302	136.918
3	164.585	164.140	162.591	159.473	153.974	144.416
4	176.776	176.180	174.108	169.968	162.794	150.582
5	184.972	184.217	181.578	176.287	167.181	152.576
6	185.980	185.333	183.100	178.676	171.061	158.287
7	199.096	198.272	195.398	189.623	179.495	162.001
8	216.896	215.896	212.412	205.413	193.174	172.434
9	225.898	224.710	220.583	212.378	198.383	175.865
10	244.435	243.217	238.968	230.425	215.431	189.471
			$w_r = 0.2$			
f [Hz]	$\mu_2 = 0.5$	$\mu_2 = 0.6$	$\mu_2 = 0.7$	$\mu_2 = 0.8$	$\mu_2 = 0.9$	$\mu_2 = 1.0$
1	130.372	130.108	129.115	126.803	121.301	100.712
2	165.537	164.905	162.647	158.114	150.573	137.944
3	189.423	188.547	185.392	178.882	167.221	145.740
4	210.370	209.195	204.960	196.194	180.468	152.419
5	221.836	220.574	216.027	206.624	189.621	154.827
6	227.918	226.446	221.134	210.098	190.281	160.162
7	244.960	243.387	237.704	225.890	204.454	164.913
8	272.209	270.326	263.513	249.319	223.448	175.859
9	293.209	290.917	282.631	265.361	234.039	179.657
10	311.516	309.246	301.037	283.905	252.558	194.046
			$w_r = 0.4$			
f [Hz]	$\mu_2 = 0.5$	$\mu_2 = 0.6$	$\mu_2 = 0.7$	$\mu_2 = 0.8$	$\mu_2 = 0.9$	$\mu_2 = 1.0$
1	140.826	140.492	139.184	136.283	130.271	101.852
2	203.553	202.225	197.089	186.114	166.884	137.668
3	239.065	237.382	230.872	216.855	191.588	145.767
4	276.049	273.866	265.398	247.060	213.592	152.724
5	292.251	289.906	280.829	261.187	225.333	155.498
6	308.409	305.770	295.539	273.311	232.232	160.473
7	331.756	328.915	317.892	293.924	249.692	165.925
8	375.161	371.817	358.831	330.532	277.985	177.170
9	417.794	413.801	398.274	364.315	300.757	181.270
10	434.675	430.699	415.243	381.526	318.649	196.020

Table 21. First ten natural frequency variations for ED3 theory of a CCFF helicoidal surface (Figure 4c) reinforced by CNTs distributed as in Figure 5c for different mass fractions w_r when varying the parameter of agglomeration μ_2 with $\mu_1 = 0.5$. The Chebyshev-Gauss-Lobatto grid distribution was employed, with $I_N = 31$, $I_M = 21$.

Theory: *ED3*					
Elastic Foundations: $\rho^{(-)} = 1800\,kg/m^3$, $\quad h_f^{(-)} = 0.15\,m$, $\quad k_{2f}^{(-)} = 20 \times 10^7\,N/m^3$, $\quad k_{3f}^{(-)} = 35 \times 10^7\,N/m^3$					
$w_r = 0.1$					
f [Hz]	$\mu_2 = 0.5$	$\mu_2 = 0.6$	$\mu_2 = 0.7$	$\mu_2 = 0.8$	$\mu_2 = 0.9$	$\mu_2 = 1.0$
1	119.831	119.536	118.460	116.069	110.954	97.923
2	149.260	149.001	148.106	146.348	143.316	136.934
3	164.665	164.220	162.668	159.547	154.043	144.473
4	176.944	176.347	174.270	170.120	162.929	150.692
5	185.132	184.376	181.736	176.440	167.319	152.674
6	186.251	185.601	183.357	178.913	171.269	158.437
7	199.453	198.625	195.740	189.942	179.770	162.172
8	217.527	216.523	213.019	205.982	193.666	172.777
9	226.023	224.835	220.709	212.508	198.524	176.005
10	245.348	244.123	239.852	231.264	216.186	190.036
$w_r = 0.2$					
f [Hz]	$\mu_2 = 0.5$	$\mu_2 = 0.6$	$\mu_2 = 0.7$	$\mu_2 = 0.8$	$\mu_2 = 0.9$	$\mu_2 = 1.0$
1	130.437	130.173	129.180	126.868	121.365	100.754
2	165.628	164.993	162.729	158.181	150.614	137.958
3	189.544	188.667	185.508	178.988	167.312	145.803
4	210.625	209.447	205.203	196.420	180.660	152.534
5	222.209	220.940	216.380	206.949	189.828	154.937
6	228.184	226.709	221.391	210.342	190.561	160.330
7	245.505	243.926	238.226	226.374	204.864	165.116
8	273.124	271.235	264.395	250.147	224.165	176.245
9	293.353	291.061	282.773	265.497	234.171	179.805
10	312.790	310.509	302.266	285.064	253.579	194.677
$w_r = 0.4$					
f [Hz]	$\mu_2 = 0.5$	$\mu_2 = 0.6$	$\mu_2 = 0.7$	$\mu_2 = 0.8$	$\mu_2 = 0.9$	$\mu_2 = 1.0$
1	140.902	140.567	139.257	136.353	130.339	101.896
2	203.733	202.401	197.258	186.262	166.988	137.680
3	239.241	237.556	231.040	217.010	191.718	145.834
4	276.411	274.225	265.746	247.387	213.870	152.843
5	292.774	290.426	281.332	261.660	225.735	155.614
6	308.769	306.127	295.887	273.641	232.520	160.653
7	332.515	329.668	318.623	294.614	250.285	166.148
8	376.390	373.033	360.016	331.658	278.974	177.584
9	417.984	413.990	398.458	364.489	300.912	181.419
10	436.360	432.364	416.868	383.072	320.016	196.689
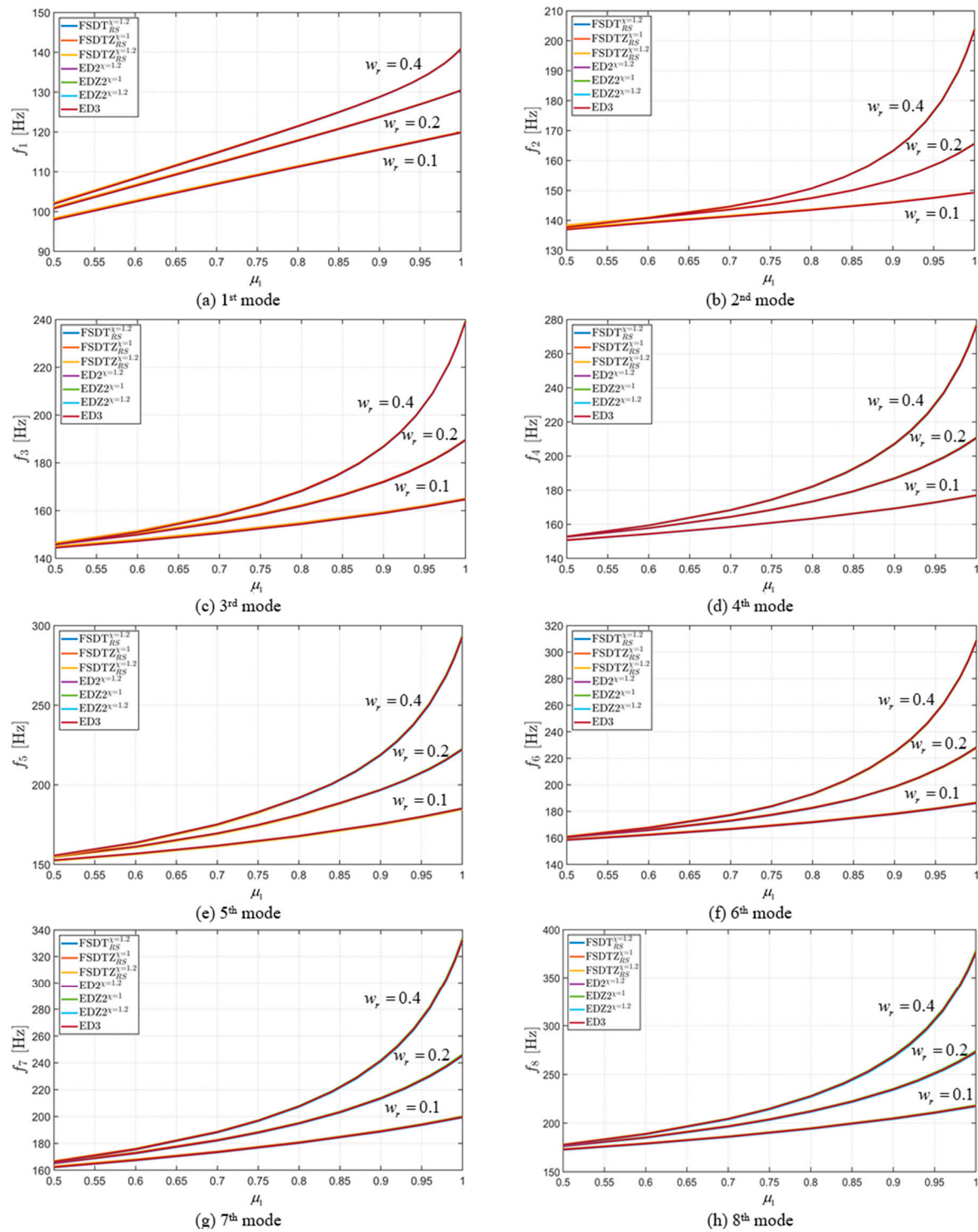
Figure 12. Frequency variations of a CCFF helicoidal surface (Figure 4c) reinforced by CNTs distributed as in Figure 5c for different mass fractions w_r when varying the parameter of agglomeration μ_1 with $\mu_2 = 1$. The Chebyshev-Gauss-Lobatto grid distribution was employed, with $I_N = 31$, $I_M = 21$. The following mode shapes are considered: (**a**) 1st mode; (**b**) 2nd mode; (**c**) 3rd mode; (**d**) 4th mode; (**e**) 5th mode; (**f**) 6th mode; (**g**) 7th mode; (**h**) 8th mode.
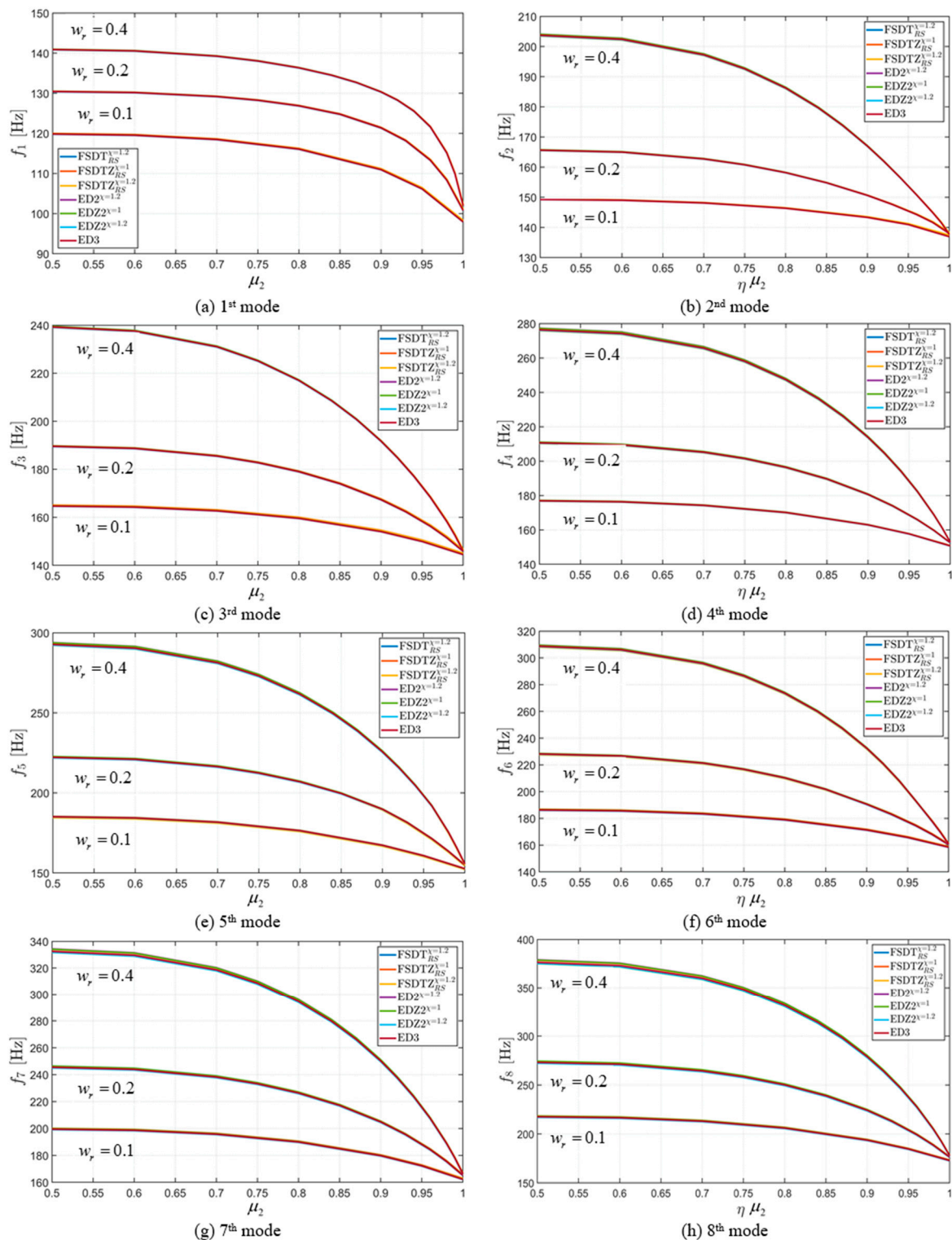
Figure 13. Frequency variations of a CCFF helicoidal surface (Figure 4c) reinforced by CNTs distributed as in Figure 5c for different mass fractions w_r when varying the parameter of agglomeration μ_2 with $\mu_1 = 0.5$. The Chebyshev-Gauss-Lobatto grid distribution was employed, with $I_N = 31$, $I_M = 21$. The following mode shapes are considered: (**a**) 1st mode; (**b**) 2nd mode; (**c**) 3rd mode; (**d**)4th mode; (**e**) 5th mode; (**f**) 6th mode; (**g**) 7th mode; (**h**) 8th mode.

5. Conclusions

In this paper, various investigations were conducted with regard to the free vibration analysis of laminated doubly-curved shells and plates resting on elastic foundation and reinforced by Carbon Nanotubes (CNTs). The results for different higher-order ESL models have been shown, which may also include the Murakami's function to capture the zig-zag effect when a soft core is considered. Once the fundamental system of equations had been developed, the corresponding differential equations were solved numerically by means of the GDQ method, due to its features of accuracy and reliability. The various parametric studies prove that dynamic behavior in terms of natural frequencies is highly affected by several mechanical parameters. In particular, the effects of Winkler-Pasternak foundation, CNT agglomeration and mass fraction were investigated and discussed through several graphs and tables. The following observations can be made:

- the choice and variation of the mechanical parameters that characterize the elastic foundation have a significant impact on the values of natural frequencies;
- interesting behaviors can be observed in terms of natural frequencies when the mechanical parameters of the foundation are increased; in particular, bifurcation points and peculiar overlapping can be noted;
- analogously, the natural frequency values are considerably affected by the agglomeration of CNTs; this aspect is extremely clear when the mass fraction of CNTs reaches higher values;
- the dynamic response of the structure can be modified by varying the parameters that define the through-the-thickness volume fraction distribution of CNTs;
- several analytical distributions can be chosen to describe peculiar through-the-thickness volume fraction distributions, such as power law, exponential and Weibull functions; it should be noted that, at the present time, these distributions are not available in FEM commercial codes;
- the comparison with the commercial FEM software shows good agreement of results, for those cases that can be analyzed and compared.

Finally, the authors believe that the present investigations could help engineers and researchers in studying and designing shell structures reinforced by CNTs and resting on elastic foundations, by providing the proper values for CNT agglomeration, and a more suitable foundation model for obtaining the optimal dynamic response.

Author Contributions: Damjan Banić, Michele Bacciocchi, Francesco Tornabene, and Antonio J. M. Ferreira contributed equally to the development of the research topic and to the writing of the manuscript.

Conflicts of Interest: The authors declare no conflict of interest.

References

1. Iijima, S. Helical Microtubles of Graphitic Carbon. *Nature* **1991**, *354*, 56–58. [CrossRef]
2. Iijima, S.; Ichihashi, T. Single-shell carbon nanotubes of 1-nm diameter. *Nature* **1993**, *363*, 603–605. [CrossRef]
3. Popov, V.N.; Van Doren, V.E.; Balkanski, M. Elastic properties of crystals of single-walled carbon nanotubes. *Solid State Commun.* **2000**, *114*, 395–399. [CrossRef]
4. Popov, V.N.; Van Doren, V.E. Elastic properties of single-walled carbon nanotubes. *Phys. Rev. B* **2000**, *61*, 3078–3084. [CrossRef]
5. Qian, D.; Wagner, G.J.; Liu, W.K.; Yu, M.-F.; Ruoff, R.S. Mechanics of carbon nanotubes. *Appl. Mech. Rev.* **2002**, *55*, 495–533. [CrossRef]
6. Thostenson, E.T.; Chou, T.-W. On the elastic properties of carbon nanotube-based composites: Modelling and characterization. *J. Phys. D Appl. Phys.* **2003**, *36*, 573–582. [CrossRef]

7. Odegard, G.M.; Gates, T.S.; Wise, K.E.; Park, C.; Siochi, E.J. Constitutive modeling of nanotube-reinforced polymer composites. *Compos. Sci. Technol.* **2003**, *63*, 1671–1687. [CrossRef]

8. Shen, L.; Li, J. Transversely isotropic elastic properties of single-walled carbon nanotubes. *Phys. Rev. B* **2004**, *69*, 1129–1133. [CrossRef]

9. Ray, M.C.; Batra, R.C. Effective Properties of Carbon Nanotube and Piezoelectric Fiber Reinforced Hybrid Smart Composites. *J. Appl. Mech.* **2009**, *76*, 540–545. [CrossRef]

10. Wang, J.F.; Liew, K.M. On the study of elastic properties of CNT-reinforced composites based on element-free MLS method with nanoscale cylindrical representative volume element. *Compos. Struct.* **2015**, *124*, 1–9. [CrossRef]

11. Liew, K.M.; Lei, Z.X.; Zhang, L.W. Mechanical analysis of functionally graded carbon nanotube reinforced composites: A review. *Compos. Struct.* **2015**, *120*, 90–97. [CrossRef]

12. Shen, H.-S. Nonlinear bending of functionally graded carbon nanotube-reinforced composite plates in thermal environments. *Compos. Struct.* **2009**, *91*, 9–19. [CrossRef]

13. Raney, J.R.; Fraternali, F.; Amendola, A.; Daraio, C. Modeling and in situ identification of material parameters for layered structures based on carbon nanotube arrays. *Compos. Struct.* **2011**, *93*, 3013–3018. [CrossRef]

14. Blesgen, T.; Fraternali, F.; Raney, J.R.; Amendola, A.; Daraio, C. Continuum limits of bistable spring models of carbon nanotube arrays accounting for material damage. *Mech. Res. Commun.* **2012**, *45*, 58–63. [CrossRef]

15. Jam, J.E.; Pourasghar, A.; Kamarian, S. Effect of the Aspect Ratio and Waviness of Carbon Nanotubes on the Vibrational Behavior of Functionally Graded Nanocomposite Cylindrical Panels. *Polym. Compos.* **2012**, *33*, 2036–2044. [CrossRef]

16. Alibeigloo, A.; Liew, K.M. Thermoelastic analysis of functionally graded carbon nanotube-reinforced composite plate using theory of elasticity. *Compos. Struct.* **2013**, *106*, 873–881. [CrossRef]

17. Alibeigloo, A. Free vibration analysis of functionally graded carbon nanotube-reinforced composite cylindrical panel embedded in piezoelectric layers by using theory of elasticity. *Eur. J. Mech.* **2014**, *44*, 104–115. [CrossRef]

18. Brischetto, S. A continuum elastic three-dimensional model for natural frequencies of single-walled carbon nanotubes. *Compos. Part B Eng.* **2014**, *61*, 222–228. [CrossRef]

19. Brischetto, S. A continuum shell model including van der Waals interaction for free vibrations of double-walled carbon nanotubes. *Comput. Model. Eng. Sci.* **2015**, *104*, 305–327.

20. Zhang, L.W.; Lei, Z.X.; Liew, K.M. Free vibration analysis of functionally graded carbon nanotube-reinforced composite triangular plates using the FSDT and element-free IMLS-Ritz method. *Compos. Struct.* **2015**, *120*, 189–199. [CrossRef]

21. Zhang, L.W.; Lei, Z.X.; Liew, K.M. Vibration characteristic of moderately thick functionally graded carbon nanotube reinforced composite skew plates. *Compos. Struct.* **2015**, *122*, 172–183. [CrossRef]

22. Lei, Z.X.; Zhang, L.W.; Liew, K.M. Free vibration analysis of laminated FG-CNT reinforced composite rectangular plates using the kp-Ritz method. *Compos. Struct.* **2015**, *127*, 245–259. [CrossRef]

23. Mareishi, S.; Kalhori, H.; Rafiee, M.; Hosseini, S.M. Nonlinear forced vibration response of smart two-phase nano-composite beams to external harmonic excitations. *Curved Layer. Struct.* **2015**, *2*, 150–161. [CrossRef]

24. Tornabene, F.; Fantuzzi, N.; Bacciocchi, M.; Viola, E. Effect of agglomeration on the natural frequencies of functionally graded carbon nanotube-reinforced laminated composite doubly-curved shells. *Compos. Part B Eng.* **2016**, *89*, 187–218. [CrossRef]

25. Tornabene, F.; Fantuzzi, N.; Bacciocchi, M. Linear Static Response of Nanocomposite Plates and Shells Reinforced by Agglomerated Carbon Nanotubes. *Compos. Part B Eng.* **2017**, *115*, 449–476. [CrossRef]

26. Fantuzzi, N.; Tornabene, F.; Bacciocchi, M.; Dimitri, R. Free vibration analysis of arbitrarily shaped Functionally Graded Carbon Nanotube-reinforced plates. *Compos. Part B Eng.* **2017**, *115*, 384–408. [CrossRef]

27. Tornabene, F.; Bacciocchi, M.; Fantuzzi, N.; Reddy, J.N. Multiscale approach for three-phase CNT/polymer/fiber laminated nanocomposite structures. *Polym. Compos.* **2017**. [CrossRef]

28. Akgöz, B.; Civalek, Ö. A size-dependent beam model for stability of axially loaded carbon nanotubes surrounded by Pasternak elastic foundation. *Compos. Struct.* **2017**, *176*, 1028–1038. [CrossRef]

29. Civalek, Ö. Free vibration of carbon nanotubes reinforced (CNTR) and functionally graded shells and plates based on FSDT via discrete singular convolution method. *Compos. Part B Eng.* **2017**, *111*, 45–59. [CrossRef]

30. Chamis, C.C. *Failure Criteria for Filamentary Composites*; TN D-5367; NASA: Washington, DC, USA, 1969.

31. Chamis, C.C. *Thermoelastic Properties of Unidirectional Filamentary Composites by a Semiempirical Micromechanics Theory*; Union Carbide Corp Cleveland Ohio Carbon Products Div: Cleveland, OH, USA, 1974.

32. Shi, D.-L.; Huang, Y.Y.; Hwang, K.-C.; Gao, H. The Effect of Nanotube Waviness and Agglomeration on the Elastic Property of Carbon Nanotube-Reinforced Composites. *J. Eng. Mater. Technol.* **2004**, *126*, 250–257. [CrossRef]

33. Mori, T.; Tanaka, K. Average stress in matrix and average elastic energy of materials with Misfitting inclusions. *Acta Metall.* **1973**, *21*, 571–574. [CrossRef]

34. Hill, R. Theory of Mechanical Properties of Fibre-Strengthened Materials: I. Elastic Behavior. *J. Mech. Phys. Solids* **1964**, *12*, 199–212. [CrossRef]

35. Hill, R. Theory of Mechanical Properties of Fibre-Strengthened Materials: II. Inelastic Behavior. *J. Mech. Phys. Solids* **1964**, *12*, 213–218. [CrossRef]

36. Hedayati, H.; Sobhani Aragh, B. Influence of graded agglomerated CNTs on vibration of CNT-reinforced annular sectorial plates resing on Pasternak foundation. *Appl. Math. Comput.* **2012**, *218*, 8715–8735.

37. Aragh, B.S.; Barati, A.H.N.; Hedayati, H. Eshelby-Mori-Tanaka approach for vibrational behavior of continuously graded carbon nanotube-reinforced cylindrical panels. *Compos. Part B Eng.* **2012**, *43*, 1943–1954. [CrossRef]

38. Aragh, B.S.; Farahani, E.B.; Barati, A.H.N. Natural frequency analysis of continuously graded carbon nanotube-reinforced cylindrical shells based on third-order shear deformation theory. *Math. Mech. Solids* **2013**, *18*, 264–284. [CrossRef]

39. Reddy, J.N. A Simple Higher-Order Theory for Laminated Composite Plates. *J. Appl. Mech.* **1984**, *51*, 745–752. [CrossRef]

40. Bert, C.W. A Critical Evaluation of New Plate Theories Applied to Laminated Composites. *Compos. Struct.* **1984**, *2*, 329–347. [CrossRef]

41. Reddy, J.N.; Liu, C.F. A higher-order shear deformation theory for laminated elastic shells. *Int. J. Eng. Sci.* **1985**, *23*, 319–330. [CrossRef]

42. Reddy, J.N. A Generalization of the Two-Dimensional Theories of Laminated Composite Plates. *Commun. Appl. Numer. Methods Biomed. Eng.* **1987**, *3*, 173–180. [CrossRef]

43. Librescu, L.; Reddy, J.N. A few remarks concerning several refined theories of anisotropic composite laminated plates. *Int. J. Eng. Sci.* **1989**, *27*, 515–527. [CrossRef]

44. Reddy, J.N. On Refined Theories of Composite Laminates. *Meccanica* **1990**, *25*, 230–238. [CrossRef]

45. Robbins, D.H.; Reddy, J.N. Modeling of Thick Composites Using a Layer-Wise Laminate Theory. *Int. J. Numer. Methods Eng.* **1993**, *36*, 655–677. [CrossRef]

46. Reddy, J.N. *Mechanics of Laminated Composite Plates and Shells*; CRC Press: Boca Raton, FL, USA, 2004.

47. Alibeigloo, A.; Shakeri, M.; Kari, M.R. Free vibration analysis of antisymmetric laminated rectangular plates with distributed patch mass using third-order shear deformation theory. *Ocean Eng.* **2008**, *35*, 183–190. [CrossRef]

48. Demasi, L. ∞3 Hierarchy plate theories for thick and thin composite plates: The generalized unified formulation. *Compos. Struct.* **2008**, *84*, 256–270. [CrossRef]

49. Amabili, M.; Reddy, J.N. A new non-linear higher-order shear deformation theory for large-amplitude vibrations of laminated doubly curved shells. *Int. J. Nonlinear Mech.* **2010**, *45*, 409–418. [CrossRef]

50. Mantari, J.L.; Oktem, A.S.; Soares, C.G. A new trigonometric layerwise shear deformation theory for the finite element analysis of laminated composite and sandwich plates. *Comput. Struct.* **2012**, *94–95*, 45–53. [CrossRef]

51. Mantari, J.L.; Soares, C.G. Generalized layerwise HSDT and finite element formulation for symmetric laminated and sandwich composite plates. *Compos. Struct.* **2013**, *105*, 319–331. [CrossRef]

52. Vo, T.P.; Thai, H.-T.; Nguyen, T.-K.; Lanc, D.; Karamanli, A. Flexural analysis of laminated composite and sandwich beams using a four-unknown shear and normal deformation theory. *Compos. Struct.* **2017**, *176*, 388–397. [CrossRef]

53. D'Ottavio, M. A Sublaminate Generalized Unified Formulation for the analysis of composite structures. *Compos. Struct.* **2016**, *142*, 187–199. [CrossRef]

54. D'Ottavio, M.; Dozio, L.; Vescovini, R.; Polit, O. Bending analysis of composite laminated and sandwich structures using sublaminate variable-kinematic Ritz models. *Compos. Struct.* **2016**, *155*, 45–62. [CrossRef]

55. Tornabene, F.; Fantuzzi, N.; Bacciocchi, M.; Reddy, J.N. An Equivalent Layer-Wise Approach for the Free Vibration Analysis of Thick and Thin Laminated Sandwich Shells. *Appl. Sci.* **2017**, *7*, 1–34. [CrossRef]

56. Tornabene, F.; Fantuzzi, N.; Bacciocchi, M. Linear Static Behavior of Damaged Laminated Composite Plates and Shells. *Materials* **2017**, *10*, 1–52. [CrossRef] [PubMed]

57. Reddy, J.N.; Chin, C.D. Thermomechanical Analysis of Functionally Graded Cylinders and Plates. *J. Therm. Stress.* **1998**, *21*, 593–626. [CrossRef]

58. Loy, C.T.; Lam, K.Y.; Reddy, J.N. Vibration of functionally graded cylindrical shells. *Int. J. Mech. Sci.* **1999**, *41*, 309–324. [CrossRef]

59. Pradhan, S.C.; Loy, C.T.; Lam, K.Y.; Reddy, J.N. Vibration characteristics of functionally graded cylindrical shells under various boundary conditions. *Appl. Acoust.* **2000**, *61*, 111–129. [CrossRef]

60. Reddy, J.N. Analysis of functionally graded plates. *Int. J. Numer. Methods Eng.* **2000**, *47*, 663–684. [CrossRef]

61. Arshad, S.H.; Naeem, M.N.; Sultana, N. Frequency analysis of functionally graded material cylindrical shells with various volume fractions laws. *J. Mech. Eng. Sci.* **2007**, *221*, 1483–1495. [CrossRef]

62. Amabili, M. *Nonlinear Vibrations and Stability of Shells and Plates*; Cambridge University Press: New York, NY, USA, 2008.

63. Reddy, J.N. Microstructure-dependent couple stress theories of functionally graded beams. *J. Mech. Phys. Solids* **2011**, *59*, 2382–2399. [CrossRef]

64. Reddy, J.N.; Kim, J. A nonlinear modified couple stress-based third-order theory of functionally graded plates. *Compos. Struct.* **2012**, *94*, 1128–1143. [CrossRef]

65. Strozzi, M.; Pellicano, F. Nonlinear vibrations of functionally graded cylindrical shells. *Thin-Walled Struct.* **2013**, *67*, 63–77. [CrossRef]

66. Kim, J.; Reddy, J.N. A general third-order theory of functionally graded plates with modified couple stress effect and the von Kármán nonlinearity: Theory and finite element analysis. *Acta Mech.* **2015**, *226*, 2973–2998. [CrossRef]

67. Sofiyev, A.H.; Kuruoglu, N. Dynamic instability of three-layered cylindrical shells containing an FGM interlayer. *Thin-Walled Struct.* **2015**, *93*, 10–21. [CrossRef]

68. Sofiyev, A.H.; Kuruoglu, N. Domains of dynamic instability of FGM conical shells under time dependent periodic loads. *Compos. Struct.* **2016**, *136*, 139–148. [CrossRef]

69. Rivera, M.G.; Reddy, J.N. Stress analysis of functionally graded shells using a 7-parameter shell element. *Mech. Res. Commun.* **2016**, *78*, 60–70. [CrossRef]

70. Tornabene, F.; Viola, E. Free Vibration Analysis of Functionally Graded Panels and Shells of Revolution. *Meccanica* **2009**, *44*, 255–281. [CrossRef]

71. Viola, E.; Tornabene, F. Free Vibrations of Three Parameter Functionally Graded Parabolic Panels of Revolution. *Mech. Res. Commun.* **2009**, *36*, 587–594. [CrossRef]

72. Tornabene, F. Free Vibration Analysis of Functionally Graded Conical, Cylindrical Shell and Annular Plate Structures with a Four-parameter Power-Law Distribution. *Comput. Methods Appl. Mech. Eng.* **2009**, *198*, 2911–2935. [CrossRef]

73. Akgöz, B.; Civalek, Ö. Bending analysis of FG microbeams resting on Winkler elastic foundation via strain gradient elasticity. *Compos. Struct.* **2015**, *134*, 294–301. [CrossRef]

74. Lanc, D.; Vo, T.P.; Turkalj, G.; Lee, J. Buckling analysis of thin-walled functionally graded sandwich box beams. *Thin-Walled Struct.* **2015**, *86*, 148–156. [CrossRef]

75. Tornabene, F.; Fantuzzi, N.; Viola, E.; Batra, R.C. Stress and strain recovery for functionally graded free-form and doubly-curved sandwich shells using higher-order equivalent single layer theory. *Compos. Struct.* **2015**, *119*, 67–89. [CrossRef]

76. Lanc, D.; Turkalj, G.; Vo, T.P.; Brnić, J. Nonlinear buckling behaviours of thin-walled functionally graded open section beams. *Compos. Struct.* **2016**, *152*, 829–839. [CrossRef]

77. Fazzolari, F.A. Reissner's Mixed Variational Theorem and Variable Kinematics in the Modelling of Laminated Composite and FGM Doubly-Curved Shells. *Compos. Part B Eng.* **2016**, *89*, 408–423. [CrossRef]

78. Fazzolari, F.A. Stability Analysis of FGM Sandwich Plates by Using Variable-kinematics Ritz Models. *Mech. Adv. Mater. Struct.* **2016**, *23*, 1104–1113. [CrossRef]

79. Tornabene, F.; Brischetto, S.; Fantuzzi, N.; Bacciocchi, M. Boundary Conditions in 2D Numerical and 3D Exact Models for Cylindrical Bending Analysis of Functionally Graded Structures. *Shock Vib.* **2016**, *2016*, 1–17. [CrossRef]

80. Brischetto, S.; Tornabene, F.; Fantuzzi, N.; Viola, E. 3D Exact and 2D Generalized Differential Quadrature Models for Free Vibration Analysis of Functionally Graded Plates and Cylinders. *Meccanica* **2016**, *51*, 2059–2098. [CrossRef]

81. Fantuzzi, N.; Brischetto, S.; Tornabene, F.; Viola, E. 2D and 3D Shell Models for the Free Vibration Investigation of Functionally Graded Cylindrical and Spherical Panels. *Compos. Struct.* **2016**, *154*, 573–590. [CrossRef]

82. Civalek, Ö. Vibration of laminated composite panels and curved plates with different types of FGM composite constituent. *Compos. Part B Eng.* **2017**, *122*, 89–108. [CrossRef]

83. Tornabene, F.; Fantuzzi, N.; Bacciocchi, M.; Viola, E.; Reddy, J.N. A Numerical Investigation on the Natural Frequencies of FGM Sandwich Shells with Variable Thickness by the Local Generalized Differential Quadrature Method. *Appl. Sci.* **2017**, *7*, 1–39. [CrossRef]

84. Barretta, R.; Feo, L.; Luciano, R. Some closed-form solutions of functionally graded beams undergoing nonuniform torsion. *Compos. Struct.* **2015**, *123*, 132–136. [CrossRef]

85. Barretta, R.; Brčić, M.; Čanađija, M.; Luciano, R.; Marotti de Sciarra, F. Application of gradient elasticity to armchair carbon nanotubes: Size effects and constitutive parameters assessment. *Eur. J. Mech. A Solids* **2017**, *65*, 1–13. [CrossRef]

86. Romano, G.; Barretta, R. Nonlocal elasticity in nanobeams: The stress-driven integral model. *Int. J. Eng. Sci.* **2017**, *115*, 14–27. [CrossRef]

87. Romano, G.; Barretta, R.; Diaco, M. On nonlocal integral models for elastic nano-beams. *Int. J. Mech. Sci.* **2017**, *131–132*, 490–499. [CrossRef]

88. Marotti de Sciarra, F.; Barretta, R. A new nonlocal bending model for Euler-Bernoulli nanobeams. *Mech. Res. Commun.* **2014**, *62*, 25–30. [CrossRef]

89. Apuzzo, A.; Barretta, R.; Luciano, R.; Marotti de Sciarra, F.; Penna, R. Free vibrations of Bernoulli-Euler nano-beams by the stress-driven nonlocal integral model. *Compos. Part B Eng.* **2017**, *123*, 105–111. [CrossRef]

90. Barretta, R. Analogies between Kirchhoff plates and Saint-Venant beams under flexure. *Acta Mech.* **2014**, *225*, 2075–2083. [CrossRef]

91. Barretta, R. On the relative position of twist and shear centres in the orthotropic and fiberwise homogeneous Saint–Venant beam theory. *Int. J. Solids Struct.* **2012**, *49*, 3038–3046. [CrossRef]

92. Barretta, R. Analogies between Kirchhoff plates and Saint-Venant beams under torsion. *Acta Mech.* **2013**, *224*, 2955–2964. [CrossRef]

93. Barretta, R. On Cesàro-Volterra Method in Orthotropic Saint-Venant Beam. *J. Elast.* **2013**, *112*, 233–253. [CrossRef]

94. Carrera, E. A refined multi-layered finite-element model applied to linear and non-linear analysis of sandwich plates. *Compos. Sci. Technol.* **1998**, *58*, 1553–1569. [CrossRef]

95. Carrera, E. Theories and Finite Elements for Multilayered, Anisotropic, Composite Plates and Shells. *Arch. Comput. Methods Eng.* **2002**, *9*, 87–140. [CrossRef]

96. Carrera, E. Theories and Finite Elements for Multilayered Plates and Shells: A Unified Compact Formulation with Numerical Assessment and Benchmarking. *Arch. Comput. Methods Eng.* **2003**, *10*, 215–296. [CrossRef]

97. Carrera, E. Historical review of zig-zag theories for multilayered plates and shells. *Appl. Mech. Rev.* **2003**, *56*, 287–308. [CrossRef]

98. Carrera, E. On the use of the Murakami's zig-zag function in the modeling of layered plates and shells. *Comput. Struct.* **2004**, *82*, 541–554. [CrossRef]

99. Tornabene, F.; Fantuzzi, N.; Bacciocchi, M.; Viola, E. *Laminated Composite Doubly-Curved Shell Structures. Differential Geometry. Higher-Order Structural Theories*; Esculapio: Bologna, Italy, 2016.

100. Tornabene, F.; Fantuzzi, N.; Bacciocchi, M.; Viola, E. *Laminated Composite Doubly-Curved Shell Structures. Differential and Integral Quadrature. Strong Formulation Finite Element Method*; Esculapio: Bologna, Italy, 2016.

101. Tornabene, F.; Viola, E.; Fantuzzi, N. General higher-order equivalent single layer theory for free vibrations of doubly-curved laminated composite shells and panels. *Compos. Struct.* **2013**, *104*, 94–117. [CrossRef]

102. Tornabene, F.; Fantuzzi, N.; Viola, E.; Carrera, E. Static Analysis of Doubly-Curved Anisotropic Shells and Panels Using CUF Approach, Differential Geometry and Differential Quadrature Method. *Compos. Struct.* **2014**, *107*, 675–697. [CrossRef]

103. Tornabene, F.; Fantuzzi, N.; Bacciocchi, M. The Local GDQ Method for the Natural Frequencies of Doubly-Curved Shells with Variable Thickness: A General Formulation. *Compos. Part B Eng.* **2016**, *92*, 265–289. [CrossRef]

104. Tornabene, F.; Fantuzzi, N.; Viola, E. Inter-Laminar Stress Recovery Procedure for Doubly-Curved, Singly-Curved, Revolution Shells with Variable Radii of Curvature and Plates Using Generalized Higher-Order Theories and the Local GDQ Method. *Mech. Adv. Mater. Struct.* **2016**, *23*, 1019–1045. [CrossRef]

105. Tornabene, F.; Fantuzzi, N.; Bacciocchi, M. The GDQ Method for the Free Vibration Analysis of Arbitrarily Shaped Laminated Composite Shells Using a NURBS-Based Isogeometric Approach. *Compos. Struct.* **2016**, *154*, 190–218. [CrossRef]

106. Bacciocchi, M.; Eisenberger, M.; Fantuzzi, N.; Tornabene, F.; Viola, E. Vibration Analysis of Variable Thickness Plates and Shells by the Generalized Differential Quadrature Method. *Compos. Struct.* **2016**, *156*, 218–237. [CrossRef]

107. Tornabene, F.; Fantuzzi, N.; Bacciocchi, M. On the Mechanics of Laminated Doubly-Curved Shells Subjected to Point and Line Loads. *Int. J. Eng. Sci.* **2016**, *109*, 115–164. [CrossRef]

108. Tornabene, F.; Fantuzzi, N.; Bacciocchi, M. A New Doubly-Curved Shell Element for the Free Vibrations of Arbitrarily Shaped Laminated Structures Based on Weak Formulation IsoGeometric Analysis. *Compos. Struct.* **2017**, *171*, 429–461. [CrossRef]

109. Tornabene, F.; Fantuzzi, N.; Bacciocchi, M. Foam core composite sandwich plates and shells with variable stiffness: Effect of the curvilinear fiber path on the modal response. *J. Sandw. Struct. Mater.* **2017**. [CrossRef]

110. Tornabene, F.; Fantuzzi, N.; Bacciocchi, M. Refined Shear Deformation Theories for Laminated Composite Arches and Beams with Variable Thickness: Natural Frequency Analysis. *Eng. Anal. Bound. Elem.* **2017**. [CrossRef]

111. Cheung, Y.K.; Zienkiewicz, O.C. Plates and tanks on elastic foundations—An application of finite element method. *Int. J. Solids Struct.* **1965**, *1*, 451–461. [CrossRef]

112. Bezine, G. A new boundary element method for bending of plates on elastic foundation. *Int. J. Solids Struct.* **1988**, *24*, 557–565. [CrossRef]

113. Katsikadelis, J.T. Large deflection analysis of plates on elastic foundation by the boundary element method. *Int. J. Solids Struct.* **1991**, *27*, 1867–1878. [CrossRef]

114. Qin, Q.H.; Diao, S. Nonlinear analysis of thick plates on an elastic foundation by HT FE with p-extension capabilities. *Int. J. Solids Struct.* **1996**, *33*, 4583–4604. [CrossRef]

115. Akbarov, S.D.; Kocatürk, T. On the bending problems of anisotropic (orthotropic) plates resting on elastic foundations that react in compression only. *Int. J. Solids Struct.* **1997**, *34*, 3673–3689. [CrossRef]

116. Shen, H.-S.; Li, Q.S. Postbuckling of shear deformable laminated plates resting on a tensionless elastic foundation subjected to mechanical or thermal loading. *Int. J. Solids Struct.* **2004**, *41*, 4769–4785. [CrossRef]

117. Civalek, O. Geometrically nonlinear dynamic analysis of doubly curved isotropic shells resting on elastic foundation by a combination of harmonic differential quadrature-finite difference methods. *Int. J. Press. Vessels Pip.* **2005**, *82*, 753–761. [CrossRef]

118. Avramidis, I.E.; Morfidis, K. Bending of beams on three-parameter elastic foundation. *Int. J. Solids Struct.* **2006**, *43*, 357–375. [CrossRef]

119. Golovko, G.B.; Lugovoi, P.Z.; Meish, V.F. Solution of axisymmetric dynamic problems for cylindrical shells on an elastic foundation. *Int. Appl. Mech.* **2007**, *43*, 785–793. [CrossRef]

120. Malekzadeh, P.; Farid, M. A DQ large deformation analysis of composite plates on nonlinear elastic foundations. *Compos. Struct.* **2007**, *79*, 251–260. [CrossRef]

121. Malekzadeh, P.; Setoodeh, A.R. Large deformation analysis of moderately thick laminated plates on nonlinear elastic foundations by DQM. *Compos. Struct.* **2007**, *80*, 569–579. [CrossRef]

122. Sofiyev, A.H. Buckling analysis of FGM circular shells under combined loads and resting on Pasternak type elastic foundations. *Mech. Res. Commun.* **2010**, *37*, 539–544. [CrossRef]

123. Wang, J.; Zhang, C. A three-parameter elastic foundation model for interface stresses in curved beams externally strengthened by a thin FRP plate. *Int. J. Solids Struct.* **2010**, *47*, 998–1006. [CrossRef]

124. Sofiyev, A.H.; Kuruoglu, N. Natural frequency of laminated orthotropic shells with different boundary conditions and resting on the Pasternak type elastic foundation. *Compos. Part B Eng.* **2011**, *42*, 1562–1570. [CrossRef]

125. Thai, H.-T.; Choi, D.-H. A refined shear deformation theory for free vibration of functionally graded plates on elastic foundation. *Compos. Part B Eng.* **2012**, *43*, 2335–2347. [CrossRef]

126. Tornabene, F.; Ceruti, A. Free-form Laminated Doubly-Curved Shells and Panels of Revolution on Winkler-Pasternak Elastic Foundations: A 2D GDQ Solution for Static and Free Vibration Analysis. *World J. Mech.* **2013**, *3*, 1–25. [CrossRef]

127. Tornabene, F.; Reddy, J.N. FGM and Laminated Doubly-Curved and degenerate Shells resting on Nonlinear Elastic Foundation: A GDQ Solution for Static Analysis with a Posteriori Stress and strain Recovery. *J. Indian Inst. Sci.* **2013**, *93*, 635–688.

128. Tornabene, F.; Fantuzzi, N.; Viola, E.; Reddy, J.N. Winkler-Pasternak Foundation Effect on the Static and Dynamic Analyses of Laminated Doubly-Curved and Degenerate Shells and Panels. *Compos. Part B Eng.* **2014**, *57*, 269–296. [CrossRef]

129. Duc, N.D.; Thang, P.T. Nonlinear response of imperfect eccentrically stiffened ceramic–metal–ceramic FGM thin circular cylindrical shells surrounded on elastic foundations and subjected to axial compression. *Compos. Struct.* **2014**, *110*, 200–206. [CrossRef]

130. Duc, N.D.; Anh, V.T.T.; Cong, P.H. Nonlinear axisymmetric response of FGM shallow spherical shells on elastic foundations under uniform external pressure and temperature. *Eur. J. Mech. A-Solids* **2014**, *45*, 80–89. [CrossRef]

131. Zhang, D.-G. Nonlinear bending analysis of FGM rectangular plates with various supported boundaries resting on two-parameter elastic foundations. *Arch. Appl. Mech.* **2014**, *84*, 1–20. [CrossRef]

132. Shariyat, M.; Asemi, K. Three-dimensional non-linear elasticity-based 3D cubic B-spline finite element shear buckling analysis of rectangular orthotropic FGM plates surrounded by elastic foundations. *Compos. Part B Eng.* **2014**, *56*, 934–947. [CrossRef]

133. Zhang, L.W.; Liew, K.M. Postbuckling analysis of axially compressed CNT reinforced functionally graded composite plates resting on Pasternak foundations using an element-free approach. *Compos. Struct.* **2016**, *138*, 40–51. [CrossRef]

134. Civalek, Ö. Nonlinear dynamic response of laminated plates resting on nonlinear elastic foundations by the discrete singular convolution-differential quadrature coupled approaches. *Compos. Part B Eng.* **2013**, *50*, 171–179. [CrossRef]

135. Tornabene, F.; Fantuzzi, N.; Bacciocchi, M.; Reddy, J.N. A Posteriori Stress and Strain Recovery Procedure for the Static Analysis of Laminated Shells Resting on Nonlinear Elastic Foundation. *Compos. Part B Eng.* **2017**, *126*, 162–191. [CrossRef]

136. Shu, C. *Differential Quadrature and Its Application in Engineering*; Springer: Berlin, Germany, 2000.

137. Tornabene, F.; Fantuzzi, N.; Ubertini, F.; Viola, E. Strong formulation finite element method based on differential quadrature: A survey. *Appl. Mech. Rev.* **2015**, *67*, 145–175. [CrossRef]

138. Viola, E.; Tornabene, F.; Fantuzzi, N.; Bacciocchi, M. Numerical Investigation of Composite Materials with Inclusions and Discontinuities. *Key Eng. Mater.* **2017**, *747*, 69–76. [CrossRef]

139. Fantuzzi, N.; Tornabene, F.; Bacciocchi, M.; Neves, A.M.A.; Ferreira, A.J.M. Stability and Accuracy of Three Fourier Expansion-Based Strong Form Finite Elements for the Free Vibration Analysis of Laminated Composite Plates. *Int. J. Numer. Methods Eng.* **2017**, *111*, 354–382. [CrossRef]

140. Tornabene, F.; Fantuzzi, N.; Bacciocchi, M. Mechanical Behaviour of Composite Cosserat Solids in Elastic Problems with Holes and Discontinuities. *Compos. Struct.* **2017**, *179*, 468–481. [CrossRef]

141. Di.Qu.M.A.S.P.A.B. Software. Available online: http://software.dicam.unibo.it/diqumaspab-project (accessed on 1 June 2017).